Stony Brook University

Derivation of the lineage and function in tumor angiogenesis of bone marrow-derived endothelial cells

A Dissertation Presented

by

Daniel Joseph Nolan

to

The Graduate School

in Partial Fulfillment of the

Requirements

for the Degree of

Doctor of Philosophy

in

Genetics

Stony Brook University

August 2007

Stony Brook University

The Graduate School

Daniel Joseph Nolan

We, the dissertation committee for the above candidate for the

Doctor of Philosophy in Genetics, hereby recommend

acceptance of this dissertation.

Dr. Vivek Mittal - Dissertation Advisor
Assistant Professor, Cold Spring Harbor Laboratories

Dr. Scott Powers – Chairperson of Defense
Associate Professor, Cold Spring Harbor Laboratories

Dr. Alea Mills
Associate Professor, Cold Spring Harbor Laboratories

Dr. Robert Lucito
Assistant Professor, Cold Spring Harbor Laboratories

Dr. Robert Benezra
Cancer Biology and Genetics, Memorial Sloan Kettering Cancer Center

This dissertation is accepted by the Graduate School

Lawrence Martin
Dean of the Graduate School

Abstract of the Dissertation

Derivation of the lineage and function in tumor angiogenesis of bone marrow-derived endothelial cells

by

Daniel Joseph Nolan

Doctor of Philosophy

in

Genetics

Stony Brook Univerisity

2007

Tumors build vessels by cooption of pre-existing vasculature and de novo recruitment of bone marrow (BM)-derived endothelial progenitor cells (EPCs). However, the contribution and the functional role of EPCs in tumor neoangiogenesis are controversial. Therefore, by using genetically marked BM progenitor cells, the precise spatial and temporal contribution of EPCs to the neovascularization of three transplanted and one spontaneous breast tumor in vivo using high-resolution microscopy and flow cytometry. Early tumors are shown to recruit BM-derived EPCs that differentiate into mature BM-derived endothelial cells (ECs) and luminally incorporate into a subset of sprouting tumor neovessels. Notably, in later tumors, these BM-derived vessels are diluted with non-BM-

derived vessels from the periphery, which accounts for purported differences in previously published reports. Furthermore, the specific ablation of BM-derived EPCs with aplpha-particle-emitting anti-VE-cadherin antibody markedly impaired tumor growth associated with reduced vascularization. Additionally, the function of EPCs was inhibited by transplanting animals with shRNA against the critical endothelial Id1 gene, delivered via lentiviral transduction of BM progenitors prior to transplantation. EPC dysfunction mimicked EPC ablation with slower tumor growth and decreased vasculature. These results demonstrate that BM-derived EPCs are critical components of the earliest phases of tumor neoangiogenesis. To address how EPCs function, a preliminary lineage within the BM progenitor population has been identified by analyzing the BM progenitor niche in resting and tumor challenged animals. Transcriptional profiling from immature cells in the BM to mature, incorporated BM-ECs reveals a switch from a pro-angiogenic EPC with the mature BM-ECs sensitized to anti-angiogenic signaling. Cumulatively, these results establish a pattern of recruitment of EPCs to early tumors to assist in the angiogenic switch. Subsequently, mature BM-ECs attempt to return the vasculature to a resting state, but are overwhelmed by the host vasculature and tumor microenvironment.

Table of Contents

List of Abbreviations……..ix
Acknowledgements……..…..xi
Chapter 1: Introduction……1
Angiogenesis overview 1
Multiple cell types aid angiogenesis 1
Table1: Select components of the tumor microenvironment 2
Targeting vasculature as a cancer therapy 5
Bone marrow contributes multiple non-hematopoietic lineages 12
Controversial reports of the contribution and identities of BM-derived cells .. 14
CHAPTER 2: Characterization and Kinetics of BM contribution to endothelium 24
Tracking bone marrow derived cells in vivo. 24
BM-derived VE-cadherin$^+$ cells precede tumor vasculature 27
BM-derived VE-cadherin$^+$ cells express various endothelial markers 31
GFP$^+$ VE-cadherin$^+$ cells do not express hematopoietic markers 40
BM-derived ECs are detected in early vasculature 44
Differentiation capacity of EPCs from BM and tumor 51
BM-derived EPCs and ECs contribute to multiple tumor models 55
BM contribution to endothelium peaks in early tumors 65
Quantitation of functional endothelium 72
Chapter 2 Discussion 79
CHAPTER 3: Targetting EPCs as an anti-angiogenic therapy 82
The monoclonal antibody E4G10 specifically recognizes VE-cadherin on EPCs 82
Tumor growth is slowed by targeting EPCs 90
Decrease in EPC contribution is associated with normalization of tumor vasculature 98
Transcription factor Id1 is expressed in tumor associated ECs and EPCs 107
Inhibition of Id1 by lentivirally delivered shRNA 111
Lentiviral delivery of shRNAs efficiently infects Lin$^-$ BM cells 118
Id shRNAs slow tumor growth with reduced angiogenesis 122
Chapter 3 Discussion 128
CHAPTER 4: Identification and analysis of the EPC lineage 133
Identification of EPC sub-populations in tumor challenged mice 137
Marker expression analysis of EPCs under tumor challenge 141
VEGFR2 is maintained in an intracellular pool of recycling endosomes 148
VEGFR2 and VE-cadherin marked cells are incapable of reconstitution 152
Chapter 4 Discussion 156

Chapter 5 Transcriptional profiling to determine the molecular mechanisms of EPC function 159
RNA isolation of flow sorted material 159
RNA and aRNA quality from flow sorted material 163
Comparison of EPCs, BM-ECs, and host-ECs from tumors 167
BM-ECs and EPCs have distinct angiogenic and ECM profiles 172
Transcriptional profiling target validation 178
Chapter 5 Discussion 182
Chapter 6 Conclusions and Perspectives 189
Materials and Methods 192
Cell lines and growth conditions 192
Designing and cloning of shRNAs 192
Lentiviral constructs, virus generation and transductions 193
BM isolation, Lin^- cell purification and transplantation. 195
Flow cytometry, tumor growth, immunohistochemistry and microscopy 195
Peripheral Blood Analysis 197
Cytospin 198
RNA Isolation and Amplification 198
Microarray and Data Analysis 199
EPC differentiation assay 200
Spontaneous tumor model 201
Conjugation of antibodies to fluorophores 201
Preparation and administration of radioimmunoconjugate 202
Statistical Analysis 203
Bibliography: 204

List of Figures and Tables

Table 1 Select components of the tumor microenvironment……...2
Figure 1 Tracking bone marrow-derived cells..... 25
Figure 2 EPCs precede tumor vascularization..... 29
Figure 3 EPCs express endothelial markers..... 32
Figure 4 Endoglin is expressed on VE-cadherin+ cells..... 35
Figure 5 VCAM expression varies on GFP+ VE-cadherin+ cells..... 38
Figure 6 EPCs do not express hematopoietic markers..... 42
Figure 7 BM-ECs contribute to early tumor vasculature..... 45
Figure 8 3-D optical sectioning microscopy is required for accurate identification of BM-EC..... 48
Figure 9EPCs derived from bone marrow and early tumor differentiate into ECs 53
Figure 10 BM contributes to melanoma endothelium 57
Figure 11 EPC recruitment to MMTV PyMT spontaneous breast tumor model.. 59
Figure 12 BM-ECs in MMTV PyMT early breast carcinoma..... 62
Figure 13 Bone marrow contribution peaks in early tumors 66
Figure 14 BM contribution to B16F0 melanoma..... 70
Figure 15 Isolectin GS IB4 specifically stains functional tumor vasculature..... 75
Figure 16 Quantitation of functional bone marrow-derived endothelium 77
Figure 17 E4G10 antibody targets monomeric VE-cadherin on EPCs..... 84
Figure 18 E4G10 recognizes EPCs, not ECs in vessels..... 86
Figure 19 VE-cadherin is not expressed on sprouting blood vessels..... 88
Figure 20 E4G10 slows LLC tumor growth 92
Figure 21 ^{225}E4G10 Reduces EPCs specifically..... 94
Figure 22 ^{225}E4G10 reduces vessel density 96
Figure 23 ^{225}E4G10 decreases dysfunctional vasculature 99
Figure 24 ^{225}E4G10 increases pericyte coverage..... 103
Figure 25 ^{225}E4G10 improves pericyte/vessel adhesion..... 105
Figure 26 Id1 is expressed in tumor ECs and EPCs 109
Figure 27 shRNA inhibition of Id1 in vitro 112
Figure 28 BMTs with TBM or Lin- cells yield identical reconstitutions 116
Figure 29 Efficient transduction of Lin- cells with shRNA lentiviral constructs 120
Figure 30 Tumor growth rates are impaired with shRNAs targeting Id1 and Id3 124
Figure 31 Id1 shRNA BMT reduces vascular density..... 126
Figure 32 VE-cadherin^{+} EPCs from Lin^{-} mobilize in response to tumor challenge 135

Figure 33 VE-cadherin sub-populations respond differently to tumor challenge139
Figure 34 VEGFR2^{+} VE-cadherin^{-} events increase in response to tumor challenge 142
Figure 35 Tumor challenge affects marker presentation on VEGFR2^{+} VE-cadherin^{-} cells..... 146
Figure 36 VEGFR2 is found on membrane and in cytoplasm..... 150
Figure 37 VE-cadherin and VEGFR2 do not define a reconstitutive population154
Figure 38 Optimizing RNA extraction from sorted cells..... 161
Figure 39 RNA quality of flow sorted and amplified material..... 165
Figure 40 Cluster Dendogram of EPCs, BM-ECs, and host-ECs from tumors.. 168
Figure 41 Scatter plot of Host-EC v BM-EC and BM-EC v EPC..... 170
Figure 42 Heat map comparing BM-ECs to EPCs 173
Table 2 Selected extracellular matrix associated genes with statistically significant changes in expression compared to BM-ECs……..176
Table 3 Selected chemokine and receptor genes with statistically significant changes in expression between Host ECs, BM-ECs, and EPCs……. 176
Figure 43 Endothelial markers and functional kinetics of tumor vasculature 180
Figure 44 Model of stabilizing BM-ECs 184
Figure 45 Model of chemokines and their role in angiogenesis 186

List of Abbreviations

BM	bone marrow
BM-EC	bone marrow-derive endothelial cell
BMT	bone marrow transplant
CCL	chemokine (C-C motif) ligand
CCR	chemokine (C-C motif) receptor
Cdh5	vascular endothelial cadherin
CXCL	chemokine (C-X-C motif) ligand
CXCR	chemokine (C-X-C motif) receptor
EC	endothelial cell
ECM	extra-cellular matrix
eEPC	embryonic endothelial progenitor cell
EPC	endothelial progenitor cell
FACS	fluorescence-activated cell sort
FGF	fibroblast growth factor
FSC	forward scatter
GFP	green fluorescent protein
GCV	ganciclovier
host-EC	host-derived endothelial cell
Lin^-	lineage depleted bone marrow progenitor cells

LLC	lewis lung carcinoma
MFI	mean fluorescent intensity
RBC	red blood cell
RIN	RNA integrity number
RMA	robust multichip analysis
shRNA	short hairpin-ribonucleic acid
SSC	side scatter
TAM	tumor associated macrophage
TEM	tumor educated macrophage
TKI	tyrosine kinase inhibitor
VCAM	vascular cell adhesion molecule
VE-cadherin	vascular endothelial cadherin
VEGF	vascular endothelial growth factor
VEGFR	vascular endothelial growth factor receptor (1,2,3)
WBC	white blood cell

Acknowledgements

The road to my PhD has been long, and many people have been there to help me make the journey. I would like to take this opportunity to thank all the people that have contributed so much to my graduate career. First, I would like to thank my advisor, Vivek Mittal, for his exceptional guidance that helped me become the scientist I am. There were uncountable conversations of brainstorming resulting in many new ways of tackling an experiment. Occasionally we followed one of his wild ideas, other times we followed one of my wild ideas. This respect and degree of freedom was instrumental in the progression of the project. I am truly appreciative of the opportunity afforded me.

There were a number of people who took the time to offer some of their experience and wisdom that made tremendous differences in my experiments. After struggling with injections, a trip to see Mike Hemann resulted in a technique that I would have never conceived on my own. I still contend he was able to do it without looking. Similarly, Barry Burbach kindly devoted the time to demonstrate how to process animals for microscopy. This has become quite a standard protocol that was used in nearly all experiments involving animal work. James Eagan demonstrated the principles of compensation in flow cytometry which was the foundation of my experience.

The second half of my time as a student revolved around sorting cells for various reasons. The planning of this project was extensive and would have required machinery not widely available and would have required enormous amounts of time in the flow facility that simply was not possible. A chance meeting with Michael Regulski in Tim Tully's laboratory changed this. With training and guidance by Nishi Sinha, I became familiar with the FACS Aria flow sorter. Without the access to this machine, much of the extensive flow sorting experiments performed would have never been feasible. The level of trust they bestowed on me to use their equipment is greatly appreciated.

Science can often be a career in navigating Catch-22 situations. In order to be relevant, you need to perform experiments that have never been done before. If they have never been done, how can you know how to do them? Chris Johns and Sohail Kahn have spent countless hours fielding my sometimes endless questions in the design and implementation of the transcriptional profiling project. Together with Anirban Paul, they were able to keep the amount of trial and error experiments to a minimum.

I would also like to acknowledge the current, former, and temporary members of the Mittal Laboratory; James Egan, Dingchen Gao, Sunita Gupta, Emily Heikamp, Azadeh Jadali, Betty Kong, Jon Marcu, Kevin McDonnell, Albert Mellick, and Wen Xue. All members of the lab have made some form of

impact on my time here, but one in particular requires special notice. Kathryn Bambino, the lab technician, shouldered a tremendous amount of responsibilities to keep science running in the Mittal Laboratory. She was an indispensable asset during large experiments when I needed a second pair of hands. Much of the work presented here would have been greatly more challenging without her help.

I would also like to thank my committee members Robert Benezra, who is also a collaborator, Robert Lucito, Alea Mills, and Scott Powers who chaired. I feel that I have had more contact with my committee than many students do. Much of this is due to working within feet of half of my committee which lead to many of the interactions having little to do with science and heaped in sarcasm, but this lead to a more open environment for when I did have a relevant question. I greatly value the comments in designing my project and interpreting my results.

Finally, I would like to thank my very understanding family. Becoming a scientist is as much of a career choice as it is a lifestyle choice. It can have demands on your time that many outside science would not understand. However, I found my family to be extremely understanding of the demands that graduate school placed on me. They have been nothing but supportive. This brings me to my wife, Marissa. The support she gave me over the last 6 years has been immeasurable. From helping me pass Biochemistry, to not letting me go home and forcing me to stay at lab, and being the largest single driving force

pushing me to succeed. I don’t know how I would have been able to do this without her.

Chapter 1: INTRODUCTION

Angiogenesis overview

The initial establishment of vasculature that occurs during embryogenesis is referred to vasculogenesis. The formation of any vessels postnataly, termed angiogenesis, was previously thought to be due the proliferation and migration of mature endothelial cells [1-3]. This notion has become more involved, as many cell types have been proven to be critical in angiogenesis [4]. Most importantly, recent studies have suggested the bone marrow as an alternative source of endothelial cells [5-7]. The understanding of the lineage and the function of bone marrow derived endothelial progenitor cells becomes extremely relevant as the role of vasculature is realized in various pathologies.

Multiple cell types aid angiogenesis

Angiogenesis is a major determinant of the progression of cancer to metastasis and mortality. The majority of solid tumor related deaths are due to the metastatic lesions that form in organs distant from the primary tumor [8-10]. The blood vessels not only provide the resources for growth, but also an avenue for metastatic dissemination. Tumor angiogenesis is a multi-step process involving tumor-derived cytokines [11], stromal cells [12, 13], fibroblasts [14-16], the extra cellular matrix (ECM) [17-19] and bone marrow (BM)-derived

components (Table 1). In particular, the BM contributes various populations of cells capable of enhancing post-natal angiogenesis [4, 20]. Many of these cell

Table1: Select components of the tumor microenvironment

Component	Function	References
EPC	Promotes vascularization of tumors	[21]
EC	Cells which directly form the vasculature supplying blood flow	[1-3, 22]
TEM	Perivascular contributor to angiogenesis of unknown function	[23, 24]
TAM	Cytokine production and matrix remodeling	[25, 26]
ECM	Degradation associated with cancer progression	[19]
Neutrophils	Production of pro-and anti-angiogenic factors	[27, 28]
Fibroblasts	Producers of growth factors, cytokines, and ECM components	[14, 15, 29]
Pericytes	Signaling and structural support cell by direct association with endothelium	[30]
cytokines	Highly varied and context dependent	[27, 31, 32]

types are of hematopoietic origin and indirectly contribute to angiogenesis by performing a perivascular role [4, 20, 33, 34]. The lineages and contributions of these cells are highly varied; for example, tumor associated macrophages (TAMs) [26, 34] which become "educated" at the site of the tumor and are capable of enhancing angiogenesis through matrix degradation and cytokine production, and can also release mutagenic oxygen and nitrogen radicals to further the instability of the cancer genome [34]. Tie-2 expressing monocytes (TEMs) are capable of enhancing angiogenesis in a paracrine manner, specifically independent from a structural contribution to the vasculature[23]. Myeloid progenitors that express vascular endothelial growth factor receptor (VEGFR)-1 are recruited, not only to the early stages of primary tumor growth, but are also suspected of altering tissues in a manner making them susceptible to colonization by metastatic cells [7, 35]. Infiltrating neutrophils have been shown to be a crucial source of matrix metalloproteinase-9 (MMP9) for extra-cellular matrix remodeling [36]. BM-derived pericyte progenitors are capable of indirect structural support to the newly formed blood vessels [30]. Other populations of BM-derived cells lack clear definitions and functions, such as BM-derived circulating cells. This broadly inclusive population is known to be attracted by vascular endothelial growth factor (VEGF) and enhances proangiogenic responses [37].

An important concept has recently emerged from studies by Indraccolo *et al* [11]. They demonstrated a difference between the initiation of angiogenesis "tripping the angiogenic switch", and "maintenance of the switch". To determine this, they used two cell lines in a xenograft tumor model; the poorly angiogenic and non-tumorigenic Molt-3 cells and the highly angiogenic, tumorigenic KSIMM cells. The authors showed that if KSIMMs were capable of tripping the angiogenic switch, Molt-3 cells were capable of maintaining it by co-injecting Molt-3 cells with heavily irradiated KSIMM cells. The KSIMMs were capable of initiating angiogenesis and quickly died. The Molt-3 cells were then capable of continuing angiogenesis and became tumorigenic. This key finding suggests that the many different lineages of cells, including BM-derived cells, have either a persistent role in tumorigenesis or play a distinct role at a defined step in the progression of tumors.

In 1997, Asahara and colleagues [5] discovered a population of endothelial progenitor cells (EPCs) circulating in the blood. These cells shared surface markers common to both endothelial and stem cells. This study isolated EPCs, which differentiated into endothelial cells (ECs) and raised the possibility that they could be used as a therapeutic agent in ischemic tissues and a target in pathologic angiogenesis. Indeed, the tracking and isolation of progenitor cells from both the BM and blood have demonstrated the ability to enhance

angiogenesis, however the results have varied between laboratories [7, 24, 38-43]. Much of this variation can be attributed to the inconsistency of the markers used to identify EPCs and the diverse sets of experiments conducted to characterized EPCs. Regardless of the inconsistencies, these reports do agree on the fact that there are EPCs that contribute to angiogenesis in a way that mature endothelial cells do not. The goals of this thesis were therefore to determine the EPC phenotype, origin, their temporal and spatial contribution to, and role in growing tumors.

Targeting vasculature as a cancer therapy

Endothelial cells present an attractive target for cancer therapeutics. One of the major reasons for this is the relative stability of the endothelial genome in comparison to tumor cells [44]. In one study of colorectal cancer, approximately 11,000 mutations were found in the tumor genome [45]. A fraction of these mutations could contribute to the resistance of cancer therapeutics. An additional property of tumor endothelial cells is that they are in direct contact with a major route of drug delivery, namely the blood flow. Lastly, each tumor has unique sets of mis-regulations, point mutations, duplications, deletions and other factors that render therapeutics useful to only a subset of tumors, whereas EPCs may provide a stable target despite differences in tumor origin.

The specific targeting of therapies to tumor endothelium is a challenging task. One potential method of addressing this is the use of gene therapy with an endothelial promoter. Such was the strategy of Greenberger *et al* [46]. An adenoviral vector was employed to deliver a chimeric death receptor under the transcriptional control of endothelium-specific pre-proendothelin-1 (PPE-1). This methodology was capable of specifically sensitizing proliferating tumor endothelial cells to the apoptotic signaling of TNFα. This treatment was capable of reducing the tumor burden in two tumor models, Lewis Lung Carcinoma (LLC) and B16F10 melanoma. There are two caveats to this particular therapy in translating results to the clinic. First, the frequent injection of large quantities of virus ($2x10^{11}$ viral particles per mouse twice in 9 days) is not feasible for human therapy. Secondly, this will target any active site of angiogenesis, including normal healing. While this strategy shows clear promise, work is needed in enhancing the efficiency and specificity of this treatment. Viral targeting, in general, requires various enhancements to increase its efficacy with respect to immunogenicity, cytotoxicity, and insertional mutagenesis[47-49].

Non-viral methodologies for gene delivery have also been investigated. The objective is to use the tumor or the nearby tumor tissue to produce anti-angiogenic factors that would locally restrict angiogenesis. Peptide-guided gene delivery is currently a feasible technology in a very early stage and requires

significant advances, reviewed in [50]. Another possibility is the injection of naked DNA; however, at an unacceptably low efficiency [51-56]. Unfortunately, this technique is typically limited to the skin or shallow muscle and would be ineffectual in deep tissues. Various other methods also exist, such as ultrasound facilitated gene transfer [57], hydrodynamics [58], cationic lipid [59], and cationic polymer mediated gene transfers [60]. However, all of these technologies currently have limitations which would not make them feasible for therapeutics in their current form.

Research is continuing towards the goal of delivering an anti-angiogenic genetic payload to either the tumor or tumor vasculature[54]. Recently, a study has successfully used gene delivery technology in an anti-angiogenic setting. Kommareddy and Amiji [61] used a gelatin-based nanoparticulate vector and delivered the soluble form of the extracellular domain of vascular endothelial growth factor receptor-1 (VEGFR1). The report demonstrates a clear reduction in tumor burden and vessel density. This is a significant advancement in the use of a non-viral gene delivery. Although the tumor was the main target, the majority of the genetic load was delivered elsewhere within the animal. While the animals were grossly healthy throughout the four week experiments, finer health measurements and prolonged exposure to this technique are needed to assess safety issues.

A cellular based delivery method has also been employed in various investigations. Embryonic endothelial progenitor cells (eEPCs) armed with a suicide gene have been shown to home to metastatic lesions in the lung [62]. The eEPCs were genetically altered to express the yeast cytosine deaminase fused to uracil phosphoribosyl transferase to be used as a catalyst to convert the relatively harmless 5-fluorocytosine (5-FC) to the cytotoxic 5-fluorouracil (5-FU), a commonly used anti-cancer drug [63, 64]. As the authors point out, eEPCs are only efficient at homing to metastatic lesions in the lung, and not to other sites. This is possibly due to the lung being the first capillary bed encountered by the cells after a venous injection. An additional problem to consider with this strategy is the incredibly efficient homing of hematopoietic stem cells to the bone marrow and their robust proliferative capabilities [65]. The triggering of the suicide gene within the progenitor niche in the BM may have adverse side effects. Whether or not eEPCs have any comparable potential has yet to be determined. Alternative cells, such as Tie2 expressing monocytes (TEMs) have also been used to target tumor sites armed with suicide genes [24]. TEMS have been shown to contribute to the angiogenesis of tumors independently of contributions to the vasculature [23]. The herpes simplex virus thymidine kinase (tk)-ganciclovier (GCV) system was lentivirally introduced to TEMs. Animals which received bone marrow transplants transduced with this vector were tumor challenged and

treated with GCV to activate the suicide gene. LLC tumors were markedly reduced in size and tumor vessel density was reduced by several fold. However, the limited fidelity of the Tie2 promoter to exclusively target TEMs may be associated with off target effects.

Targeting growth factors that promote the vascularization of tumors has proved to be the most feasible anti-angiogenic therapeutic approach in the clinic [66]. In particular, the targeting of VEGF has been has been attempted in clinical trials. This can be achieved by either targeting the cytokine or its receptors. One of the more notable attempts at this has been Bevacizumab, an antibody that targets VEGF [67]. Bevacizumab was the first drug approved by the Food and Drug Administration (FDA) targeting tumor angiogenesis for metastatic colorectal cancer. Phase III clinical trials of Bevacizumab in have shown to enhance survival rate, response rate, and duration of response when combined with conventional chemotherapies as a first line treatment for metastatic colorectal cancer. This treatment will serve as a benchmark for future anti-angiogenic therapies. Unfortunately, Bevacizumab does have its limitations, as it is ineffectual in refractory metastatic breast cancer [68] and is associated with notable side effects.

In addition to Bevacizumab [69] there are now various other therapeutic agents capable of targeting angiogenesis. Sunitinib [70], sorafenib [71], and

various small molecule tyrosine kinase inhibitors (TKIs) [72-78] are either approved for various types of tumors, or are currently in Phase II and III clinical trials. While the data from these trials is still early, various unanticipated results have arisen from their use. Recent studies have shown long term treatment has been associated with reduced left ventricular ejection fraction (LVEF) [79, 80]. Bleeding complications have also been observed ranging from minor nose bleeds to potentially fatal bleeding in the lungs with both Bevacizumab and TKIs [81-83] in up to 44% and 26% of patients respectively. Complications involved with normal healing after surgeries almost quadrupled in patients receiving Bevacizumab in combination with chemotherapy [84]. Thrombic events, another potentially life threatening side-effect, has also been observed when anti-angiogenic therapies are combined with chemotherapies[85-87]. Hypertension is one of the most common side-effects of anti-angiogenic therapies , occurring from 15-60% depending on the agent [88-90]. Disturbances in normal kidney function have been found in Bevacizumab patients, but these were not considered life threatening [91, 92]. Finally, increased plasma levels of VEGF have been observed when patients were treated with anti-angiogenic TKIs. The concern here is that increased growth factors may have deleterious effects once the patients are removed from the anti-angiogenic therapies by instigating a large wave of tumor angiogenesis [93, 94]. For a comprehensive review of the

toxicities of anti-angiogenic therapies, see Verheul and Pinedo, 2007 [66]. These drugs have established the effectiveness of anti-angiogenic therapies in improving the health of patients, and the associated toxicities suggest the need for the development of more specific therapies to be developed.

A concerning feature of targeting only a single pro-angiogenic cytokine is the potential for compensation by alternative pro-angiogenic pathways. Indeed, it has been demonstrated that FGF signaling is up-regulated after a prolonged and persistent VEGF signaling blockade. Casanovas *et al* [95] showed that blocking either VEGFR2 alone, or in combination with VEGFR1, decreased tumor burden associated with decreased vessel density in a pancreatic tumor model. However, prolonged VEGFR2 suppression resulted in rebounding tumors with an invasive phenotype that was not dependent on VEGFR2 signaling. VEGFR2 was persistent in its lack of activation, however the tumor up-regulated several pro-angiogenic cytokines including FGF1, FGF2, FGF7, EphrinA1, EphA2, and Angiopoietin1. The authors observed that in addition to inhibiting VEGF, the inhibition of FGF was essential for maintaining an impaired tumor growth. Thus, it is possible that the evasion of a single style of anti-angiogenic therapy may be common among tumors.

Various other anti-angiogenic strategies have been tested; however, none present themselves as a "magic bullet". Due to the redundancies in the pathways

of vasculature formation, hazardous off-target effects, and the adaptive abilities of tumors, it is likely that any true increase in life expectancy (measured in years, not months) will require an elaborate cocktail of anti-cancer therapies. Various aspects of anti-angiogenic therapies must be evaluated (in addition to targeting pro-angiogenic hematopoietic cells) to determine the most effective combinations with chemotherapies in various tumor pathologies. It has already been demonstrated that there are significant differences in tumor responses to different angiogenic blockades, and even variations based on the timing of drug administration [96]. Research in the field of anti-angiogenic therapies are truly at an early stage; however, these early therapies and findings show great promise and will be the basis for the future elucidation of the keys to targeting angiogenesis and creating truly successful therapies.

Bone marrow contributes multiple non-hematopoietic lineages

The hypoxic and cytokine rich environment of the tumor is analogous in many ways to a wound. Indeed, in other models of tissue damage, there is significant evidence for the contribution of BM-derived ECs. The majority is diversified data across multiple healing models including skin flap healing, cardiac repair, and hind limb ischemia.

One promising avenue of research is cardiac repair, and its enhancement by BM-derived cells. It was the goal of Orlich *et al* [39] to characterize which

cell types contribute to cardiac repair and the parameters of healing. The reason for this research is the inability of existing myocytes to replace the necrotic tissues of the heart after myocardial infarction. Donor BM constitutively expressing GFP under the B-actin GFP promoter was used as a means of tracking BM-derived cells in WT recipients. Orlich was capable of finding multiple cell types contributing to the healed heart. Notably, after the differentiation and incorporation of BM-derived cells, c-Kit (a progenitor marker [97]) expression was lost. Specifically, the neovasculature within the damaged region of the heart was 44% GFP^+. He was also capable of detecting myocytes and smooth muscle cells derived from the implanted BM based on GFP expression. Importantly, Orlich was capable of measuring an increase in cardiac function as measured by left ventricular end-diastolic pressure (LVEDP) and developed pressure (LVDP), among other cardiac parameters.

BM derived endothelial cells are found in various wound healing contexts. In human patients, it has been demonstrated that BM is capable of contributing to both epithelial and endothelial fates [98]. In this context, female cancer patients that received BM from male donors were subjected to lung biopsies. FISH staining for a Y chromosome was capable of discerning donor from host cells. A similar strategy was also used to analyze kidney tissue [99]. BM derived cells, again tracked by Y chromosome FISH, were found in the epithelium and, to a

lesser extent, to the endothelium. Importantly, the authors distinguished incorporated cells from hematopoietic cells in close association with the endothelium by co-staining with the hematopoietic marker F4/80. These various studies show the wide range of progenitor cells residing in the BM and emphasize the proper identification of each cell type for proper isolation.

Controversial reports of the contribution and identities of BM-derived cells

In the last decade, research of BM-derived endothelial cells has lead to varying reports on the existence and contribution of BM-ECs. There are several aspects to this controversy. First is the choice of technologies to detect the BM-derived endothelial cells. Some of the initial reports of BM contribution to endothelium used light microscopy and a Lac-Z reporter system[7, 43]. As pointed out by DePalma and colleagues and others, this method is incapable of discerning perivascular contributions of other BM-derived cells from bona fide vessel-incorporated BM-ECs [24, 100]. However, the shortcoming of this particular technology in no way disproves or marginalizes the existence of BM-ECs. In fact, DePalma and Naldini went to great lengths in their attempts to disprove the existence of BM-ECs. However, these experiments only proved that BM-ECs do not form the tumor neovasculature in its entirety, which is far from disproving their existence. Grunewald's research was addressing the recruitment of BM-derived cells in response to VEGF expression and also made the

assumption that BM-ECs would form entire vessels [37]. In their attempt to discern whether or not their model was capable of recruiting BM-ECs, they specifically sought "strings" of BM-ECs.

The notion that BM-ECs have the capacity to form entirely functioning vessels is illogical. As Asahara initially established, EPCs can be found as single cells in circulating blood. If entire vessels, or sections of vessels, were formed by EPCs alone, without neighboring endothelium, there would be several insurmountable problems for the establishment of proper vasculature. First, the progression of arterial to venous blood flow may be compromised by either improper architecture or discontinuity. One end of the vasculature must be capable of connecting to an artery, while distant, yet connected cells, must connect to a vein. Secondly, spontaneous vessel formation would be possible from EPCs alone that would have no association with established vasculature. It is therefore more feasible that EPCs function in a cooperative manner with established vasculature by forming chimeric vessels.

Regardless of assumptions made about the behavior of BM-ECs or the technology used to detect BM-ECs, other discrepancies arose from the use of varying genetic models to track BM-ECs in bone marrow transplant experiments. Lyden *et al* used genetic models that gave no preference to any specific lineage by using ubiquitous promoters to drive a transgene [7]. This reasoning made

minimal assumptions about the biology of a poorly understood cell type and resulted in their successful detection of BM-ECs. Zhang *et al* used an universal endothelial promoter, VEGFR2, which had already had its expression confirmed in EPCs [5, 43]. However, others used promoters that did not have established progenitor or endothelial expression [41] or used gene delivery technologies that had incomplete fidelity with true gene expression [24]. Specifically, Gothert *et al* used the tamoxifen inducible endothelial-SCL-Cre-ERT promoter to detect BM-derived cells. This promoter was used in conjunction with either B-galactosidase (Lac-Z) or enhanced yellow fluorescent protein (EYFP). Gothert was incapable of detecting BM-ECs, and thus concluded they did not contribute to tumor endothelium. When tumors were grown in these transgenic animals, as much as 30% of the tumor vasculature failed to be detectible by this promoter strategy. This result suggests either heterogeneity of endothelial cells within tumors, or that the promoter had incomplete fidelity. This lack of fidelity was also made evident in the detection of the reporters in the myeloid and erythroid lineages. The most serious concern regarding the usefulness of this promoter in BM-EC biology is the lack of reporter expression in the BM. Other issues arose in this investigation as well, including variability in the degree of reconstitution (likely do to a minimal amount of transplanted BM) and the exclusive study of large, established tumors.

DePalma and Naldini [24] made additional assumptions in their attempts to disprove the contribution of BM to tumor endothelium. BM-ECs are not necessarily equivalent to endothelial cells recruited from the neighboring vasculature. If both populations of cells were phenotypically identical, why would there be a need for BM-ECs? If BM-ECs truly did express Tie2, it is possible that alternative promoter elements could be responsible for its expression compared to host-ECs. Regardless, DePalma and colleagues used a lentiviral based Tie2 promoter driving GFP to detect BM-ECs. The transgenic animal, derived from random integration, failed to achieve high fidelity. Indeed, their data shows large populations of cells immunoreactive for Tie2 protein, but showed no promoter activity driving GFP by flow cytometry. Conversely, there was a significant population with an active promoter that had no discernible Tie2 immunoreactivity. Acknowledging the possibility that a constitutive promoter would give superior detection, additional analysis was done. However, tumor analysis in a BM transplanted animal with a constitutive GFP reporter was limited in comparison with the Tie2 investigation and performed on tumors as old as 4 weeks. This study could therefore not be reliable in addressing the contribution of BM-ECs or their regulation of Tie2.

Furthermore, the repertoire of cell surface receptors expressed on endothelial cells is diverse, but many markers are far from exclusive to the

endothelial lineage [101]. Therefore, care must be taken in the identification of endothelial cells by receptor expression. For example, a publication by Granss' group described a continually increasing level of contribution of BM-ECs to two spontaneous tumor types [42]. However, their definition of ECs was based on CD31 (PECAM1) expression. While CD31 is usually used as an endothelial marker, it is expressed on some hematopoietic cells [102, 103] . Therefore, the increased contribution of BM to the endothelium may have been an increase in the amount of $CD31^+$ hematopoietic cells homing to the tumor [104].

Often, *in vitro* data has been especially confounding with regards to marker analysis and lineage. Many studies have used CFU-EC (colony forming unit-endothelial cell) assays to determine if a cell, typically isolated from blood, had the potential to be both a progenitor and endothelial cell. Conclusions utilizing this assay have focused on either pathological condition causing the increase in EPCs, or marker analysis, which purportedly enhances the definition of EPCs [105-114]. Intriguingly, it has been reported that monocytes can be stimulated to express endothelial markers and contribute to vessels formation. Schmeisser *et al* further showed that these cells can, under continuous and prolonged exposure to angiogenic stimuli, simultaneously express endothelial (von Wildebrand Factor, VE-cadherin, and ec-NOS) and hematopoietic (CD45, CD68, and HAM56) markers [103]. These populations of monocytes were

confirmed to lack any endothelial marker expression at the time of harvest by RT-PCR and flow cytometric analysis. Schmeisser first analyzed the populations after exposure to angiogenic cytokines at 2 weeks and found that up to 50% of cells began to express endothelial markers. An additional two weeks of angiogenic stimuli resulted in greater than 95% of monocytes expressing endothelial markers. It is worth noting that these cells failed to express VEGFR2, a receptor critical for the proper function of endothelial cells [115-117]. While the authors present the possibility that monocytes have the plasticity to become ECs, it is also possible that 4 weeks of exposure to high amounts of angiogenic stimuli resulted in the expression of EC markers. Indeed, the lack of VEGFR2 expression questions weather these can be truly considered ECs.

An example of how *in vitro* CFU-EC experiments could be misleading to the experimenters was performed in the Dimmeler laboratory [118]. The study sought to expand the understanding of the extent of the EPCs functionality in neovascularization. $CD14^+$, a monocyte marker, and $CD14^-$ cells were isolated from the peripheral blood and cultivated. No difference was found in their ability to form CFU-ECs. Even more striking, neither of the isolated cell populations was capable of enhancing neovascularization in ischemic mice after harvest. However, upon *ex vivo* angiogenic stimulation and differentiation, they gained the ability to aid in the revascularization of ischemic limbs regardless of their

classification by CD14. Their conclusions, which rely heavily on their *in vitro* differentiation results, are that EPCs can be derived from multiple populations in the peripheral blood. While heterogeneity in the EPC lineage is a distinct possibility, the reliance on *in vitro* data poses intriguing alternative possibilities. These results sound strikingly familiar to the properties of tumor educated macrophages which gain pro-angiogenic properties after stimulation [34]. Additionally, there may be dozens of BM-derived cells that contribute to the neovascularization process, only one of which being a true EPC. Possibly, non-endothelial cells have been confused for EPCs. Recent work from Yoder *et al*, [119] has questioned the relevance of CFU-EC assays all together. This work has quite eloquently demonstrated that positive colonies in CFU-EC assays are diverse in their lineages. Yoder was capable of demonstrating that hematopoietic and non-endothelial cells were capable of reporting as EPCs in CFU-EC assay with an alarming false-positive rate. Thus bona fide EPCs are significantly rarer than once thought. As the authors of this study conclude, many previous findings must now be re-evaluated. This includes any work that relied on CFU-EC assays and concluded hematopoietic cells are capable of endothelial differentiation.

Inconsistent data is also found in non-tumor settings. A study by Balsam *et al* [40], tried to repeat the results of Orlich by again isolating lineage depleted (Lin^-) c-Kit^+ cells, injecting these cells into ischemic myocardium, and testing for

improved functions and the BM-derived cells associated with it. Balsam did find improved cardiac function, in agreement with Orlich, but to a lesser extent. This study failed to find BM-derived myocytes or BM-derived ECs. The major cellular contribution from the injection of BM cells was determined to be hematopoietic. They conclude that Lin^- $c\text{-}Kit^+$ cells are committed to a hematopoietic fate and do not contribute to either the myocyte or endothelial lineage.

A careful analysis of the work between Orlich and Balsam revealed a key distinction between the definitions of cells they studied. Orlich employed a flow sorting purification method for all markers, including c-Kit, and was capable of detecting both hematopoietic and non hematopoietic cells. Balsam used a purification technique utilizing antibodies conjugated to magnetics for the isolation of progenitors and only detected hematopoietic contributions in the damaged hearts. This is a critical detail when considering the work by Katayama *et al* [120], which describes the differences between $c\text{-}Kit^{HIGH}$ and $c\text{-}Kit^{LOW}$ expression on hematopoietic progenitors. Katayama was capable of discerning that $c\text{-}Kit^{HIGH}$ expressers were actively cycling cells in contrast to $c\text{-}Kit^{LOW}$ cells which were more primitive and quiescent. Flow sorting of progenitors has the capacity to be more sensitive to c-Kit expression than the magnetic strategy employed by Balsam. The reconciliation offered by Balsam was an assumed

difference in surgical techniques, but no specifics were given. An alternative resolution between the data of Orlich and Balsam is that Orlich was capable of isolating a more primitive and quiescent population of cells which contained various progenitors capable of endothelial and cardiac differentiation. Conversely, Balsam injected mostly actively cycling c-Kit expressing cells overwhelmingly representing hematopoietic cells. As Balsam wisely points out, more preclinical experimental data is required to explain the phenomenon of BM contribution to ischemic myocardium. A more complete understanding of BM-derived lineages, including endothelial progenitor cell lineage, would allow for a more precise study of cellular contributions to healing. This could ultimately lead to highly specific cellular injections of only beneficial cell types.

Finally, through these various reports, there has been little if any consistency in the tumor type, staging, and marker analysis. Variation was as extreme as comparing day 2 [7] tumors of minimal size to tumors developing for several weeks of very large sizes [24]. The lack of consistency between reports is not surprising when there is no consensus on what technology to use to detect BM-ECs, what reporters to use, which receptors to follow, which assays are reliable, and when to analyze the specimens.

The state of research focusing on BM contribution to the endothelium in tumor angiogenesis is therefore in a degree of turmoil. The clinic is beginning to

see the profound potential of anti-angiogenic therapies, while at the same time realizing that even more specificity is required in the treatments. Unfortunately, this specificity is not currently attainable, due to the lack of agreement about the proper definitions regarding which cells are capable of promoting tumor progression. The body of research I have conducted has addressed this controversial topic by focusing on bone marrow-derived endothelial progenitor cells and resolving a significant portion of their nature. The key findings were the dissection of their spatial and temporal contributions, along with an in-depth characterization of the markers. Furthermore, I have compelling evidence demonstrating that the specific ablation of EPCs can confer substantial therapeutic benefits. Lastly, I have begun to unravel the functions of EPCs and BM-ECs to understand their role beyond the simple "pro-angiogenic" description they currently hold.

CHAPTER 2: Characterization and Kinetics of BM contribution to endothelium

Tracking bone marrow derived cells in vivo.

In order to determine the contribution of the BM-derived EPCs to the formation of tumor neovasculature, I performed bone marrow transplantation (BMT) experiments. To track BM-derived cells *in vivo*, GFP^+ BM cells were isolated from C57BL/6-Tg (ACTbEGFP) mice and transplanted into lethally irradiated age matched, syngeneic, non-GFP recipients (Figure 1A). The syngenicity was required to allow transplants from donor animals into fully immunocompetant recipients.

Analysis of bone marrow and peripheral blood (4-weeks post transplantation), showed greater than 95% reconstitution of recipient hematopoiesis by the donor BM-derived GFP^+ transplanted progenitor cells (Figure 1B). Flow cytometric analysis of the BM also showed high amounts of GFP^+ cells (data not shown), indicating stable replacement of original host stem-cell population by the donor cells.

Following BM reconstitution of WT recipients with donor BM, a variety of transplantable syngeneic tumors (LLC, B6RV2 lymphoma, and B16F0 melanomas) or spontaneous tumor models (MMTV- PyMT breast tumors) were used to determine the contribution of BM-derived cells to growing tumors.

Figure 1: Tracking bone marrow-derived cells

A: Schematic representation of a bone marrow transplantation experiment. Bone marrow from GFP^+ donor animals (C57BL/6-Tg (ACTbEGFP)10sb/J or FVB.Cg-Tg(GFPU)5Nagy/J) was harvested. These cells were then injected into WT animals after a sub-lethal dose of irradiation (1100 Rads). After 4 weeks of reconstitution, animals were challenged with tumors. **B:** Flow cytometric analysis was used to quantitate the amount of GFP^+ cells in the blood of WT animals, GFP^+ BM donors, and WT GFP^+ BM recipients. Note: Reconstitution percentage is calculated according to a comparison with the donor animals, not the absolute number of WBC with detectable GFP signal.

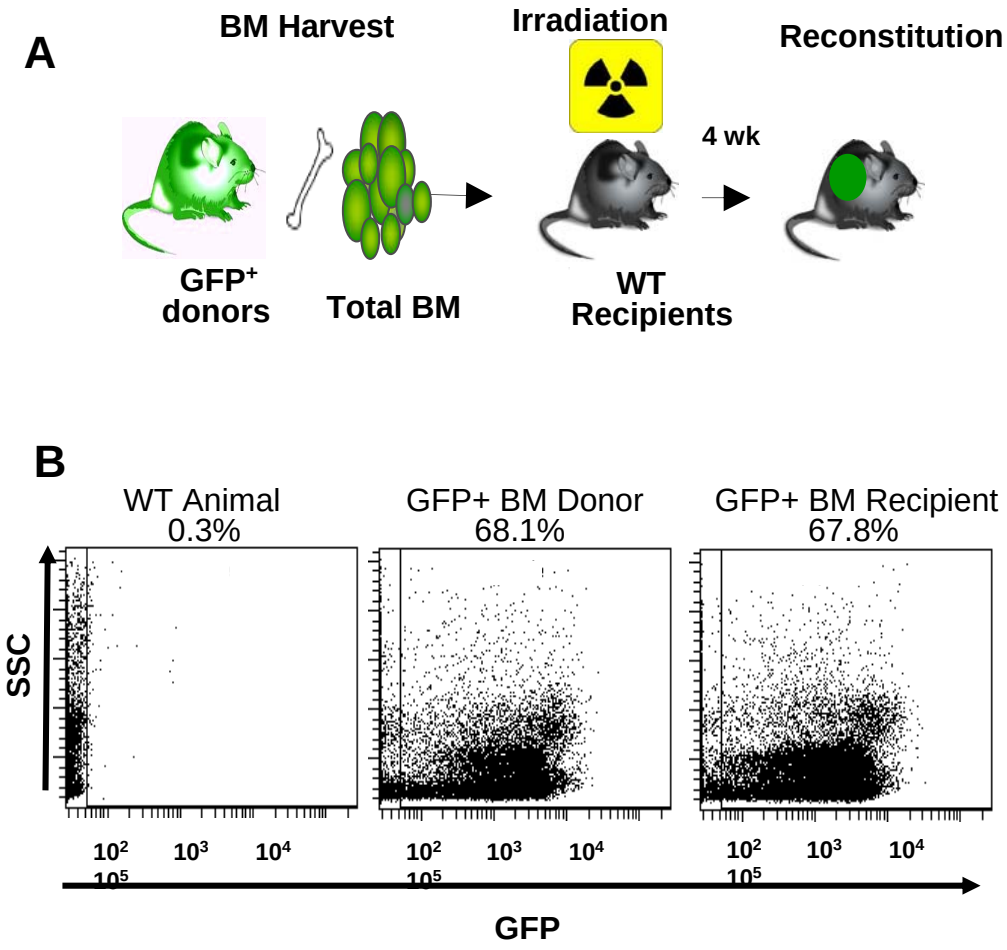
A
BM Harvest
Irradiation
Reconstitution
4 wk
GFP+ donors
Total BM
WT Recipients
B
WT Animal 0.3%
GFP+ BM Donor 68.1%
GFP+ BM Recipient 67.8%
SSC
GFP
10^2
10^3
10^4
10^5

Figure 1

BM-derived VE-cadherin$^+$ cells precede tumor vasculature

The C57BL/6 inbred strain is permissive of tissue transplants from other C57BL/6 animals. The Lewis Lung Carcinoma (LLC) was isolated from C57BL/6 animals and has long been used as an implantable tumor model [121]. Efforts have been focused on xenograft models for studying tumor development, as these models presented several advantages. Xenograft models have 100% penetrance; all implanted animals will form tumors. All xenografts progressed to large vascularized tumors without any lag phase. Most importantly, this model afforded a consistency between animal subjects. This allowed small distinctions in staging to be observed between groups over small periods of time. The variability in onset, penetrance, and growth rate of other tumor models (spontaneous and mutagenic) would have been too confounding to find patterns or make firm conclusions. However, the confirmation of the findings from xenografts in a spontaneous model was then used to establish the relevance of any observations.

When animals were confirmed to be fully reconstituted from GFP$^+$ donor bone marrow by analysis of peripheral blood, they were challenged with LLC tumors. A random group of animals was first sacrificed at day 4 post tumor implant. At this point, gross visual examination suggested a lack of vasculature in the pale tumor plug. Immunofluorescent staining of these tumors confirmed that

the vasculature had not yet infiltrated the tumor bed. At this point, however, a large infiltration of BM-derived cells (Figure 2A) was observed within the tumor boarder (dotted line separates host from tumor). The overwhelming majority of these infiltrating cells are hematopoietic, as noted by their co-expression of CD45 (Figure 2B.) CD45, which has functions that vary in context and splice variant dependent manners, is considered an indicator of hematopoietic cells [122-125].

The vasculature was stained with endothelial markers, CD31 and VE-cadherin. CD31 (PECAM-1) is involved in the adhesion of leukocytes and their extravasation [102]. VE-cadherin is an endothelial specific marker, which is located at the cell-cell contacts and forming part of the intracellular junctions of endothelial cells [126]. Interestingly, there were a number of BM-derived (GFP^+) VE-$cadherin^+$ cells that had infiltrated the tumor bed. They are single cells, as opposed to a continuous blood vessel. They are also rounded, in contrast to the elongated shape of mature endothelial cells. The differences suggested these cells are distinct from endothelial cells. I therefore investigated these cells further to determine if these cells were EPCs.

Figure 2: EPCs precede tumor vascularization

A: A representative fluorescent image showing recruitment of BM-derived GFP^+ $VE\text{-}cadherin^+$ EPCs at the periphery of early non-vascularized LLC tumors (day 4-6, n=15). CD31+ mature vessels are observed in the host tissue but not in the tumors. The dotted line separates the host tissue from the tumor. Scale bar, 100 μm. **B:** The bone marrow-derived cells were assayed for their presentation of the CD45 antigen by flow cytometry. All GFP+ cells were gated (left) and the level of CD45 determined (right, Alexa Fluor 750).

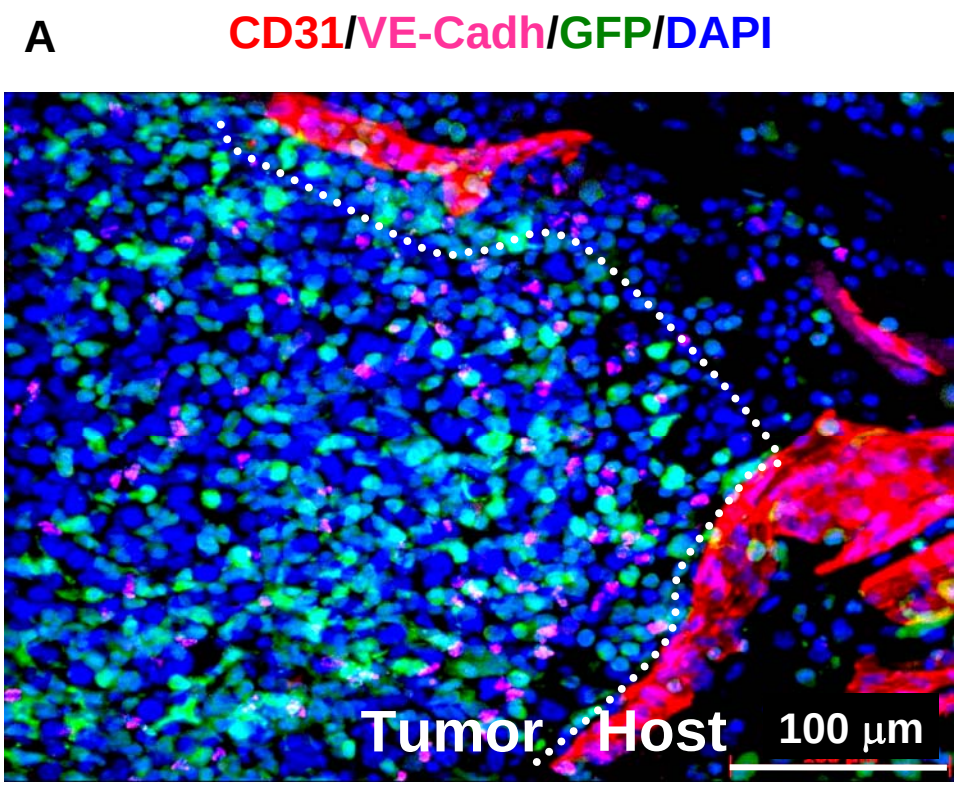
A
CD31/VE-Cadh/GFP/DAPI
Tumor
Host
100 μm

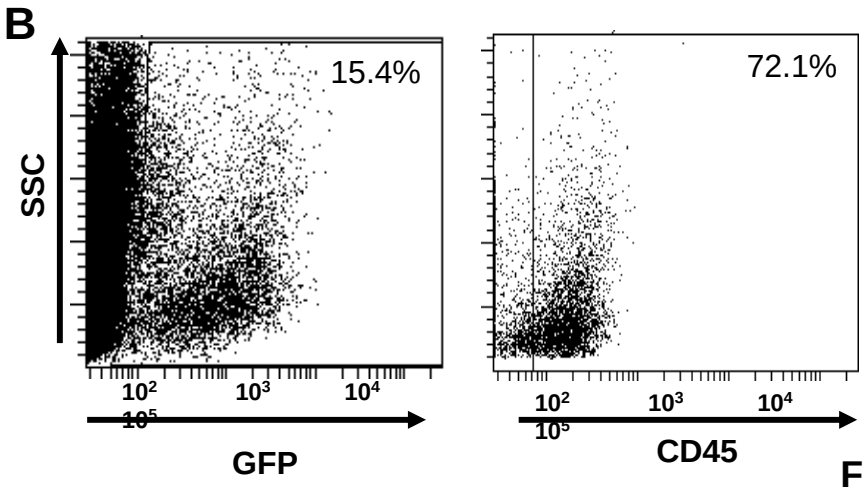
B
SSC
15.4%
72.1%
10²
10³
10⁴
10⁵
GFP
CD45

Figure 2

BM-derived VE-cadherin$^+$ cells express various endothelial markers

Staining for various endothelial markers was performed to investigate whether GFP$^+$ VE-cadherin$^+$ cells are EPCs. The GFP$^+$ VE-cadherin$^+$ cells, while morphologically distinct, share certain surface markers with mature endothelial cells. VE-cadherin is expressed uniformly on the surface of these BM-derived cells (Figure 3A, B), but is restricted to the intracellular junctions between adjacent endothelial cells. Vascular endothelial growth factor receptor 2 (VEGFR2/Flk1/KDR), a receptor tyrosine kinase, is an endothelial specific marker. VEGFR2 was used as a marker in the original definition of EPCs by Asahara [5]. The interaction between cytokine and receptor has a profound role on the development of the early vasculature and subsequent vascular remodeling in the adult [127]. Therefore, it was expected that an EPC in tumors would be positive for VEGFR2. Figure 3A shows that GFP$^+$ VE-cadherin$^+$ cells also express VEGFR2.

GFP$^+$ VE-cadherin$^+$ cells also express endothelial marker CD31, however at a lower level than observed in mature endothelial cells (Figure 3B). Quantitation of the fluorescent signal by microscopy showed an approximately 10-fold reduced CD31 signal (Figure 3C). One of the main functions of CD31 on a mature EC is to facilitate the extravasation of leukocytes from the blood stream.

Figure 3: EPCs express endothelial markers

Multichannel fluorescent images showing **A:** GFP^+ VE-$cadherin^+$ $VEGFR2^+$ EPCs (arrows). **B:** GFP^+ VE-$cadherin^+$ $CD31^+$ EPC (arrows) at the periphery of LLC tumors (day 4). Scale bar, 20 μm**. C:** GFP+ VE-cadherin+ Prominin1+ EPCs (day 4 LLC) Fluorescent signals are shown individually or after merging. Scale bar, 20 μm. **D:** Tumor (day 6) showing both a mature EC (M) and a EPC (IM). Quantitation using Axiovision 4.5 software shows greater than 10-fold lower CD31 signal intensity in an EPC relative to mature EC. Error bars represent the standard error of the mean. Scale bar, 50 μm.

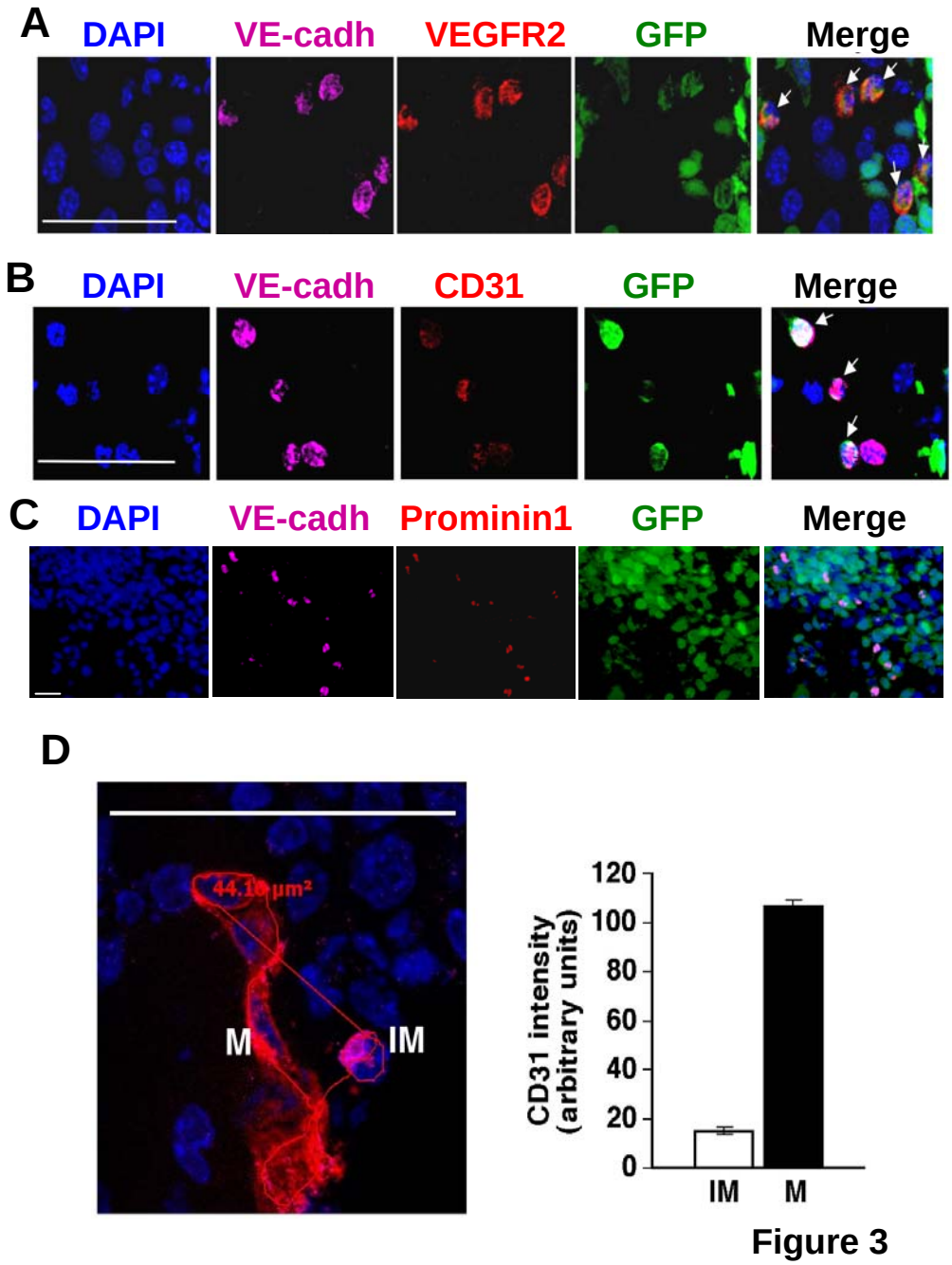
A
DAPI
VE-cadh
VEGFR2
GFP
Merge
B
DAPI
VE-cadh
CD31
GFP
Merge
C
DAPI
VE-cadh
Prominin1
GFP
Merge
D
44.18 µm²
M
IM
CD31 intensity (arbitrary units)
120
100
80
60
40
20
0
IM
M

Figure 3

Specifically, the interaction between CD31 on the endothelial cells and the leukocytes appears to be the transmigration between endothelial cells after the leukocyte has tightly adhered to the endothelial cell. Blocking antibodies to CD31, or incubation with soluble receptor is capable of blocking leukocyte transmigration [128]. Considering the function of CD31, it is not surprising a candidate EPCs would have very little expressed on the surface.

Prominin 1 is a transmembrane antigen which is preferentially expressed on BM progenitor cells [129]. It has been demonstrated as a characteristic marker of EPCs [105]. To date, the function of Prominin 1 remains unknown [130]. Early tumors stained with VE-cadherin and Prominin 1 show their colocalization on GFP^+ cells.

Endoglin (CD105) has been previously demonstrated to be associated with actively or recently proliferating endothelial cells as an accessory component of the TGFβ binding receptor complex [131]. It is mostly restricted to expression on endothelial cells [132]. Recent work has demonstrated that tumor vasculature, in particular, strongly expresses Endoglin [133, 134] and can be used as an prognostic indicator [135, 136]. For example, increased density of endoglin positive vessels indicates a poor prognosis for patients[137]. The risk of developing metastatic lesions has also been demonstrated to be correlated with

Figure 4: Endoglin is expressed on VE-cadherin^{+} cells

A: Representative fluorescent images of an early LLC tumor (day 6) with GFP marking BM-derived cells (green), VE-cadherin marking blood vessels and EPCs (magenta), Endoglin marking blood vessels and EPCs (red), and DAPI marking nuclei (blue). Panels are shown as individual colors with DAPI, or as a merge. Scale bar, 20 μm**. B:** Representative flow cytometry plot analyzing the expression of Endoglin on VE-cadherin^{+} GFP^{+} CD31^{low} CD11b^{-} cells.

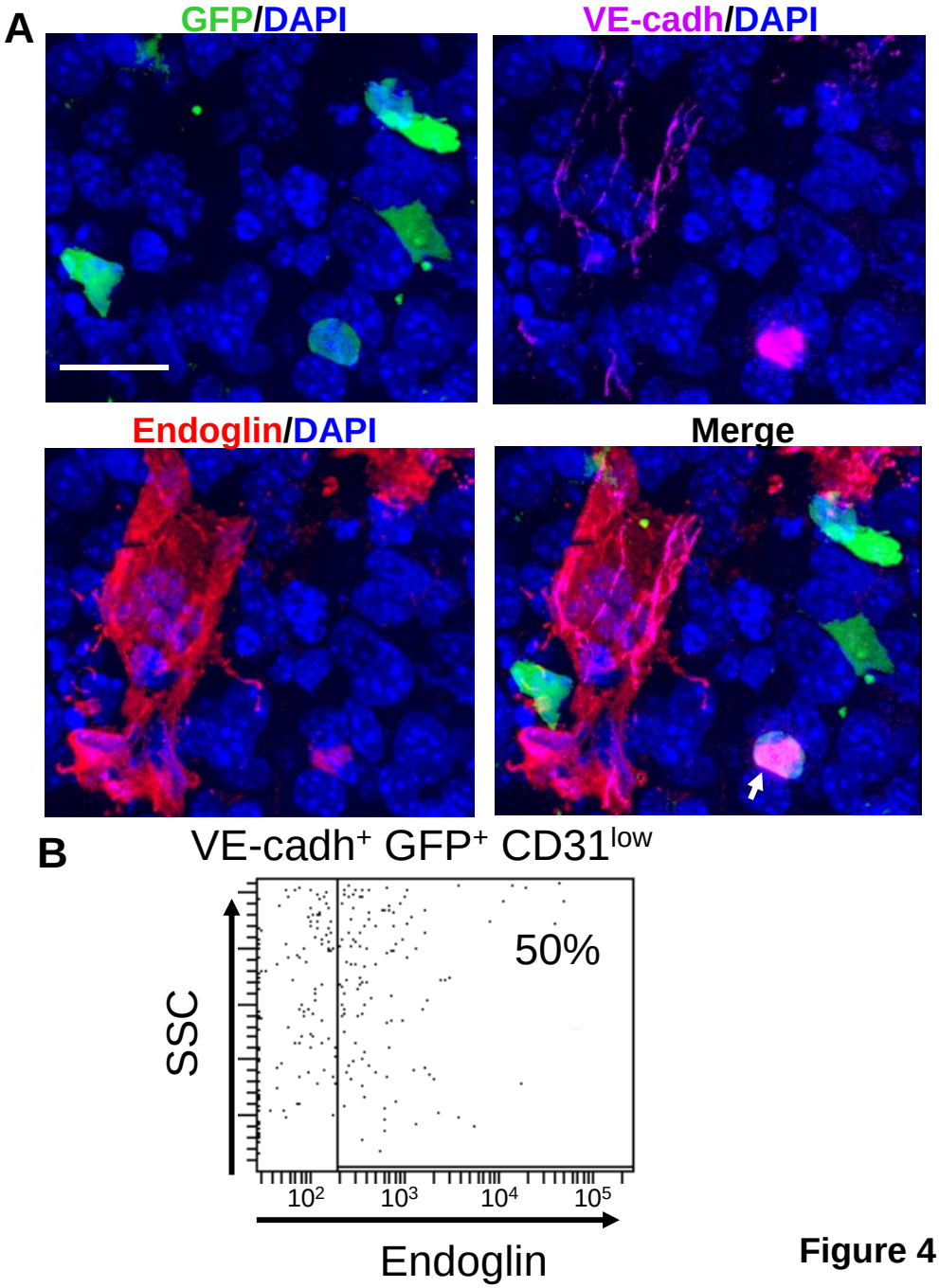
A
GFP/DAPI
VE-cadh/DAPI
Endoglin/DAPI
Merge
B
VE-cadh+ GFP+ CD31low
50%
SSC
10^2
10^3
10^4
10^5
Endoglin

Figure 4

increased Endoglin expression [138]. GFP^+ VE-$cadherin^+$ cells express Endoglin at varying levels (Figure 4A, B). This difference in intensity on VE-cadherin cells may be indicative of varied states of activation or differentiation in growing tumors.

Vascular cell adhesion molecule, VCAM, is an endothelial marker that is involved in the adhesion between endothelial cells and leukocytes. VCAM binds to the receptor very late activation antigen-4 (VLA-4) expressed on monocytes and lymphocytes [139, 140]. GFP^+ VE-$cadherin^+$ cells display an intriguing pattern of VCAM expression with little to none at the tumor periphery with increasing levels within the tumor mass (Figure 5). There are two possible explanations for this observation. The first possibility is that levels of VCAM expression may be associated with differentiation into mature ECs. The second possibility is that the GFP^+ VE-$cadherin^+$ cells may be sensitive to their location within the tumor and are capable of regulating their VCAM expression accordingly. Considering the role of VCAM in binding to receptors on leukocytes, it may be suggestive of a hematopoietic accessory cell in the construction of neovasculature via their association with GFP^+ VE-$cadherin^+$ cells.

Figure 5: VCAM expression varies on GFP+ VE-cadherin^{+} cells

A: Representative fluorescent image of an early vascularized tumor (LLC, day 6) with the tumor/skin boundary oriented towards the right and the tumor core oriented at the left. GFP is marking BM-derived cells (green), VE-cadherin marking blood vessels and EPCs (red), VCAM marking blood vessels and EPCs (magenta), CD31 marking blood vessels (cyan) and DAPI marking nuclei (blue). Select EPCs are circled and numbered. Scale Bar 100 μm. **B:** Marked cells in **A** showing the variation of VCAM expression on EPCs. **C:** Quantitation of VCAM expression using Axiovision 4.5 software of the selected cells (A,B). Error bars represent standard deviation.

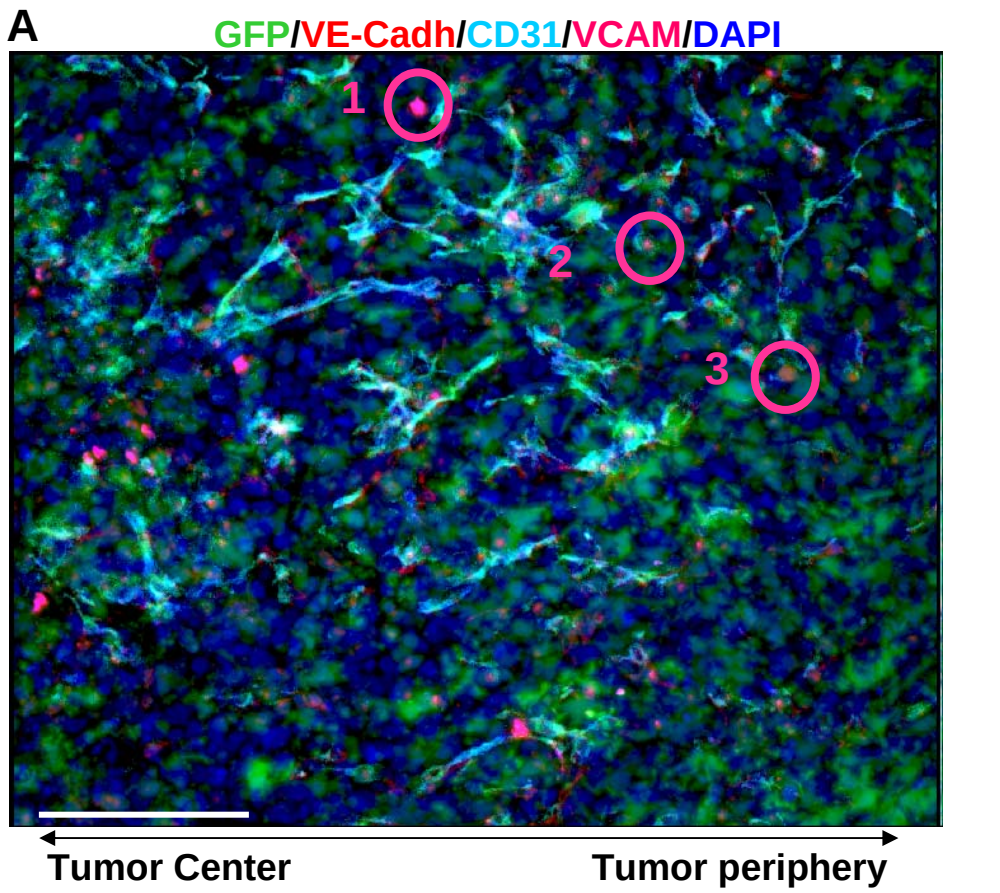
A
GFP/VE-Cadh/CD31/VCAM/DAPI
1
2
3
Tumor Center
Tumor periphery
B
1
2
3
C
VCAM intensity
arbitrary units
200
160
120
80
40
0
1
2
3

Figure 5

GFP$^+$ VE-cadherin$^+$ cells do not express hematopoietic markers

A concern when analyzing the BM contribution to tumor endothelium is the ability to discern hematopoietic from endothelial contributions. As previously mentioned [24], contribution of BM-derived endothelial cells could be confounded by the intimate association of hematopoietic cells with the tumor vasculature. There are also publications which describe hematopoietic cells expressing some endothelial markers [103] therefore warranting a comprehensive hematopoietic marker analysis.

CD11b is associated with integrin mediated signaling on various populations of monocytes and macrophages [141]. As shown in Figure 6A, the GFP$^+$ CD11b$^+$ cells were quite polymorphous. The neighboring GFP$^+$ VE-cadherin$^+$ cells were CD11b$^-$ and have a smaller and rounder morphology. Additionally, GFP$^+$ VE-cadherin$^+$ cells did not stain for CD45RB (Figure 6B), a marker of T cells, B cells, monocytes and macrophages [142]. GFP$^+$ VE-cadherin$^+$ cells were also assayed for the presence of CD41. CD41 is a marker of megakaryocytes, platelets, and some hematopoietic progenitors [143]. Lineage depleted (Lin$^-$) cells from the BM were cytospun onto a glass slide and stained for VE-cadherin and CD41. CD41 stained megakaryocytes, depicted by large cells; however, VE-cadherin$^+$ cells were devoid of CD41 staining (Figure 6C). Collectively, these analyses, along with those for various progenitor and

endothelial markers, demonstrate that the GFP^+ VE-$cadherin^+$ cells are distinct from the hematopoietic lineage strengthening their candidacy as bona fide EPCs.

Figure 6: EPCs do not express hematopoietic markers

High resolution image of a day 4 LLC tumor showing that the BM-derived GFP^+ $VE\text{-}cadherin^+$ cells lack hematopoietic marker **A:** CD11b, Scale bar, 50μm. **B:** CD45RB. Scale bar, 50 μm **C:** CD41 (cytospun Lin- BM cells). Scale bar, 20 μm. White arrows denote BM-derived $VE\text{-}cadherin^+$ cells and yellow arrows denote $CD11b^+$ and $CD45^+$ cells.

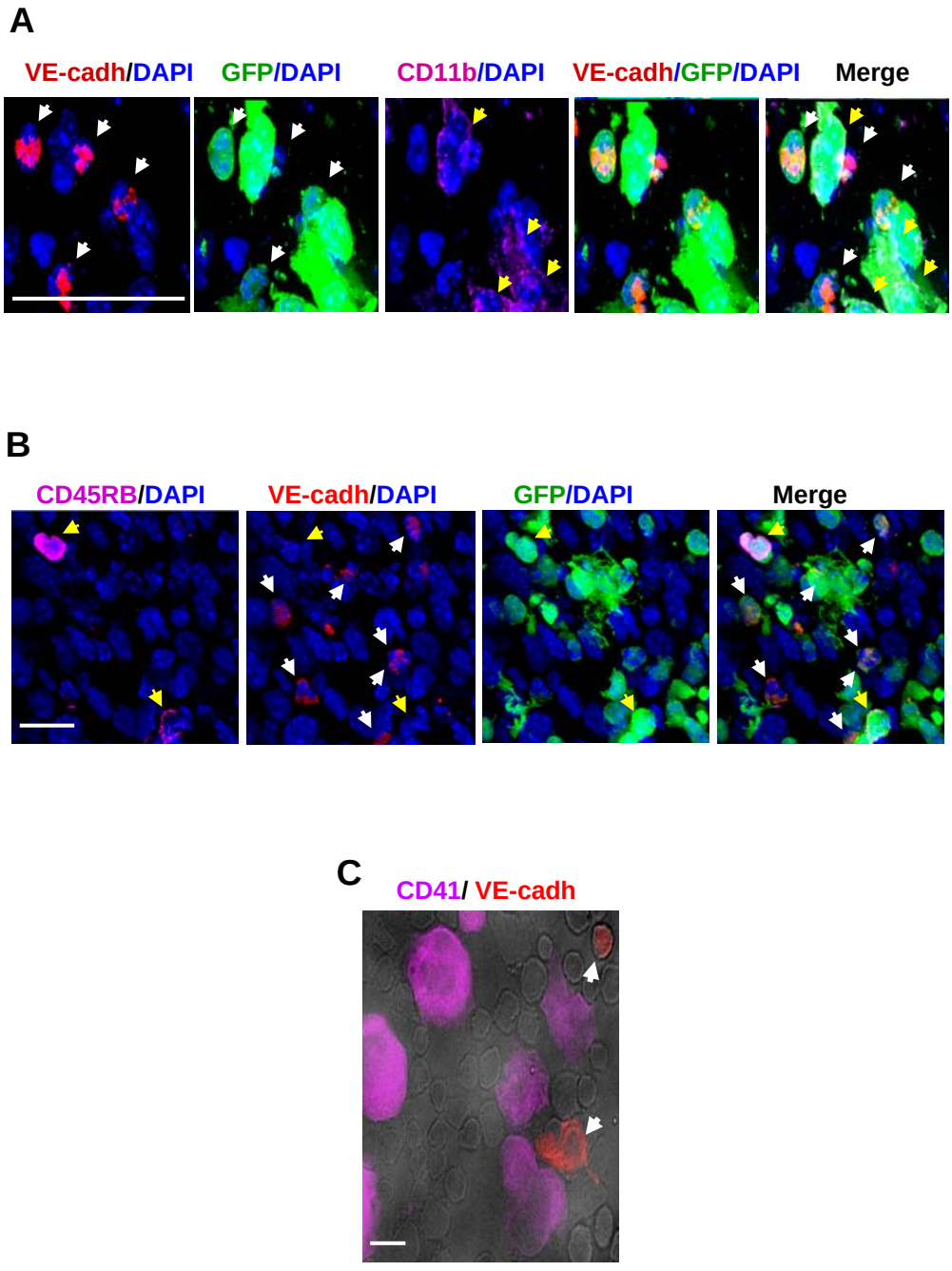
A
VE-cadh/DAPI
GFP/DAPI
CD11b/DAPI
VE-cadh/GFP/DAPI
Merge
B
CD45RB/DAPI
VE-cadh/DAPI
GFP/DAPI
Merge
C
CD41/ VE-cadh

Figure 6

BM-derived ECs are detected in early vasculature

Analysis of LLC tumors at days 6-8 after implantation showed a highly vascularized tumor compared to early stage tumors (day 4). Gross visual analysis of tumors at this time of harvest showed pink and red tumors, as opposed to the white tumors of day 4. Immunofluorescent analysis of tumors showed vessels of various sizes mainly concentrated at the tumor periphery (Figure 7A). At this stage, there is a profound infiltration of BM-derived GFP^+ hematopoietic cells. The majority of vessels appeared at the same location as the GFP^+ VE-$cadherin^+$ presumptive EPCs in earlier tumors.

To determine if GFP^+ cells were vessel incorporated ECs, high resolution microscopic analysis was performed. BM-derived cells exhibited hallmarks of a mature EC, such as spindle-like morphology, high surface CD31 expression, and characteristic VE-cadherin staining at the intercellular adherens junctions (Figure 7B). Compare this VE-cadherin staining at the intracellular junctions of the mature BM-derived cell to the ubiquitous VE-cadherin staining of the GFP^+ VE-$cadherin^+$ cells (Figures 2-6). Optical sectioning (Z-stack resolution of 0.275 μm, 30μm thick) further confirmed that the BM-derived EC had a single nucleus, and that the GFP and CD31 signals were localized to the same individual cell, indicating that the incorporated EC was derived from the BM. It is worth noting that under all circumstances, BM-derived ECs were found in chimeric vessels

Figure 7: BM-ECs contribute to early tumor vasculature

A: A representative fluorescent image showing $CD31^+$ mature vessels in LLC tumors (day 6-8, n=15). Arrows depict incorporated BM-derived ECs in these vessels. Scale bar, 200 μm. The dotted line separates the host tissue from the tumor. **B:** High resolution image of a representative blood vessel showing an incorporated mature BM-derived GFP^+ $CD31^+$ VE-$cadherin^+$ co-expressing cell (arrow). The lumen of the vessel (L) and VE-cadherin staining the adherens junctions between ECs are shown. Scale bar, 20 μm.

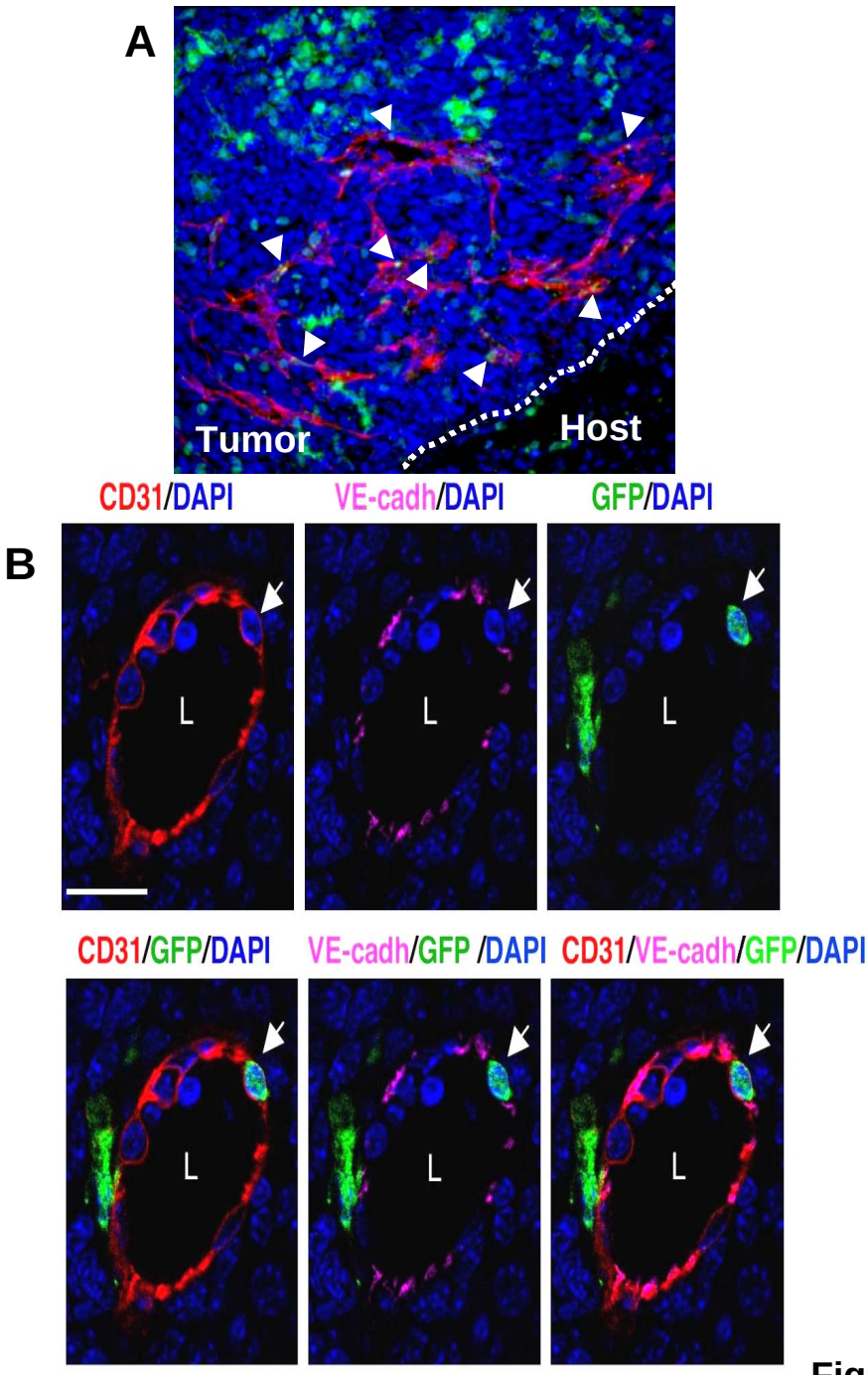
A
Tumor
Host
B
CD31/DAPI
VE-cadh/DAPI
GFP/DAPI
L
CD31/GFP/DAPI
VE-cadh/GFP /DAPI
CD31/VE-cadh/GFP/DAPI

Figure 7

with non-BM-derived ECs as opposed to vessels comprised exclusively of BM-derived ECs.

High resolution microscopy allowed the confirmation of bona fide BM-ECs (Figure 8A) and exclude false positives comprised of perivascular GFP^+ cells intimately associated with vessels (Figure 8B,C). A comparison of techniques for immunofluorescent detection shows that optical sectioning in 3D is capable of making these distinctions. Figure 8A depicts a BM-EC with a single nucleus, confirmed GFP signal within the $CD31^+$ cell membrane, VE-cadherin at the intracellular junctions, that is part of a vessel. The crosshairs denote a single point in the XY, XZ, and YZ planes. Figure 8B depicts a blood vessel imaged with and without optical sectioning. Optical sectioning is capable of filtering out the signal from above and below the plane of focus. The out-of-focus signal is capable of making one cell appear to have the fluorescent characteristics of the adjacent cells. However, under the examination of optical sectioning technology, it becomes clear that the GFP signal is originating from a cell adjacent to the endothelial cells (Figure 8B).

Additionally, bona fide BM-ECs must be analyzed in 3D. An individual cell may be in such a configuration adjacent to endothelial cells that it appears to be an endothelial cell itself, even with optical sectioning (Figure 8C). However, when viewed in the XZ and YZ planes, it again becomes apparent that the GFP

Figure 8: 3-D optical sectioning microscopy is required for accurate identification of BM-EC

A: Optical sectioning of a vessel containing a bona fide BM-derived endothelial cell showing GFP localized within a $CD31^+$ membrane with VE-cadherin staining intracellular junctions between Host-derived ECs. **B:** Comparison of traditional fluorescent microscopy (left) of a potential BM-derived endothelial cell with optical sectioning microscopy (right) of the same vessel revealing this as a false-positive event. **C**: Optical sectioning of a vessel that appears to have a BM-derived endothelial cell in the XY plane, however XZ and YZ planes reveal this false-positive GFP signal to be localized to a non-endothelial cell.

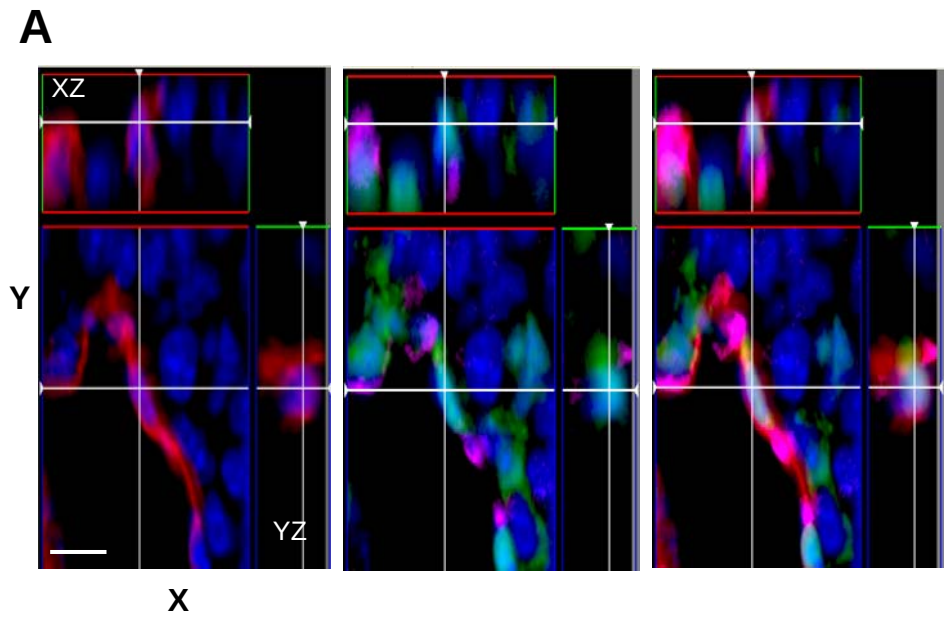

CD31/VE-Cadh/GFP/DAPI

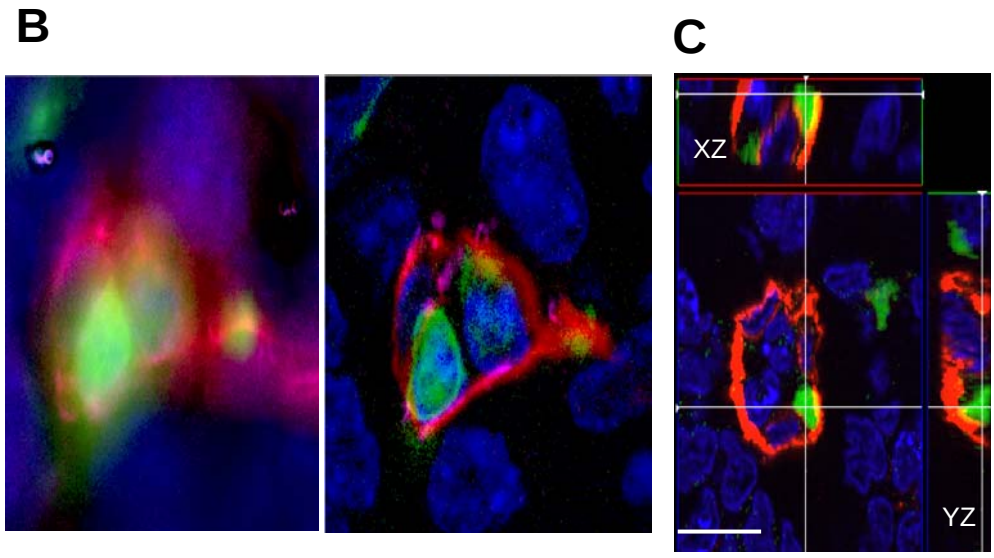

Figure 8

signal is coming from a cell with an intimate association with the thin endothelial cells. Therefore, only the most rigorous analysis of tumor endothelium via high resolution microscopy with optical sectioning microscopy and 3D analysis is able to confirm BM-EC contribution by excluding the possibility of perivascular associations. This scrutiny has been applied to all BM-ECs quantitated and characterized in this study.

Differentiation capacity of EPCs from BM and tumor

I have shown that EPCs are recruited to early tumors and BM-ECs are luminally incorporated into vessels shortly thereafter. However, these results do not establish a precursor product relationship. I therefore sought to isolate EPCs from both the bone marrow and from growing tumors and to demonstrate that GFP^+ VE-$cadherin^+$ cells had the capacity to differentiate into mature endothelial cells, contribute to vascular networks, and were truly EPCs. Due to the inconsistencies in *in vitro* differentiation that relied upon colony formation [103, 118, 119], I decided to use a differentiation assay that more closely resembled *in vivo* differentiation conditions by co-culturing the EPCs with mature endothelial cells.

First, I sorted GFP^+ EPCs (Lin^- VE-$cadherin^+$) from the bone marrow by flow cytometry (Figure 9A), and co-cultured them with spontaneously immortalized murine endothelial cells, mHEVc [144], in matrigel. Notably, mHEVcs in culture have lost CD31 and VE-cadherin expression, but have retained VCAM expression [144]. The extra-cellular matrix containing matrigel would allow for the formation of 3D structures which resemble vascular networks. By 12 hours, GFP^+ VE-$cadherin^+$ cells had not differentiated into endothelial cells and remained VCAM negative (Figure 9). The observation that the cellular input was lacking VCAM expression was in agreement with the notion that VCAM

becomes expressed as GFP^+ VE-$cadherin^+$ cells begin to differentiate (Figure 5). By day 2, GFP^+ BM-ECs that had incorporated into the growing vascular networks were detected (Figure 9C). These incorporated GFP^+ BM-derived ECs expressed VCAM and CD31 (data not shown). High resolution microscopy confirmed that the incorporated EC was indeed derived from the GFP^+ VE-$cadherin^+$ cells. I next determined whether there was continuity between the VE-$cadherin^+$ Lin- cells and the GFP^+ VE-$cadherin^+$ cells recruited to early tumors by testing whether they could also differentiate into endothelial cells and incorporate into neovessels. GFP^+ VE-$cadherin^+$ $CD11b^-$ cells were flow sorted from early tumors (day 4, Figure 9D). EPCs further identified as $CD31^{low}$ were co-cultured with mHEVcs in matrigel. By day 2, GFP^+ EPCs had differentiated into GFP^+ ECs and incorporated into the vascular networks (Figure 9E).

In contrast, GFP^+ $CD11b^+$ hematopoietic cells isolated from the same early tumors neither differentiated into endothelial cells (note the polymorphous shape and lack of VCAM) nor incorporated into vessels (Figure 9F). Collectively, these results demonstrate that GFP^+ VE-$cadherin^+$ cells, whether derived from the BM compartment or early tumors, are truly EPCs and contribute to the endothelial lineage.

Figure 9: EPCs derived from bone marrow and early tumor differentiate into ECs

A: Scatter plot showing VE-cadherin expressing EPCs in the BM-derived Lin- CD11b- fraction (green box). **B**: Immunostaining of co-cultured BM-derived GFP^+ EPCs and mature ECs (non-GFP) in 3D matrigel at 12 hours. A high resolution image showing an unincorporated, BM-derived GFP^+ $VCAM^-$ EPC (white arrow, right panels). **C**: Multiple BM-derived ECs (GFP^+ $VCAM^+$, yellow arrows) that have incorporated into vascular tubes 48 hours following co-culture. A high resolution image showing an incorporated BM-derived GFP+ EC (right panels, yellow arrow). **D**: Scatter plot showing GFP+ cells from day 4 LLC tumors. GFP^+ VE-$cadherin^+$ $CD11b^-$ EPCs (green box) and GFP^+ VE-$cadherin^-$ $CD11b^+$ hematopoietic cells (blue box) were live sorted. **E:** Immunostaining of co-cultured BM-derived GFP+ EPCs sorted in D and mature ECs (non-GFP) in 3D matrigel at 48 hours. High resolution microscopy showing an incorporated BM-derived GFP^+ $VCAM^+$ EC (yellow arrow). **F:** Immunostaining of co-cultured GFP^+ $CD11b^+$ hematopoietic cells sorted in D and mature ECs (non-GFP) in 3D matrigel at 48 hours. High resolution microscopy showing an unincorporated BM-derived GFP^+ $VCAM^-$ cell (white arrow). All scale bars are 10 μm. SSC-A denotes side scatter values.

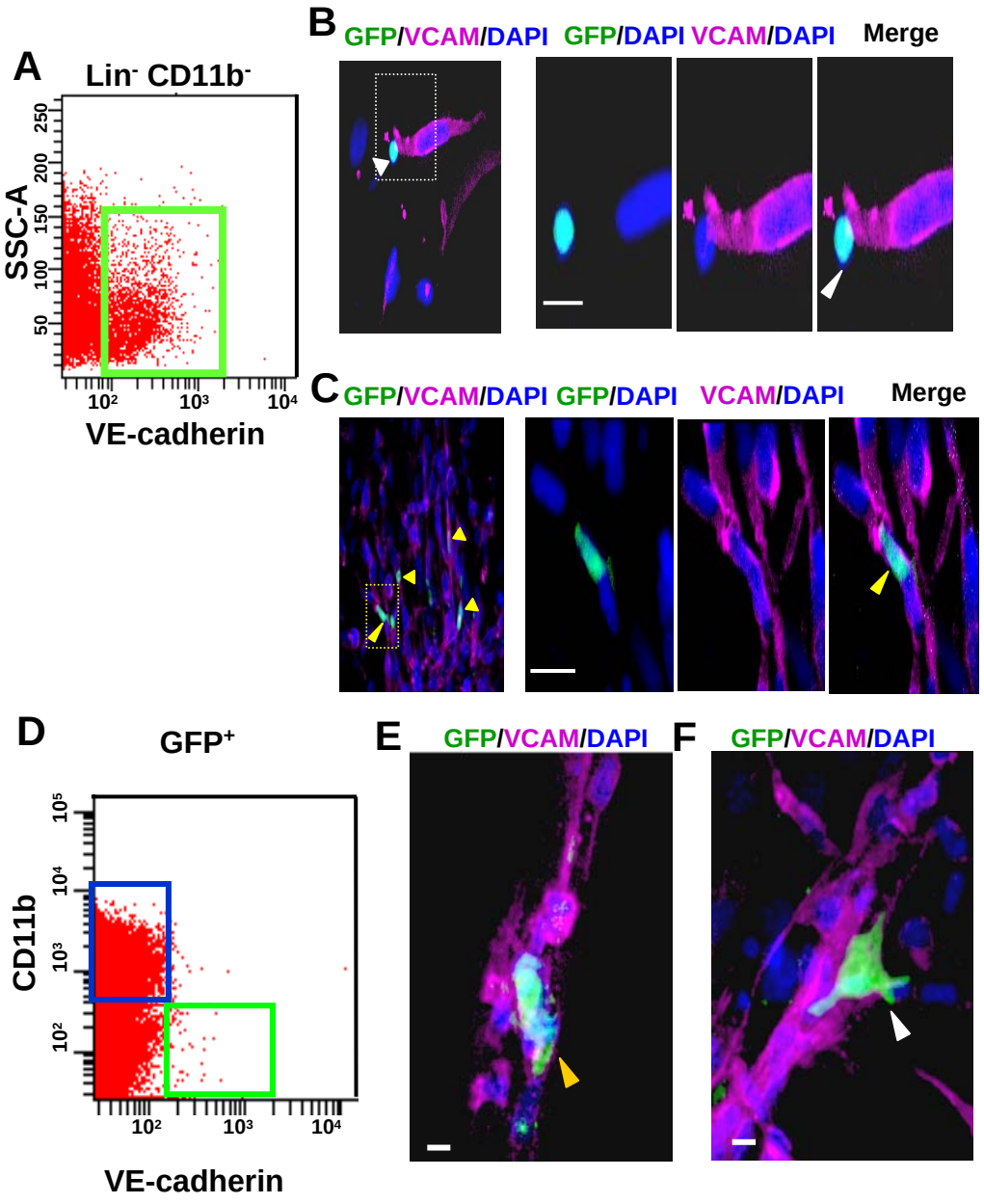
A
Lin- CD11b-
SSC-A
250
200
150
100
50
10²
10³
10⁴
VE-cadherin
B
GFP/VCAM/DAPI
GFP/DAPI
VCAM/DAPI
Merge
C
GFP/VCAM/DAPI
GFP/DAPI
VCAM/DAPI
Merge
D
GFP+
CD11b
10⁵
10⁴
10³
10²
10²
10³
10⁴
VE-cadherin
E
GFP/VCAM/DAPI
F
GFP/VCAM/DAPI

Figure 9

BM-derived EPCs and ECs contribute to multiple tumor models

To determine whether the contribution of BM-derived EPCs to vessel formation was a general phenomenon in tumors, additional tumor models were studied. The B16F0 melanoma cell line was derived from a spontaneous tumor and capable of *in vitro* expansion and implantation. Intradermal implantation of B16F0 cells is considered an orthotopic tumor model since injection is in the organ of origin [145]. Histological analysis of B16F0 melanomas revealed a similar pattern to that observed with LLCs with respect to vascular recruitment.

Analysis of early tumors, day 5, revealed a largely avascular tumor mass with the expected infiltration of BM-derived cells (Figure 10A), as shown with the LLC model. A small percentage of BM infiltration was composed of VE-cadherin^{+} EPCs (yellow arrows). As with the LLCs, the EPCs had entered the tumor prior to the recruitment of neovasculature. Note the only vessel in Figure 10A is at the tumor-host border. Day 8 tumors were also analyzed for the presence of BM-ECs. Indeed, BM-derived cells were found to contribute to the endothelium of melanomas (Figure 10B). Quantitation, performed by flow cytometry, confirmed the contribution of BM-ECs to melanoma endothelium at day 8 to be approximately 10% (Figure 10C).

In order to confirm that these events are also taking place in spontaneous tumors, a similar analysis was performed in breast tumors arising in MMTV-

PyMT transgenic mice [146]. In these animals the PyMT oncogene is expressed under the transcriptional control of the mouse mammary tumor virus promoter/enhancer specifically in the mammary epithelium [146]. The PyMT transgene activates pathways similar to that induced by ErbB2 [147], and importantly, this murine tumor model recapitulates human breast cancer progression from early nonmalignant hyperplasia (~ 6 weeks of age) and adenoma (8 to 9 weeks of age), to early and late malignant adenocarcinoma (8 to 12 weeks of age) [148]. This spontaneous tumor model is syngenic with the FVB/NJ inbred strain of mice. These mice are not syngenic with the C57Bl/6 GFP^+ donor used in previous experiments. Therefore, FVB/NJ GFP^+ transgenic mice, which also ubiquitously drive GFP expression under a CMV-enhanced b-actin promoter, were used as BM donors. The contribution of BM-derived EPCs and luminally incorporated endothelial cells to these mammary tumors were then studied. Early adenomas (~8 wk of age) were identified as closely packed multifocal acini surrounded by pre-existing host vessels. Adenomas at this stage had not yet recruited neovasculature from the preexisting vessels, and very few GFP^+ BM cells were observed infiltrating the adenoma mass (Figure. 11A). A subset of adenomas progressing into early carcinoma (9 weeks) were detected by their larger sizes and the lack of a clear border (compare Figures 11A to 11B).

Figure 10: BM contributes to melanoma endothelium

A: A representative fluorescent image showing recruitment of donor BM-derived GFP^+ VE-cadherin$^+$ EPCs (yellow arrows) at the periphery of early melanomas (day 5). Scale bar, 200 μm. **B:** High resolution images showing mature vessels in melanoma tumors (day 8). Arrow depicts an incorporated BM-derived ECs (GFP^+ $CD31^+$Isoectin$^+$) in these vessels. Scale bar, 20 μm. **C:** The percentage of BM contribution to melanoma endothelium was quantitated as the fraction of $CD31^+$ Isolectin$^+$ $CD11b^-$ cells which were also GFP^+ in day 8 tumors. Error bars represent standard deviation.

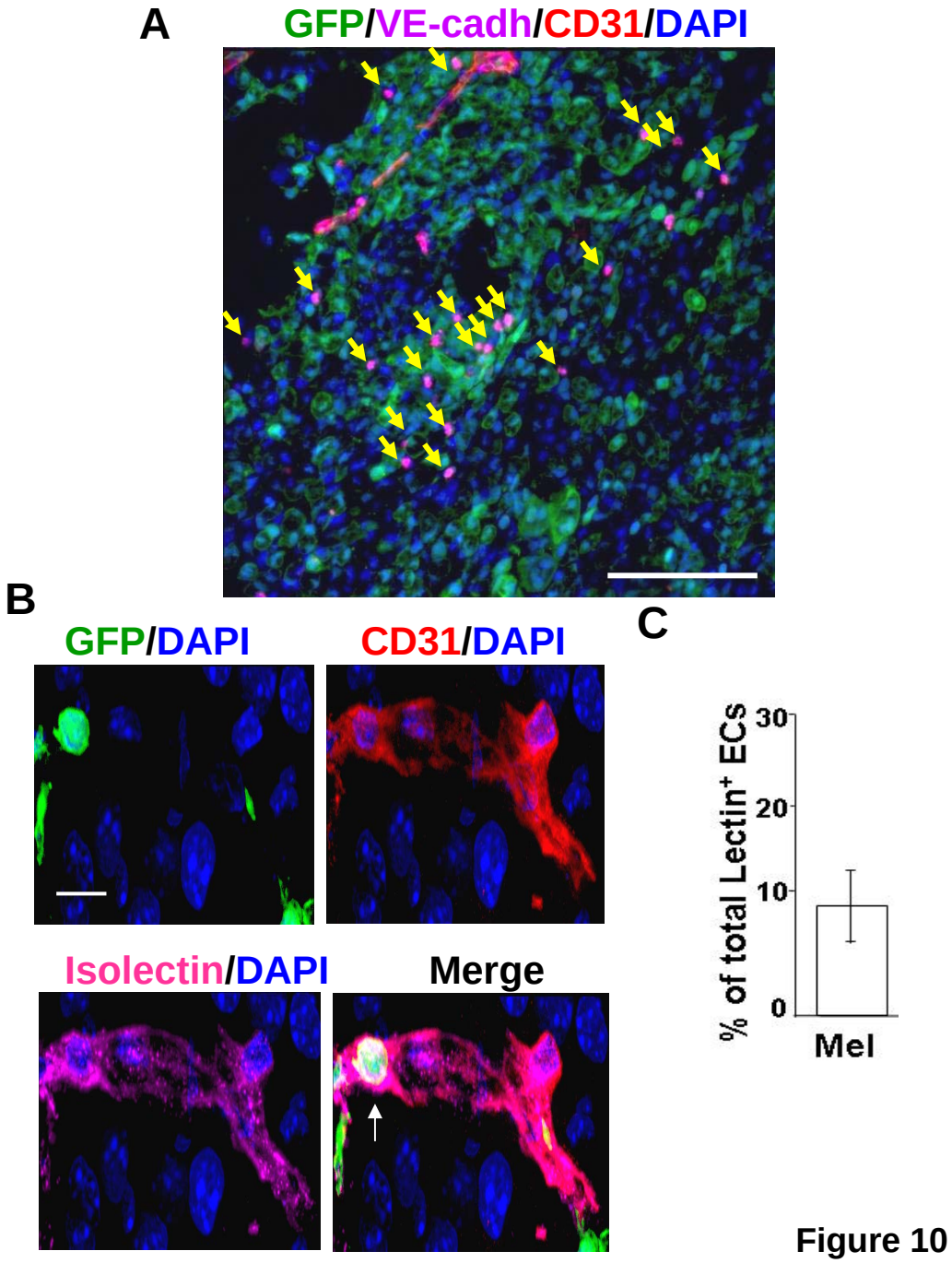
A
GFP/VE-cadh/CD31/DAPI
B
GFP/DAPI
CD31/DAPI
Isolectin/DAPI
Merge
C
% of total Lectin+ ECs
30
20
10
0
Mel

Figure 10

Figure 11: EPC recruitment to MMTV PyMT spontaneous breast tumor model

A: Primary adenoma lesions in mammary gland sections from a PyMT mouse at 8 weeks of age. Pre-existing $CD31^+$ vessels are observed surrounding the adenomas. Scale bar, 100 μm. **B:** Recruitment of BM-derived GFP^+ VE-$cadherin^+$ EPCs (arrows) at the periphery of the avascular adenoma-carcinoma progression is shown (9 weeks). Scale bar, 100 μm.

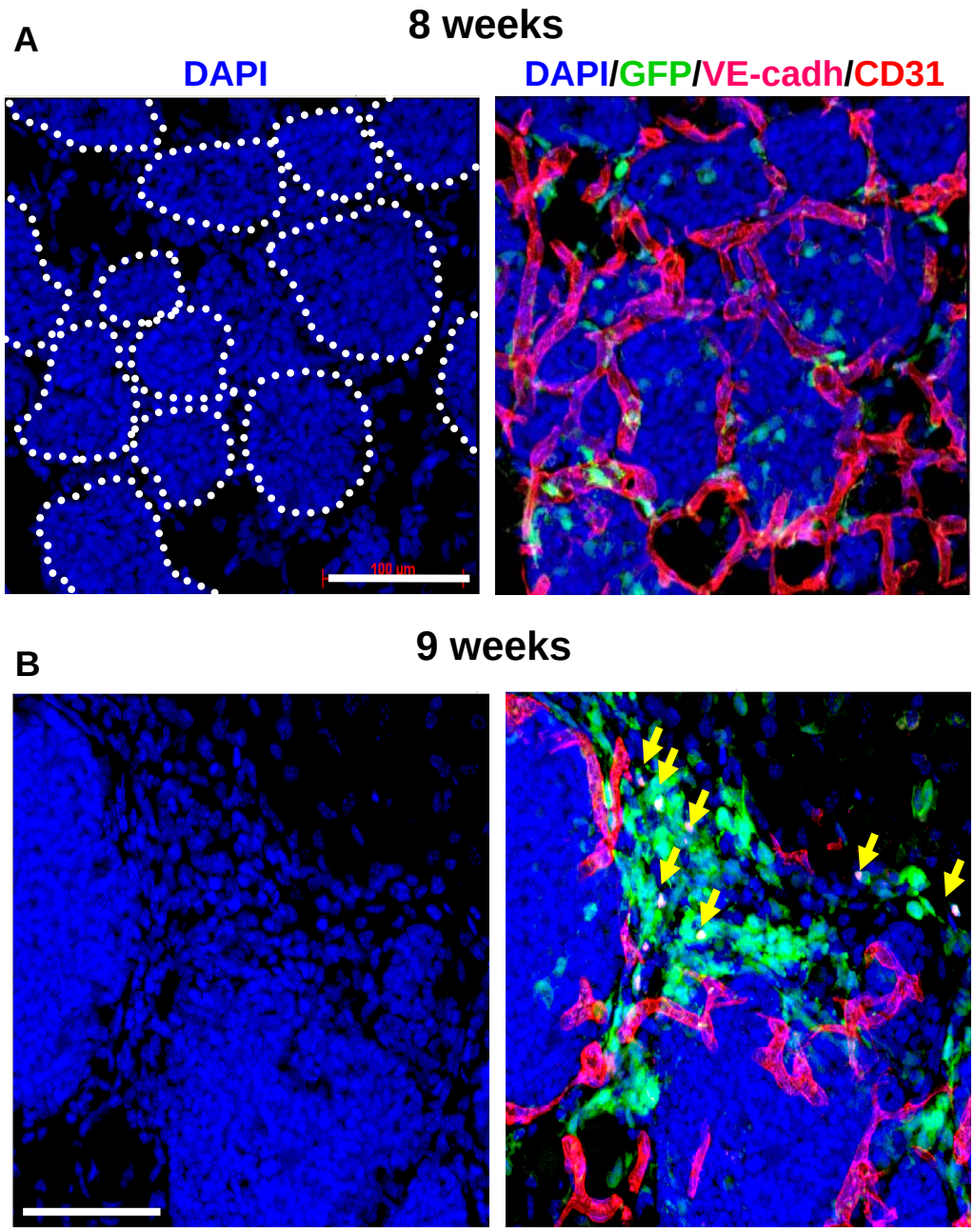

Figure 11

These progressing tumors showed foci of BM-derived GFP^+ cells including VE-cadherin$^+$ EPCs (Figure 11B, arrows). Such foci of BM-derived cell infiltration have been previously observed in adenomas [148]. Analysis of early carcinomas (10 weeks of age) showed high density of BM infiltration and increased vessel density. These vascular tumors were characterized by the presence of $CD31^+$ neovessels of various sizes (Figure 12A). Closer inspection of these sprouting nascent vessels showed there were incorporated BM-derived GFP^+ $CD31^+$ ECs (Figure 12B). In this model, quantitation of luminally incorporated BM-derived ECs by flow cytometry was technically challenging for two reasons. Due to the closely packed, multifocal nature of breast tumor development, different stages of tumor development could not be isolated to homogeneity. The mammary fat pad is very well vascularized prior to the formation of tumors (Figure 11A). This makes discerning pre-existing vasculature from nascent tumor vasculature impossible by flow cytometry. Defining the boarders of each individual tumor and manual scoring was not an ideal option as the growth of one tumor would undoubtedly have an effect on neighboring tumor foci; however, the nature of spontaneous tumor model made manual microscopic quantitation the most logical. I therefore performed vessel counts by microscopy of mammary fat pads from 10 week old animals, dominated

Figure 12: BM-ECs in MMTV PyMT early breast carcinoma

A: An early carcinoma showing recruited $CD31^+$ mature vessels in the tumor mass (10 weeks of age). Arrow depicts incorporated BM-derived ECs in a vessel. Scale bar, 100 mm. **B:** High resolution image of a representative blood vessel (box in A) showing an incorporated mature BM-derived GFP^+ $CD31^+$ co-expressing cell (arrow). Scale bar, 20 mm. DAPI was used to stain the nucleus of all cells

10weeks

A

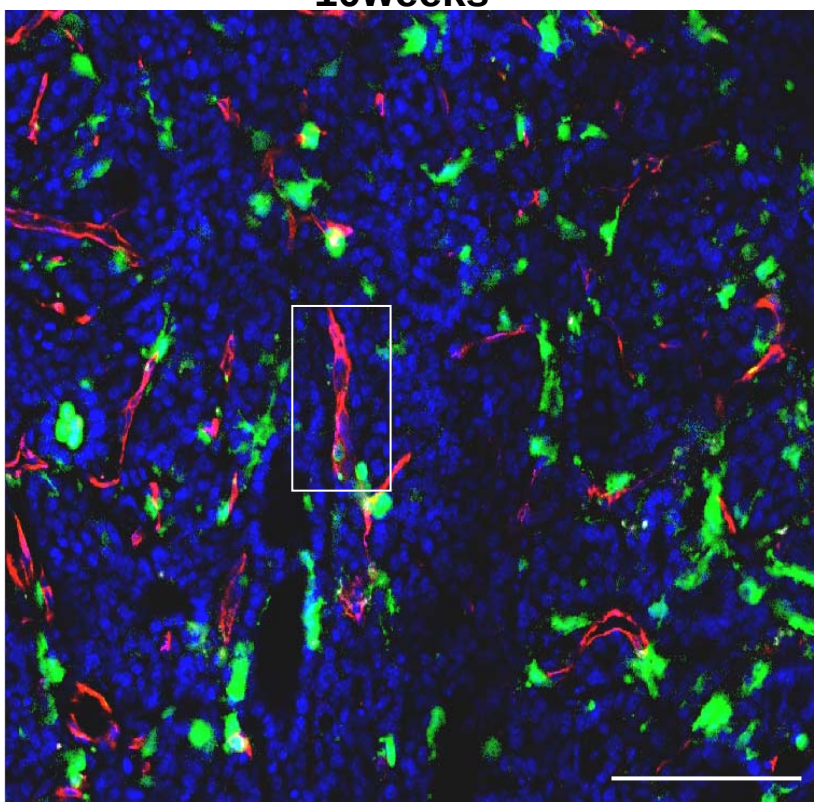

B

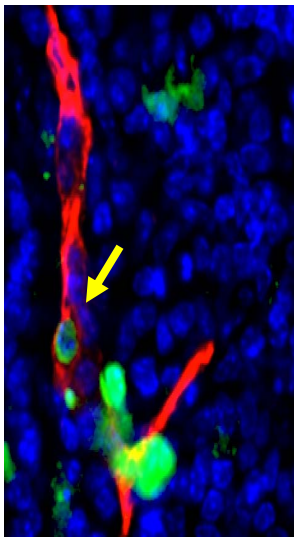

Figure 12

by early carcinomas which showed that approximately 5-10% of host vessels had incorporated BM-derived GFP^+endothelial cells (GFP^+ VE-$cadherin^+$ $CD31^+$). Older animals bore fat pads that were far too varied in stage to make reliable counts.

The observation that BM-derived EPCs precede host-ECs, and that BM-ECs contribute to neovascularization in early stages of melanomas, spontaneous breast tumors, and B6RV2 lymphomas (data not shown) was consistent with that observed in LLC tumors, highlighting the general relevance of these cells in tumor neovascularization.

BM contribution to endothelium peaks in early tumors

The observation that BM-derived EPC precede the angiogenic switch suggested a possibility that EPC contribution may be an early event during tumor growth. This also suggests that in other studies, analysis of later tumors may have confounded the detection of EPCs and BM-ECs. I therefore determined the EPC contribution as a function of tumor growth. BMT animals (n=20) were challenged with LLC tumors and analyzed at day 4 (early tumors prior to angiogenic switch), days 6-10 (mid-staged tumors shortly after angiogenic switch), days 14-28 (large and highly progressed tumors).

Flow cytometric analysis was performed to determine the relative numbers of BM-derived EPCs (GFP^+ VE-$cadherin^+$ $CD31^{low}$ $CD11b^-$) and non-BM-derived ECs (GFP^- VE-$cadherin^+$ $CD31^{high}$ $CD11b^-$) at different stages of tumor growth (Figure 13A). BM-derived EPCs comprised of 25%–35% of the total ECs in the early phases of tumor growth (days 4–6), and this contribution decreased by approximately fourfold in late tumors (day 14), consistent with histological analysis (Figure 13B). Notably, in late tumors there was an enhanced recruitment of local non-BM-derived GFP^- ECs (65%–75%, days 10–14), which diluted the observed contribution of BM-derived EPCs. As these host-ECs became rapidly more abundant, the relative contribution of EPCs to the pool of endothelial cells became less significant. I next quantified luminally incorporated BM-derived

Figure 13: Bone marrow contribution peaks in early tumors
A: Flow cytometry analysis of LLC tumors (day 4 -14; n= 5 per group), showing relative contribution of BM-derived EPCs (GFP^+ VE-$cadherin^+$ $CD31^{low}$ $CD11b^-$), and host-derived ECs (GFP^- VE-$cadherin^+$ $CD31^+CD11b^-$). Total number of cells analyzed were $2x10^5$ per animal. Each analysis was performed in duplicate, and the numbers denote averages obtained from different samples. Error bars represent standard deviations. This analysis was repeated and identical trends were observed. **B:** Quantitation of EPCs in LLC tumors (days 4-28) via microscopy. 6 non sequential sections and 20 images per tumor were analyzed, z-stacks evaluated for each section. **C:** Quantification of vessels in LLC tumors (day 4- 28) with incorporated BM-derived ECs (GFP^+CD31^+VE-$cadherin^+$), a minimum of 400 vessels counted per time point from 6 non sequential sections and 20 images per tumor, z-stacks evaluated for each section. Error bars represent standard deviations.

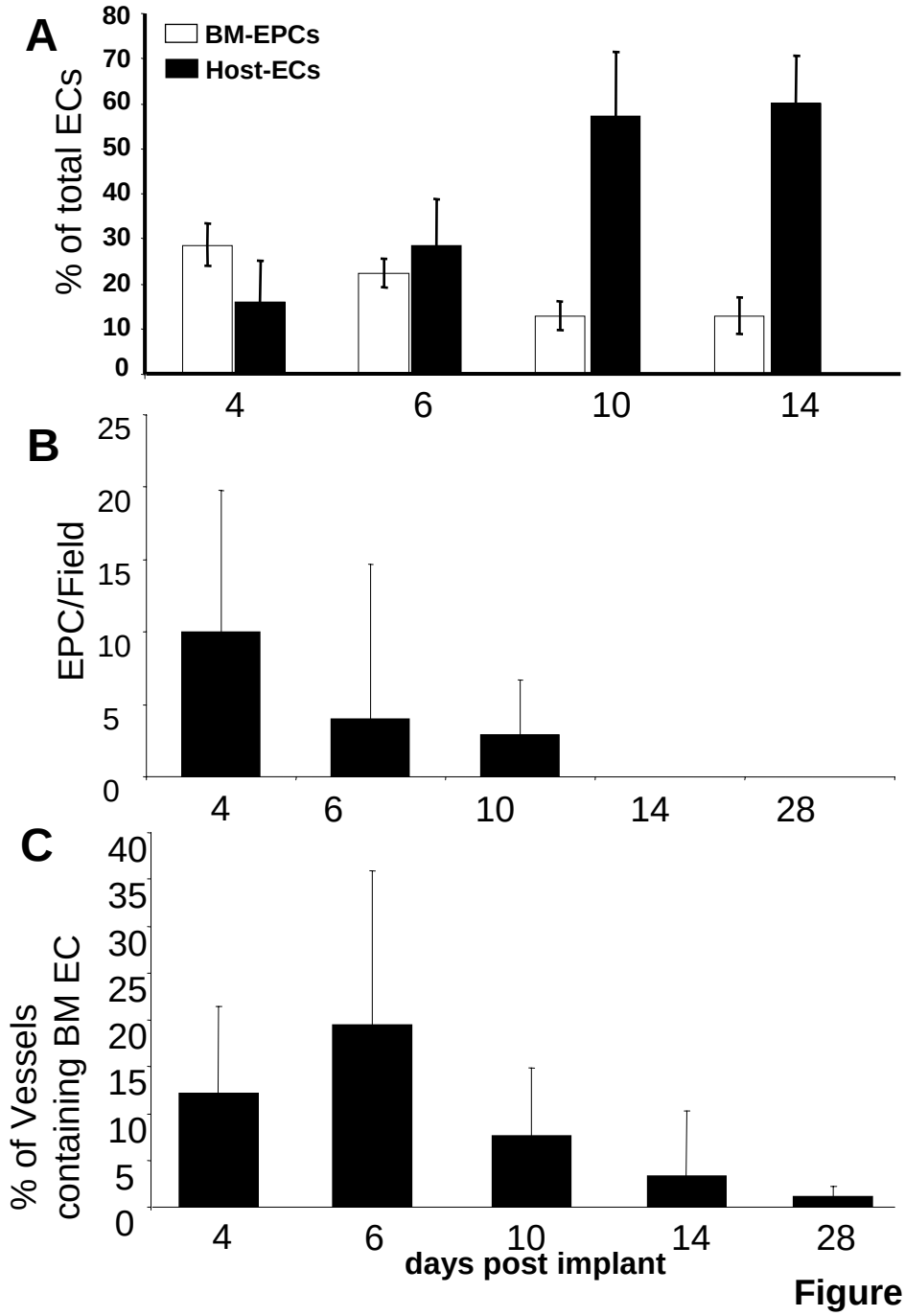
A
BM-EPCs
Host-ECs
% of total ECs
80
70
60
50
40
30
20
10
0
4
6
10
14
B
EPC/Field
25
20
15
10
5
0
4
6
10
14
28
C
% of Vessels containing BM EC
40
35
30
25
20
15
10
5
0
4
6
10
14
28
days post implant

Figure 13

ECs in tumor vessels. Vessel counts from optically sectioned tumors showed that ~20% of vessels had incorporated BM-derived ECs (GFP^+ $VE^-cadherin^+$ $CD31^+$) at day 6 (Figure 13C), and these chimeric vessels markedly decreased with time (<1% remaining after 4 wk).

The peak of EPC contribution was followed by a peak in BM-EC contribution. All BM-ECs counted were scrutinized as described earlier with optical sectioning technology and in 3D. Day 6 tumors possessed approximately 25% BM-derived vessels, which was the peak of BM contribution to the endothelium. This contribution quickly tapered off as the large infiltration of host endothelial cells diluted the BM-ECs. By day 28 tumors, less than 1% of vessels contained a BM-EC.

I next sought to discern if the kinetics of BM contribution to the endothelium was specific to the LLC tumor model, or if it was a general phenomenon across varying tumor models. B16F0 melanomas were subjected to a similar flow cytometric analysis. The B16F0 orthotopic model had a longer latency between implantation and growth, as compared to LLCs, but grew rapidly thereafter. For this reason, tumors at days 5, 8, and 14 were studied. EPCs were again seen to have a decreasing contribution to the tumor endothelium (Figure 14A). Host ECs were again seen to have a small contribution in early tumors, in agreement with

immunofluorescent analysis, followed by a large influx of host ECs (Figure 14A). Analysis reveled that EPCs have a higher representation in early tumors that decreased approximately 3 fold in later tumors, a pattern also

observed with LLC tumors. Quantitation of BM-EC contribution to the endothelium by flow cytometry ($CD31^{high}$ $Isolectin^{+}$ GFP^{+} $CD11b^{-}$) showed an approximate two fold decrease from day 5 to day 14 tumors (Figure 14B). The comparable patterns of EPC and BM-EC kinetics in these two distinct tumor models is contrasted by 5-7 fold less endothelium present in B16F0 tumors compared to LLC tumors (Figure 14C) suggesting that tumors may have a similar reliance on EPCs, despite differing angiogenic properties.

Figure14: BM contribution to B16F0 melanoma

A: Flow cytometric analysis of B16F0 tumors (day 5 -14; n= 5-7 per group), showing relative contribution of BM-derived EPCs (GFP^+ VE-$cadherin^+$ $CD31^{low}$, $CD11b^-$), and host-derived ECs (GFP^- VE-$cadherin^+$ $CD31^+$, $Isolectin^+$, $CD11b^-$). Total number of cells analyzed were $2x10^5$ per animal. **B:** The abundance of BM-ECs (GFP^+ VE-$cadherin^+$ $CD31^{low}$, $Isolectin^+$ $CD11b^-$) was quantitated also by flow cytometry. Error bars represent standard deviations. **C:** Endothelial cells were quantitated by flow cytometry day 14 LLC and B16F0 tumors. Error bars represent standard deviation.

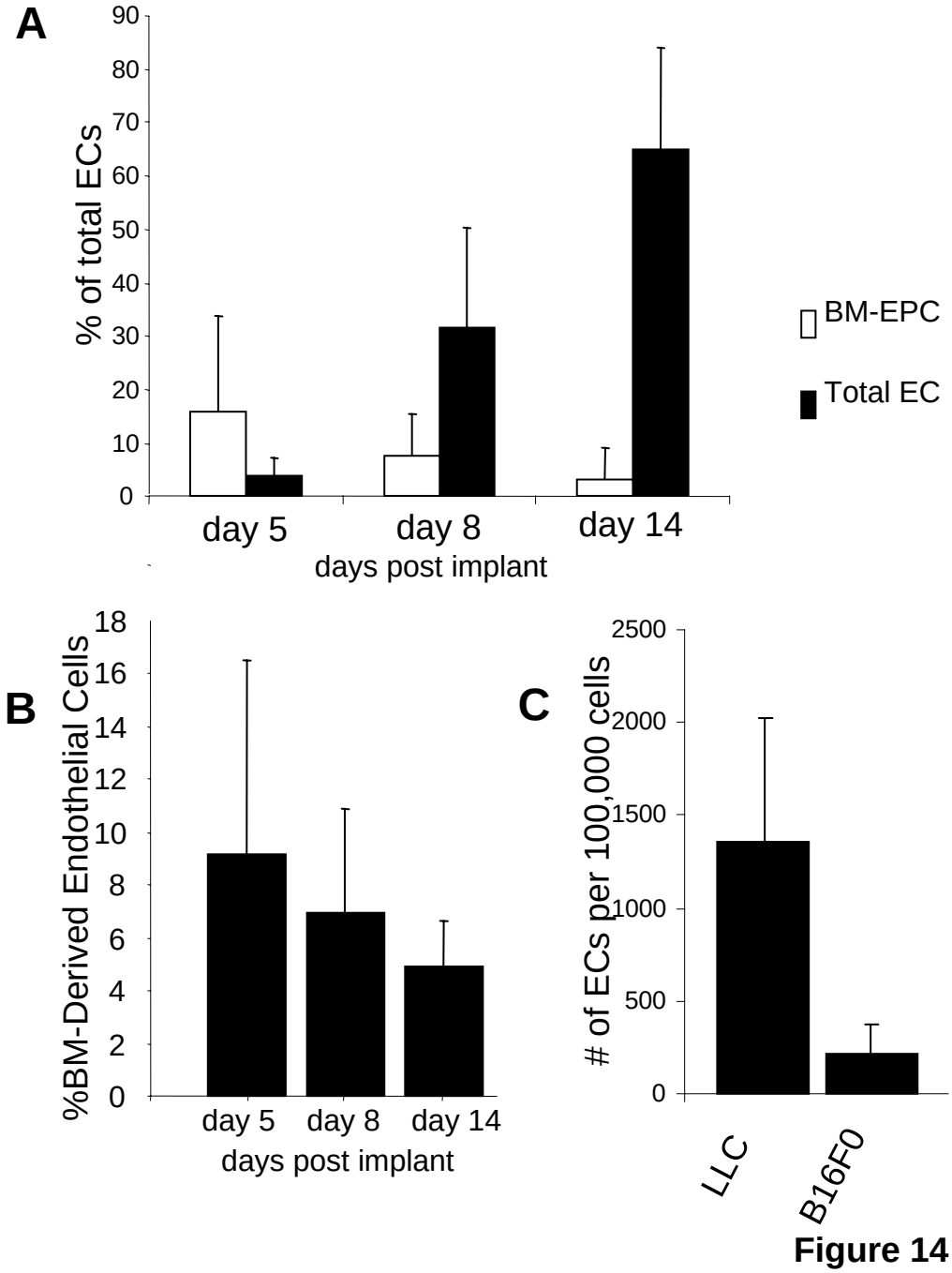
A
90
80
70
60
50
40
30
20
10
0
% of total ECs
BM-EPC
Total EC
day 5
day 8
day 14
days post implant
B
18
16
14
12
10
8
6
4
2
0
%BM-Derived Endothelial Cells
day 5
day 8
day 14
days post implant
C
2500
2000
1500
1000
500
0
# of ECs per 100,000 cells
LLC
B16F0

Figure 14

Quantitation of functional endothelium

As an approach to determine luminally incorporated BM-derived ECs in tumor vessels, I sough to use flow cytometric analysis. Flow cytometry has several major advantages in BM-EC detection. First, flow cytometry can screen several thousand endothelial cells from multiple animals in the same time it would take to acquire a single 3D, optically sectioned 1600μm^2 section of tumor. Flow cytometry also is devoid of bias once the control samples have established the parameters for accurate gating of GFP to distinguish BM-derived cells from Host-derived cells. Most importantly, the analysis of single cell suspensions is not confounded by any GFP signal from neighboring cells. Unfortunately, flow cytometry does have one major disadvantage; it gives no structural information, whereas microscopic analysis clearly demonstrates vessel integration.

The injection of a fluorescent dye into the blood stream of a living mouse to visualize the vasculature has been previously performed [149]. Therefore, flow cytometric identification of an endothelial cell as part of a functioning blood vessel is possible by using a fluorescent marker to determine if it was in contact with blood-flow. Various lectins and agglutinins have been used for their binding affinity to endothelium. Isolectin GS-IB_4, isolated from the seeds of the African legume *Griffonia simplicifolia* has been used in both immunofluorescent and flow cytometric analysis of endothelial cells in various species [150]. Isolectin was

capable of brightly and specifically binding to the tumor endothelium, as visualized in Figure 15A. Importantly, isolectin was not a ubiquitous marker of the endothelium within the tumor; it was only capable of binding vessels with active blood flow. A contrasting approach would have been to use a dye that lacked specificity to mark contact with blood flow. The choleratoxin β-subunit binds to galactosyl moieties, which are markers of lipid rafts [151]. In contrast, choleratoxin readily stained large portions of the tumor that were not vasculature (Figure 15B, white arrows). The dye leaked through leaky tumor vasculature or on intravassated hematopoietic cells. 50μg of isolectin GS-IB_4 was therefore used to mark the functional endothelium of tumors. This is evidenced by the lack of isolectin staining in some of the tumor blood vessels (yellow arrow).

Animals with an early vascularized tumor (day 8) were injected with fluorescent isolectin via tail vein prior to sacrifice. Animals were then subjected to cardiac perfusion with PBS, as usual. This perfusion would clear any unbound isolectin in the vasculature. Tumors were prepared in a single-cell suspension for flow cytometric staining with antibodies to CD31 and CD11b. Endothelial cells were gated based on their expression of CD31 and lack of CD11b (Figure 16A, blue box). As this population may still contain hematopoietic cells expressing CD31 [102], only cells bound to isolectin were further analyzed (red box). Their expression of CD31 and their ability to bind the isolectin dye confirmed their

endothelial identity. Of these endothelial cells, 16.5% were found to be BM-derived ($CD31^{high}$ $Isolectin^{+}$ GFP^{+} $CD11b^{-}$). Microscopic analysis of isolectin injected tumors confirmed that isolectin was capable of specifically binding to the luminal surface of host and BM-derived endothelial cells (Figure 16B).

Figure 15: Isolectin GS IB_4 specifically stains functional tumor vasculature

Representative image showing that the Isolectin staining was tightly confined to the endothelial cells comprising the nascent vasculature (tumors, day 6) as compared to Choleratoxin b subunit. Tumor vasculature in animals perfused with **A:** Isolectin GS-IB_4 (Alexa Fluor 647) and stained with CD31 (Alexa Fluor 568). Yellow arrows highlight a non-functioning vessel. **B**: Choleratoxin (Alexa Fluor 647) and stained with CD31 (Alexa Fluor 568). White arrows indicate leakage of choleratoxin into the tumor mass. Scale bars, 50 μm.

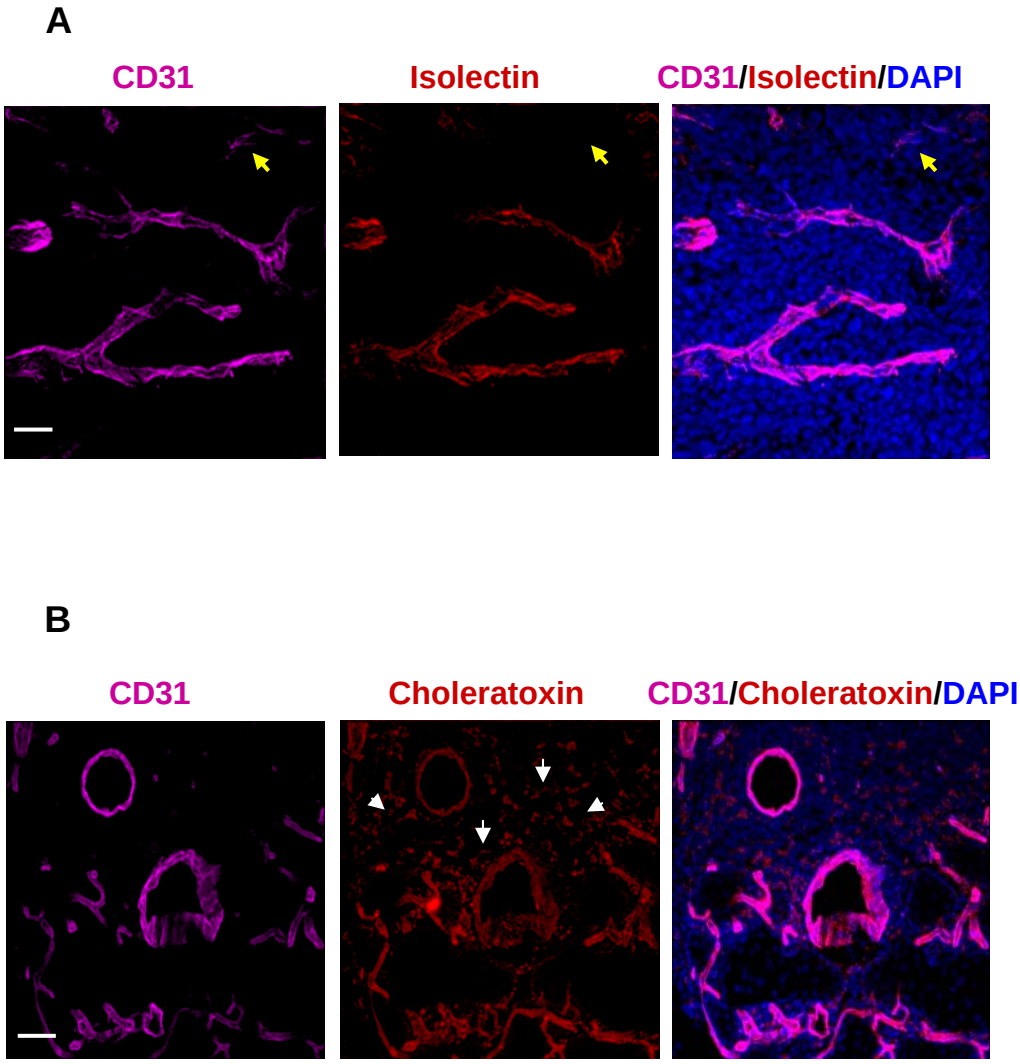
A
CD31
Isolectin
CD31/Isolectin/DAPI
B
CD31
Choleratoxin
CD31/Choleratoxin/DAPI

Figure 15

Figure 16: Quantitation of functional bone marrow-derived endothelium

A: Flow cytometric analysis of early tumors (LLC, day 8) perfused with isolectin. Endothelial cells were selected for their high expression of CD31 and lack of CD11b (left panel). Endothelial cells were considered functional if they were also positive for isolectin GS IB4 (middle panel). The detection of GFP in 16% of the functional endothelium confirms the bone marrow derivation of a subset of tumor endothelium (right panel). **B:** High resolution microscopic analysis of a BM-EC displays isolectin preferentially bound to the luminal surface of the vessel. L, lumen. Scale bar, 10μm.

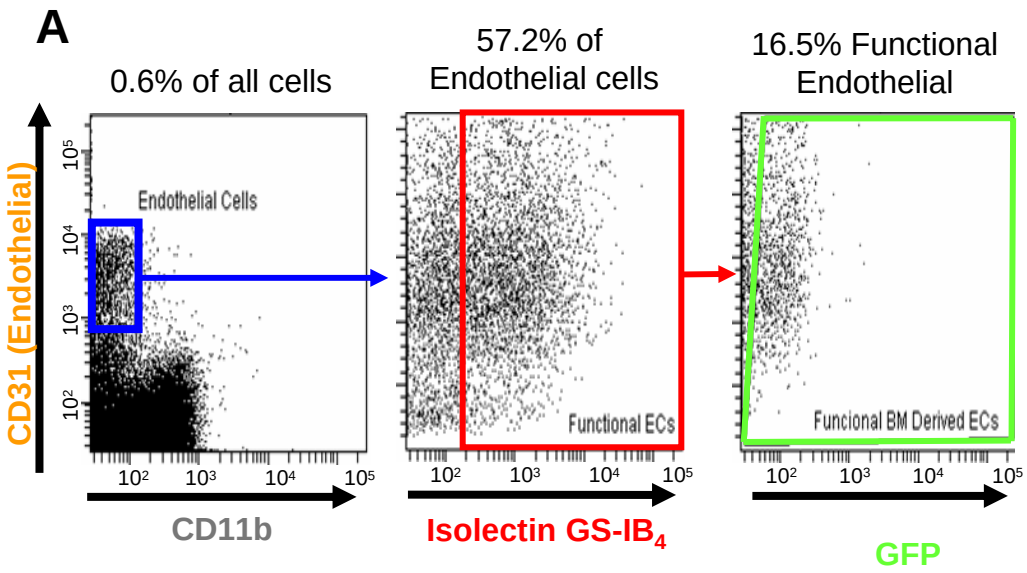
A
0.6% of all cells
57.2% of Endothelial cells
16.5% Functional Endothelial
CD31 (Endothelial)
Endothelial Cells
Functional ECs
Funcional BM Derived ECs
CD11b
Isolectin GS-IB4
GFP

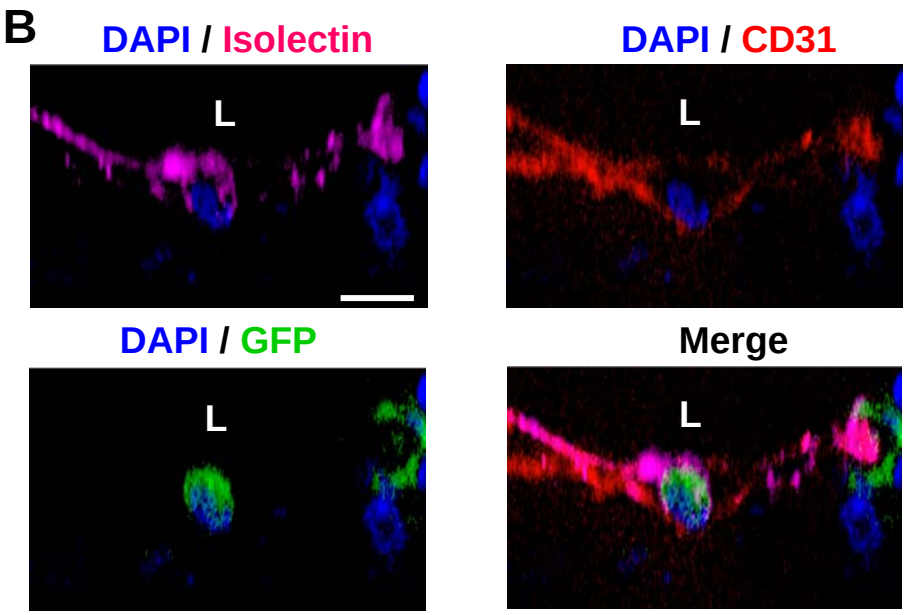
B
DAPI / Isolectin
DAPI / CD31
DAPI / GFP
Merge
L

Figure 16

Chapter 2 Discussion

This study has provided evidence that BM-derived EPCs, as defined by the cell surface expression of VE-cadherin, VEGFR2, $CD31^{low}$, Endoglin and Prominin I /AC133, differentiate into mature endothelial cells and contribute structurally to tumor angiogenesis. Further analysis demonstrated that the EPCs are distinct from other hematopoietic and pro-angiogenic BM-derived cell types such as Tie2-expressing monocytes [23], macrophages [34], recruited BM-derived circulating cells [37], pericyte progenitors [30], infiltrating neutrophils [36]. and vascular leukocytes [152]. These distinctions are based on specific presentation of cell surface receptors and the fact that BM-ECs are incorporated into the vasculature as opposed to a perivascular role.

Analysis of multiple tumor types showed that EPCs differentiate into mature ECs and luminally incorporate into neovessels, clearly demonstrating the derivation of tumor vasculature from transplanted BM cells. The specific recruitment of EPCs to both spontaneous and transplanted tumors highlights the general relevance of these cells in tumor angiogenesis. The three tumor models (LLC, B16F0, breast) each presented a unique vascular profile; however, all these models retained the similar pattern of EPC recruitment prior to neovascularization. These observations suggest that an anti-EPC therapeutic approach may be promising in targeting a variety of tumors.

A systematic kinetic analysis showed that EPCs are recruited to the tumor periphery preceding vessel formation, and are luminally incorporated into a subset of sprouting neovessels in early tumors. Noticeably, these chimeric BM-derived vessels were eventually diluted with host-derived vessels, thereby explaining the low contribution observed by other investigators in large, established tumors [23, 24, 38, 41, 100, 153]. Possibly, de Palma and colleagues were unable to detect BM-derived tumor endothelial cells not only due to the analysis of late tumors (4 weeks), but also because the Tie2 promoter in their study does not mark all the $Tie2^+$ mature endothelial cells or bona fide EPCs. In their study, the reporter GFP gene was not driven by the endogenous Tie2 promoter. Instead, the Tie2 promoter driving the GFP gene was introduced by a lentiviral construct into murine embryonic stem cells. Therefore, it is possible that random integration of lentiviral vectors may have failed to identify the true repopulating EPCs. Additionally, it is possible that that alternative promoter elements contribute to the transcription of Tie2 between host-ECs and BM-ECs. In a similar study, using an endothelial-specific (SCL) inducible Cre recombinase to activate a stop-floxed β-galactosidase gene, Gothert et al. argue the lack of BM–precursor contribution to the tumor endothelium. The SCL promoter does not mark the progenitors in the BM, but was used to identify BM-derived cells that mature in the periphery. Regardless of the promoter here, the lack of $LacZ^+$ peripheral

vessels observed at 14 days post-implantation is in agreement with our data that BM-derived chimeric vessels are diluted by mature peripheral vessels in later tumors.

Evidence for the contribution of EPCs to ischemic revascularization resulting from severe vascular injury has been reported both in humans and mice. For example, Minami and colleagues have shown that circulating endothelial cells engraft luminally into 15 to 29% of the vessels of the transplanted heart in patients with sex mismatched heart transplants [154]. These data suggest that during acute vascular injury, the demand for neoangiogenesis increases to a point where there is a profound contribution of circulating host-derived endothelial cells to neoangiogenesis. Similarly, during the angiogenic switch, as it may occur in the early phases of tumor growth, the rapid demand for neo-angiogenesis may facilitate the recruitment of BM-derived EPCs, as observed in our investigation. The presence of EPCs in tumors, prior to recruitment of host vasculature, raises the possibility that the BM-derived EPCs play a critical role in initiating the recruitment of non-BM derived vessels to the tumors. At this stage, EPC differentiation and luminal incorporation of BM-derived EC may be necessary for providing structural support and guidance to these nascent vessels.

CHAPTER 3: Targeting EPCs as an anti-angiogenic therapy

The monoclonal antibody E4G10 specifically recognizes VE-cadherin on EPCs

To determine if the BM-derived EPCs had a functional role in angiogenesis-mediated tumor growth, EPCs were selectively ablated. The monoclonal antibody E4G10 specifically recognizes the exposed monomeric epitope on the immediate N-terminus of VE-cadherin, which becomes masked upon trans-dimerization in mature endothelial cells in vessels (Figure 17A) [155]. Bulk injections of the antibody had previously shown that E4G10 was capable of decreasing tumor volume [156] at early time points [96]. However, there was no convincing data presented that E4G10 was capable of targeting mature vasculature. I hypothesized that the VE-cadherin would only be exposed as a monomer on EPCs due to their lack of contact with mature endothelial cells, as depicted in Figure 17B, and was therefore the true target of E4G10.

I next determined whether E4G10 recognizes the monomeric VE-cadherin on EPCs, but not the dimerized form present on vessel incorporated endothelial cells (Figure 18). Indeed five color immunofluorescent imaging was required to determine EPC specificity with respect to BM-origin (GFP, color 1), blood vessels by CD31 (Alexa Fluor 750, color 2), the detection of all VE-cadherin on blood vessels and EPCs by a pan-VE-cadherin antibody clone 11D4.1 (Alexa

Fluor 568, color 3), VE-cadherin in monomeric form by E4G10 (Alexa Fluor 647, color 4), and the ability to distinguish one cell from another (DAPI, color 5).

I confirmed that E4G10 recognizes VE-cadherin on the EPCs, but not in mature endothelial cells comprising the nascent early tumor neovessels (Figure 18 white arrows), compared to the pan VE-cadherin antibody 11D4.1 (VE-cadh^{pan}) that recognized both the monomeric VE-cadherin on EPCs and homodimerized VE-cadherin on endothelial cells in vessels (red arrows). Indeed, no vessels within any region of the tumor could be found with E4G10 staining at cell-cell junctions. In addition, the N-terminal VE-cadherin epitope was exposed in neither the luminally incorporated BM-derived GFP^{+} endothelial cells (data not shown), nor the endothelial cell projections of sprouting nascent vessels in early tumors (Figure 19). It was therefore concluded that E4G10 could be used to specifically target EPCs but not normal physiological or tumor vasculature.

Figure 17: E4G10 antibody targets monomeric VE-cadherin on EPCs

A: Structural homology model of VE-cadherin based on the crystal structure of C-Cadherin, adapted from May *et al* 2005 [130]. Monomeric and homodimeric forms display how the E4G10 epitope (red) is masked upon dimerization. **B:** Model of the presentation of VE-cadherin on the surfaces of EPCs and mature vessels.

A

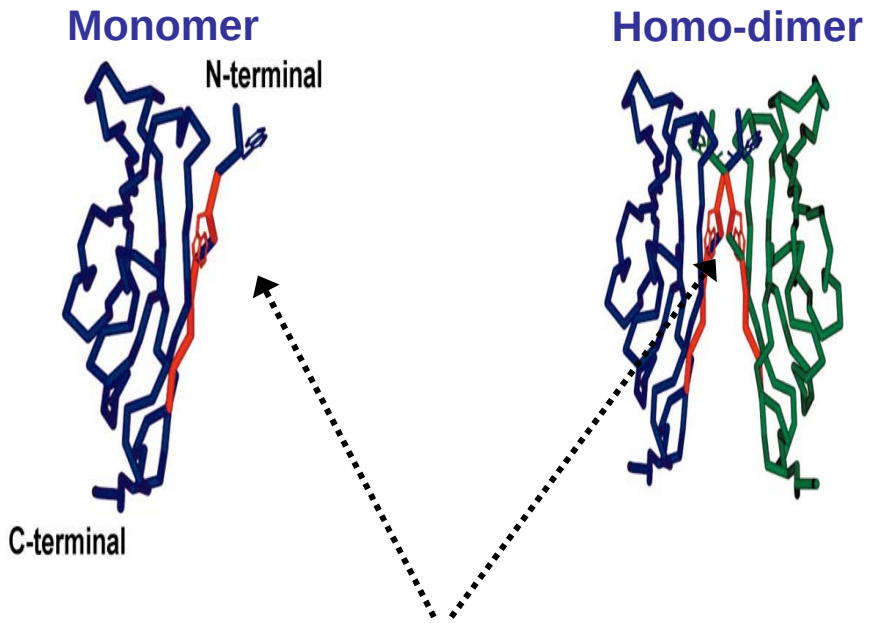

May *et al, Blood 2005*

B

Epitope of E4G10

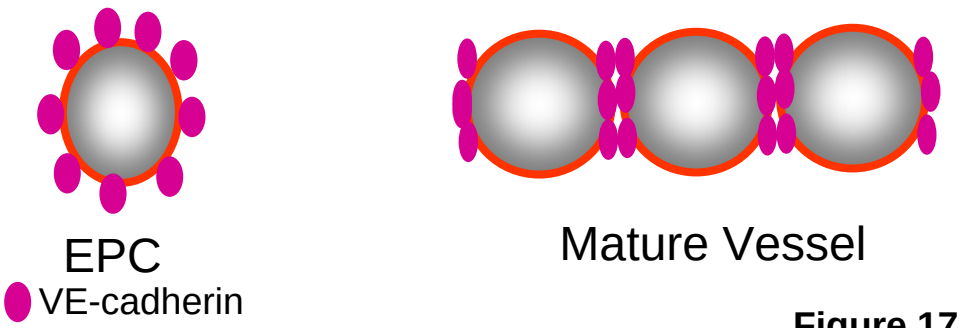

Figure 17

Figure 18: E4G10 recognizes EPCs, not ECs in vessels

Five color immunostaining of early LLC tumors (day 6) with VE-cadherin antibody E4G10 (white arrows), pan VE-cadherin antibody 11D4.1 (VE-cadh^{pan}, red arrows) and CD31. E4G10 exclusively staining EPCs is shown (double red and white arrows). Scale bar, 20 μm.

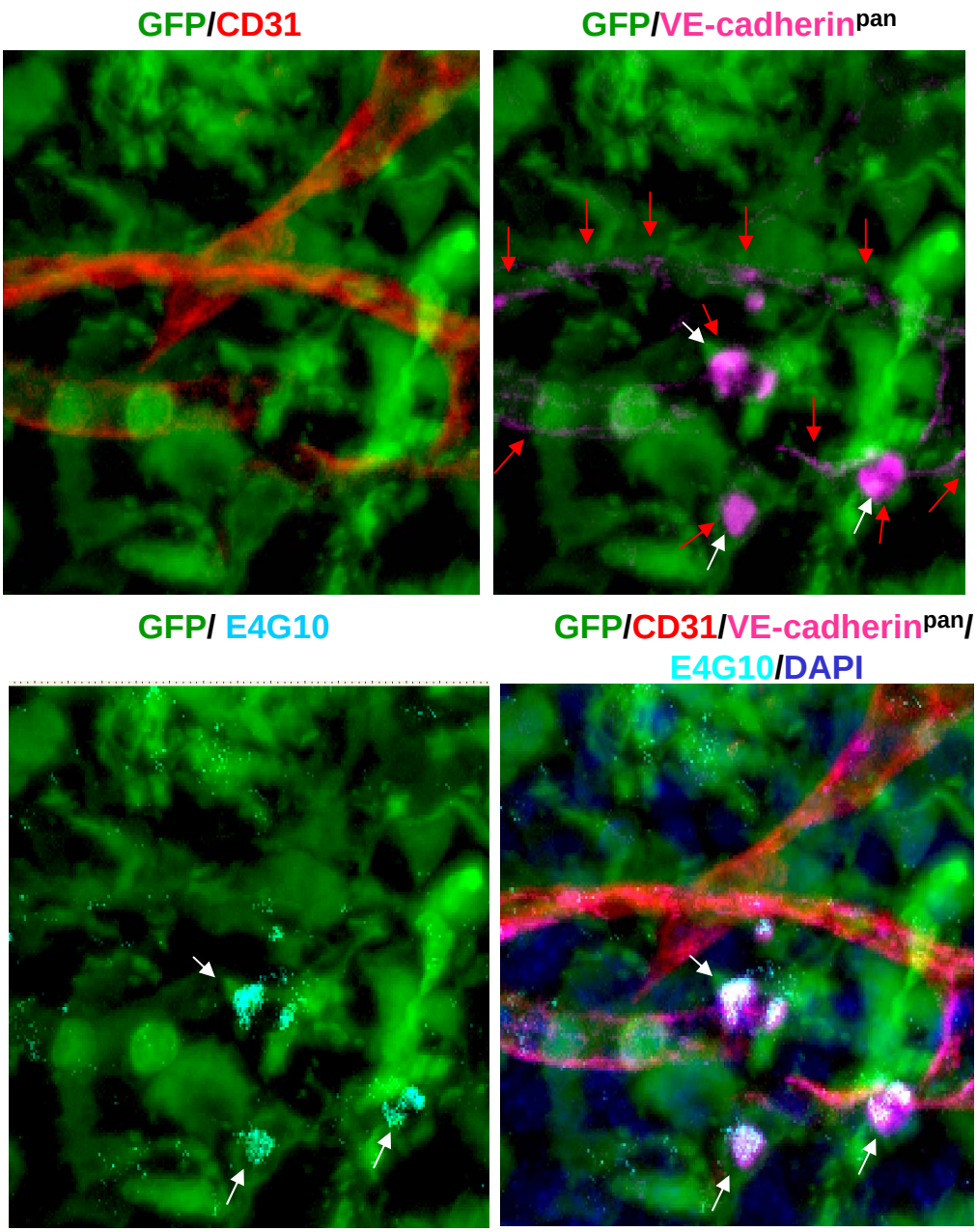
GFP/CD31
GFP/VE-cadherin pan
GFP/ E4G10
GFP/CD31/VE-cadherin pan/
E4G10/DAPI

Figure 18

Figure 19: VE-cadherin is not expressed on sprouting blood vessels

A: Immunostaining of early tumors (day 6) with CD31 and a pan VE-cadherin antibody. Low magnification image showing endothelial projections of the invading tumor vasculature. Yellow arrows depict VE-cadherin^{+} EPCs in the vicinity. Scale bar 20μm. **B:** Higher magnification of the area denoted by a rectangle (in A) depicting that the endothelial projections are devoid of VE-cadherin (white arrows).

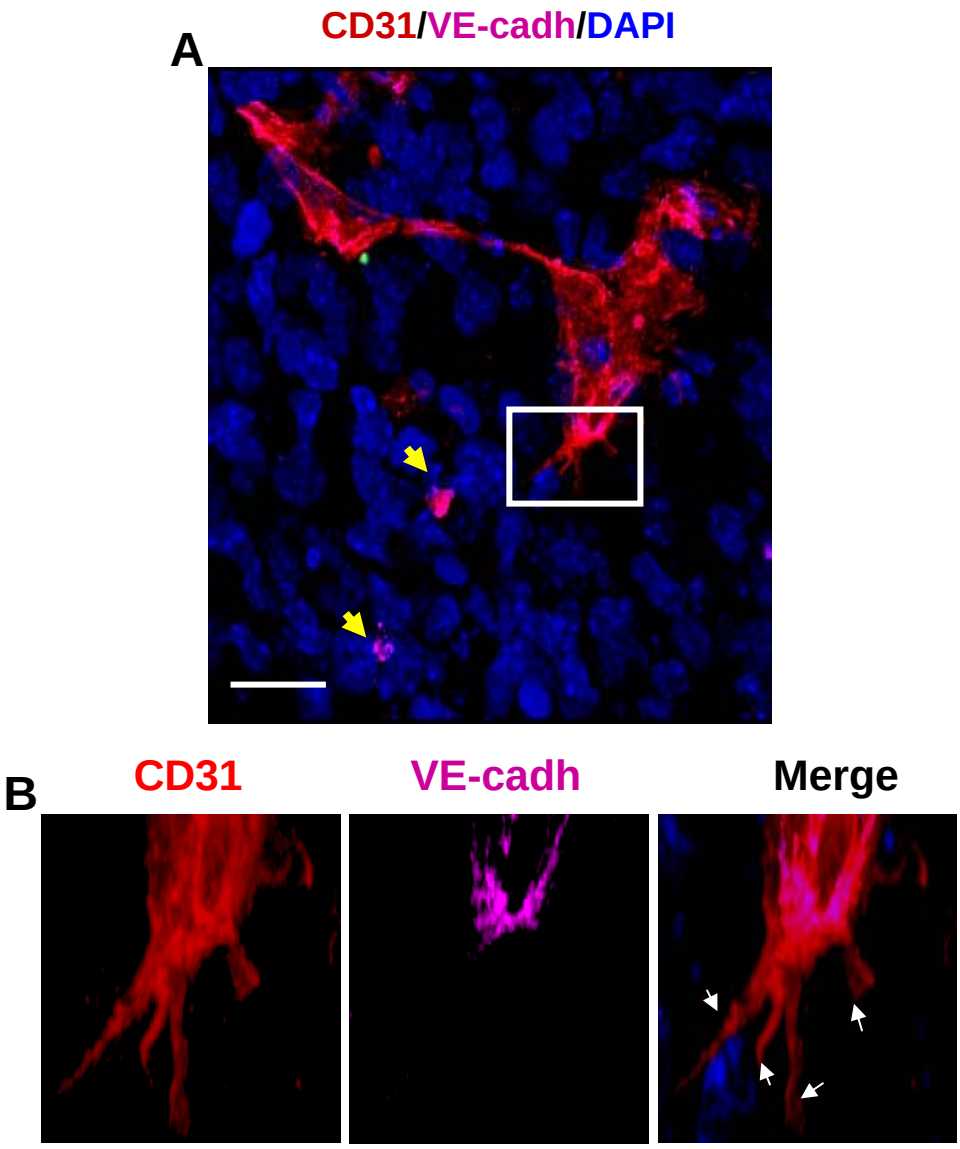

Figure 19

Tumor growth is slowed by targeting EPCs

The cytotoxic potency of E4G10 was enhanced by coupling the antibody to an alpha particle emitting isotope, actinium-225 (^{225}Ac) [157], so that target cells could be effectively killed at low concentrations of the antibody. Due to the short effective range of ^{225}AC, the collateral damage to the neighboring cells would be insignificant [158]. Administration of ^{225}Ac-labeled E4G10 (50 nCi, 0.6μg antibody per administration/animal) via retro-orbital injections at days 3, 5, 8, and 12 post tumor implantation reduced accumulated LLC tumor burden per animal by approximately 40% (day 14, p=0.001) compared to the administration of equivalent amounts of ^{225}Ac-labeled IgG isotype control mixed with unlabeled E4G10 (Figure 20). This control assured that the growth inhibition was specific to the ablation of EPCs as opposed to any minor VE-cadherin blockade by E4G10 or systemic or nonspecific response to the radioactivity.

The impaired tumor growth was associated with a marked reduction in EPC contribution (>45%, p=0.004) as determined by flow cytometry (Figure 21A) and confirmed by histology (Figure 21C). Ablation of VE-cadherin$^+$ cells was specific, since no detectable change was observed in other BM-derived GFP$^+$ infiltrating cell populations, including the CD11b$^+$ hematopoietic cells available in the immediate proximity (Figure 21B, p=0.86). There was no discernable difference to the total number of endothelial cells specifically at day 6 (p=0.6),

again attesting to the specificity of ^{225}E4G10 to EPCs and not tumor vasculature.

Notably, ablation of VE-cadherin^{+} EPCs resulted in a 40% reduction in BM-derived luminally incorporated ECs at day 6 (GFP^{+} CD31^{+} Isolectin^{+} CD11b^{-}, $p=0.016$), and a dramatic reduction in vessel density ($p=0.006$) in later tumors (Figure 22). No gross or histopathological toxicity was observed in normal tissues or their vasculature at the dosage administered. There were also no discernable toxic effects on the remaining tumor vasculature in the treated animals. Taken together, these results suggest that ablation of EPCs results in marked delay in tumor growth associated with decreased vessel density.

Figure 20: E4G10 slows LLC tumor growth

LLC tumor volume at day 14 in animals administered with isotype control ^{225}Act-IgG and unlabeled E4G10 or ^{225}Act-E4G10 antibody (n= 5, 10 respectively per group). Error bars represent standard deviation.

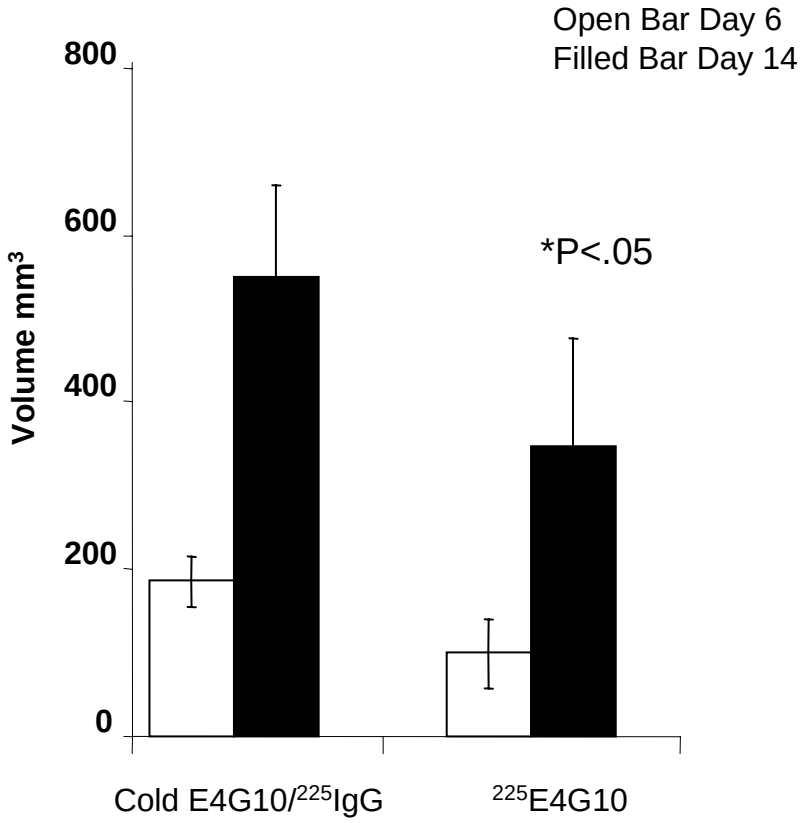
Open Bar Day 6
Filled Bar Day 14
800
600
400
200
0
Volume mm³
*P<.05
Cold E4G10/225IgG
225E4G10

Figure 20

Figure 21: ^{225}E4G10 Reduces EPCs specifically

A: Number of BM-derived EPCs (GFP^+ VE-cadherin$^+$ $CD31^{low}$ $CD11b^-$) cells in early tumors (day 6) in animals administered with control or ^{225}Act-E4G10 antibody at day 3 and 5 post tumor innoculation (n= 5,10 respectively, $1x10^5$ events counted per n). Bars denote averages. **B:** BM-derived GFP^+ $CD11b^+$ cells in tumors from animals treated as in A (n= 5, 10 respectively, $1x10^5$ events counted per n). Bars denote averages. **C:** Representative microscopy of control and treated tumors depicting the reduction of EPCs in treated tumors (yellow arrows).

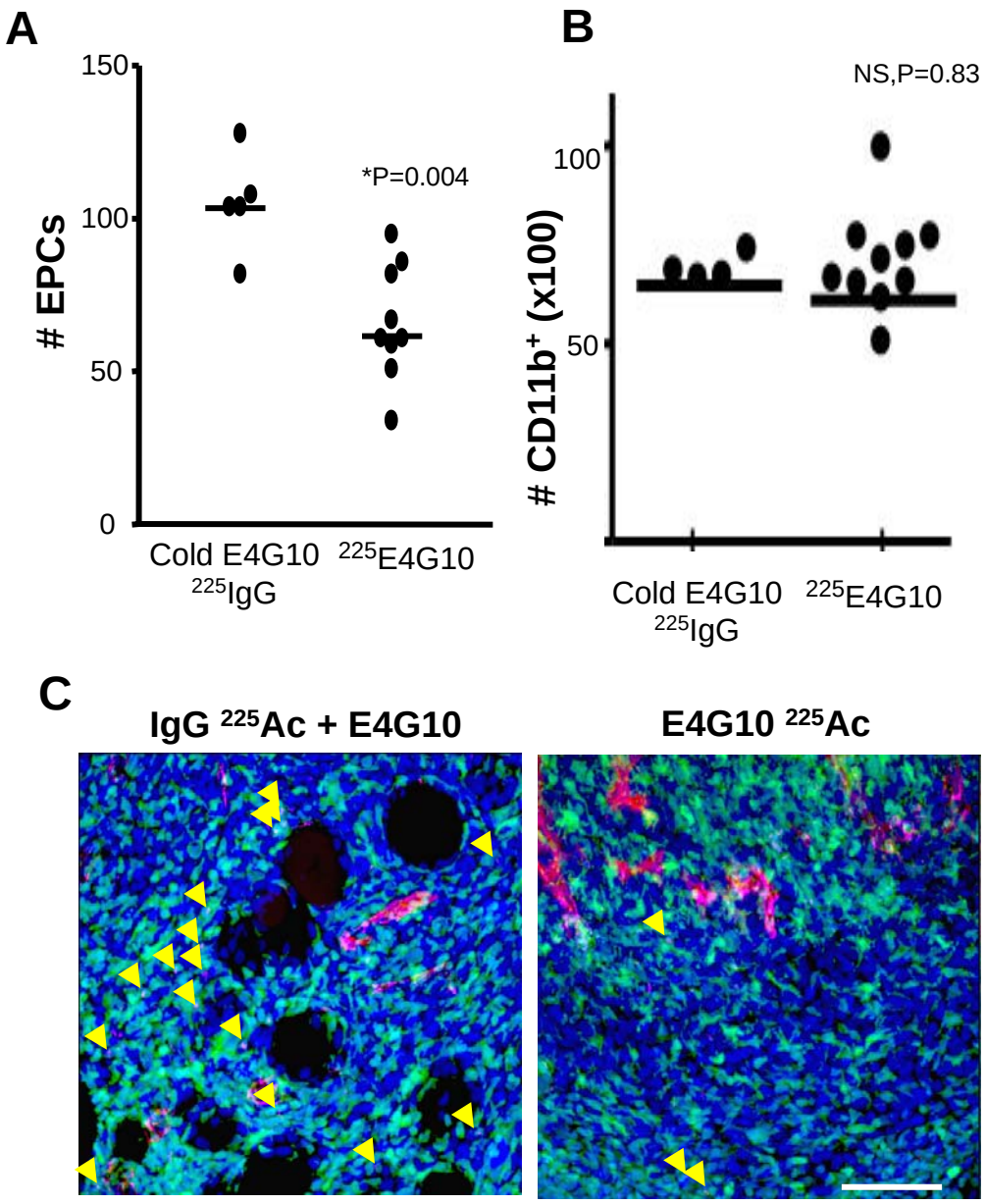
A
150
100
50
0
EPCs
*P=0.004
Cold E4G10 225IgG
225E4G10
B
NS,P=0.83
100
50
CD11b+ (x100)
Cold E4G10 225IgG
225E4G10
C
IgG 225Ac + E4G10
E4G10 225Ac
DAPI / GFP / VE-cadherin / Isolectin IB4

Figure 21

Figure 22: ^{225}E4G10 reduces vessel density

A: Vessel density in tumors in animals treated with control and test antibody (day 14, n= 5, 7 respectively per group). **B:** CD31 immunostaining of tumor sections (day 14) isolated from E4G10-treated and control-treated animals. Scale bar, 50 μm. Error bars represent standard deviations. * represents significant by t-test (* $p<0.05$).

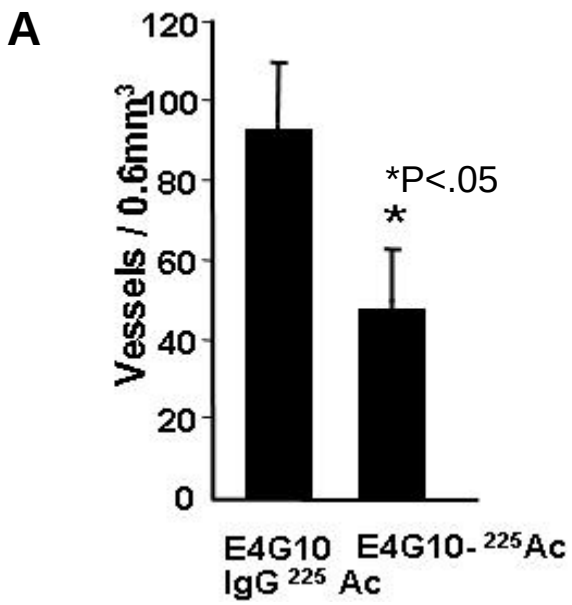
A
120
100
80
60
40
20
0
Vessels / 0.6mm3
*P<.05
*
E4G10
IgG 225 Ac
E4G10- 225Ac

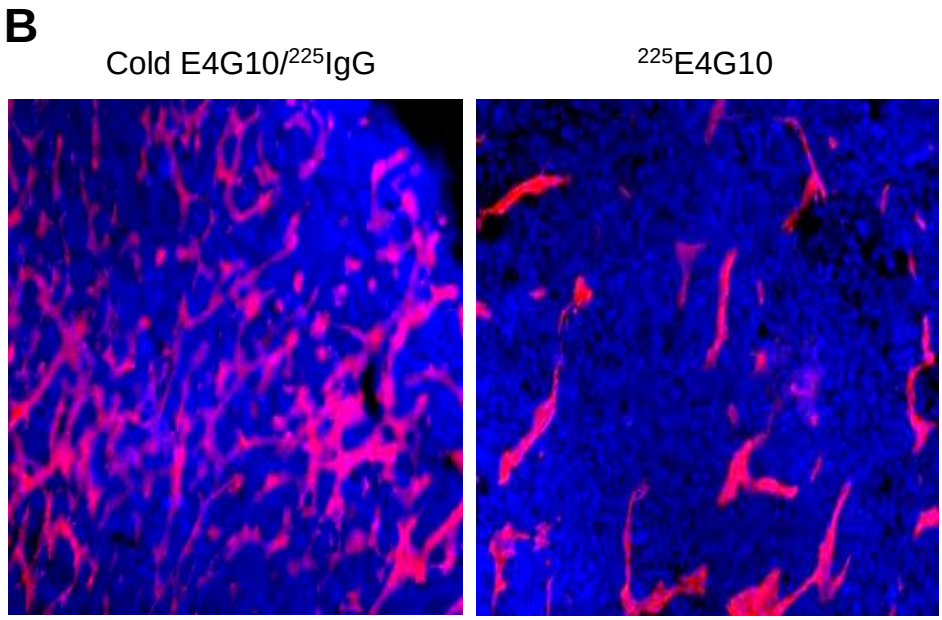
B
Cold E4G10/225IgG
225E4G10

Figure 22

Decrease in EPC contribution is associated with normalization of tumor vasculature

There has been an emerging concept in the field of anti-angiogenic therapies in the last several years, proposed by Rakesh Jain termed vessel normalization [159]. Jain highlights the fact that anti-angiogenic therapies have failed to yield long-term survival benefits in patients [160]. Jain has attributed this, in part, to a previously unrealized patterning change in the vasculature of tumors in response to anti-angiogenic therapy. Normalization is the temporary return to relatively normal vessel architecture within the tumor before complete recession of vessels in response to anti-angiogenic therapies. Typically, this normalization occurs within a short window of time when the efficacy of chemotherapy would be enhanced due to improved delivery through the normalized vasculature [161]. The hallmarks of normalization compared to regular tumor vasculature are an organized architecture, high pericyte coverage, aberrant basement membranes, lower vessel density, reduced permeability, high drug penetration, and low interstitial pressure.

Figure 23: ^{225}E4G10 decreases dysfunctional vasculature

A: Quantitative analysis based on flow cytometry of endothelial cells in control and treated day 14 LLC tumors. Dysfunctional vasculature was defined as $CD31^{high}$ $CD11b^{-}$ $Isolectin^{-}$, regardless of GFP expression. **B:** Mean fluorescent intensity (MFI) of the endothelial cells between control and treated animals, n= 5 and 10 respectively. Error bars represent standard deviation.

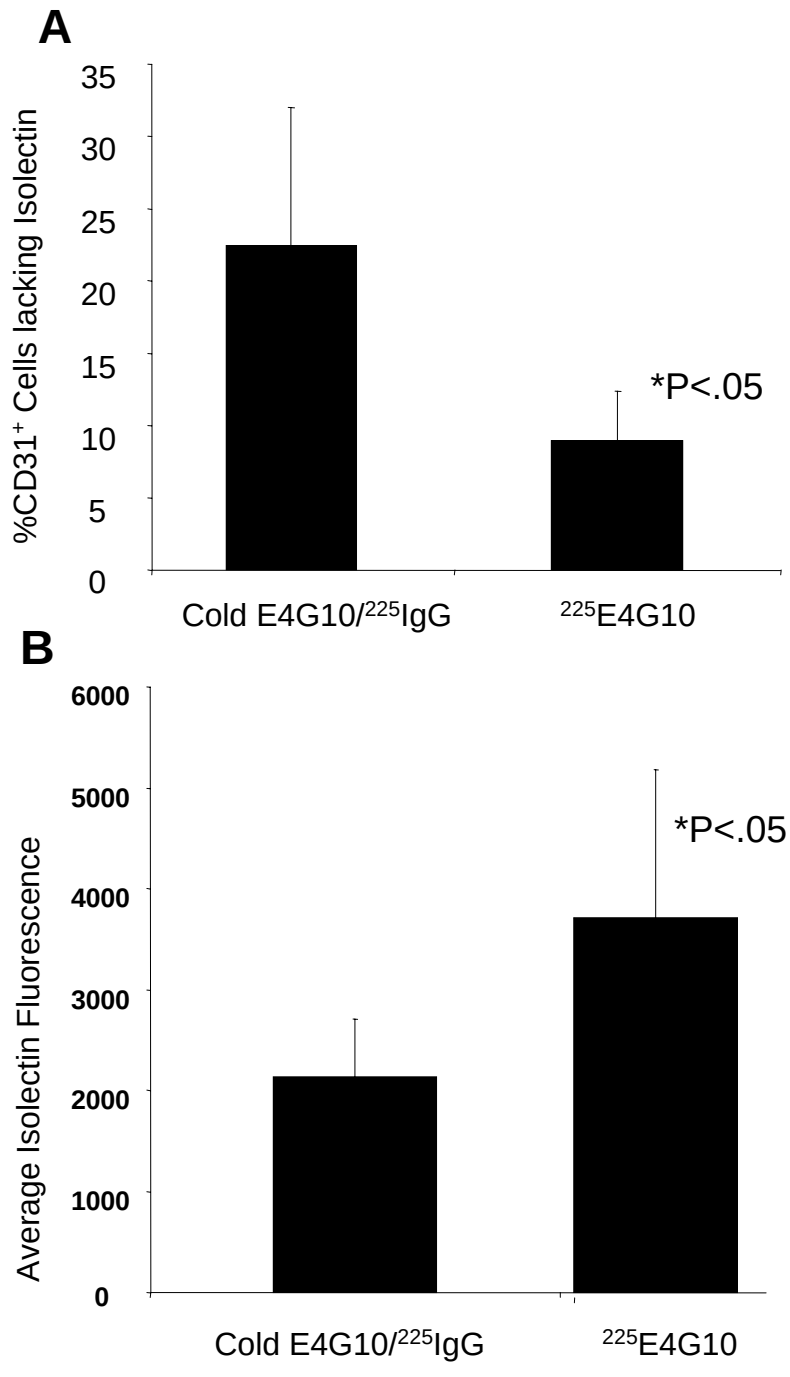
A
%CD31+ Cells lacking Isolectin
35
30
25
20
15
10
5
0
*P<.05
Cold E4G10/225IgG
225E4G10
B
Average Isolectin Fluorescence
6000
5000
4000
3000
2000
1000
0
*P<.05
Cold E4G10/225IgG
225E4G10

Figure 23

The first clue to the effect that EPC ablation had on tumor vasculature was the change in the isolectin profile of ^{225}E4G10 treated tumor endothelium. Surprisingly, EPC ablation resulted in the decrease of dysfunctional vasculature (Figure 23A). This was determined by quantitation of the $CD31^{+}$ $CD11b^{-}$ cells and the percentage of these cells that were able to bind Isolectin. This particular measurement is interesting, but circumstantial, due to the fact that CD31 may also be expressed on non-endothelial cells [102]. However, the mean fluorescent intensity (MFI) of the endothelial cells, which is indicative of the amount of blood flow they were exposed to, was increased nearly two fold (Figure 23B). As isolectin MFI and overall endothelial functionality has never before been used as a marker of normalization, additional confirmation was required. I therefore quantitated pericyte coverage by α-smooth muscle actin staining, which is a widely accepted measurement of normalized vasculature. Indeed, ^{225}E4G10 treated tumors had more than two fold increase in the pericyte coverage over control treated cohorts (Figure 24A, B). Three-dimensional images were used to create surface map models of the blood vessels. In addition to increased pericyte coverage, the pericytes appeared to be more tightly adherent to the blood vessels. Note that the pericyte coverage in control treated tumors was only loosely connected (Figure 25, white arrows) in comparison to the EPC ablated tumors. Finally, untreated tumors were lacking proper support and appeared ribbon-like,

as opposed to an open blood vessel (Figure 25). In addition to the isolectin data, the inclusion of more widely accepted parameters to measure normalization confirms the notion that the ablation of EPCs indeed does cause the vasculature to normalize. This notion was further validated in collaboration with Dr. David Scheinberg looking at the LnCap prostate tumor model. ^{225}E4G10 treatment here also normalized the vasculature, and enhanced the survival of animals when combined with chemotherapy [162].

Figure 24: ^{225}E4G10 increases pericyte coverage

A: Day 14 tumors of treated and untreated animals were stained for isolectin as an endothelial marker (green), and a smooth muscle actin (SMA, magenta) as a marker of pericyte coverage. B: Microscopic analysis from A was quantitated in control and treated animal groups, n=5and 7 respectively. Error bars represent standard deviation.

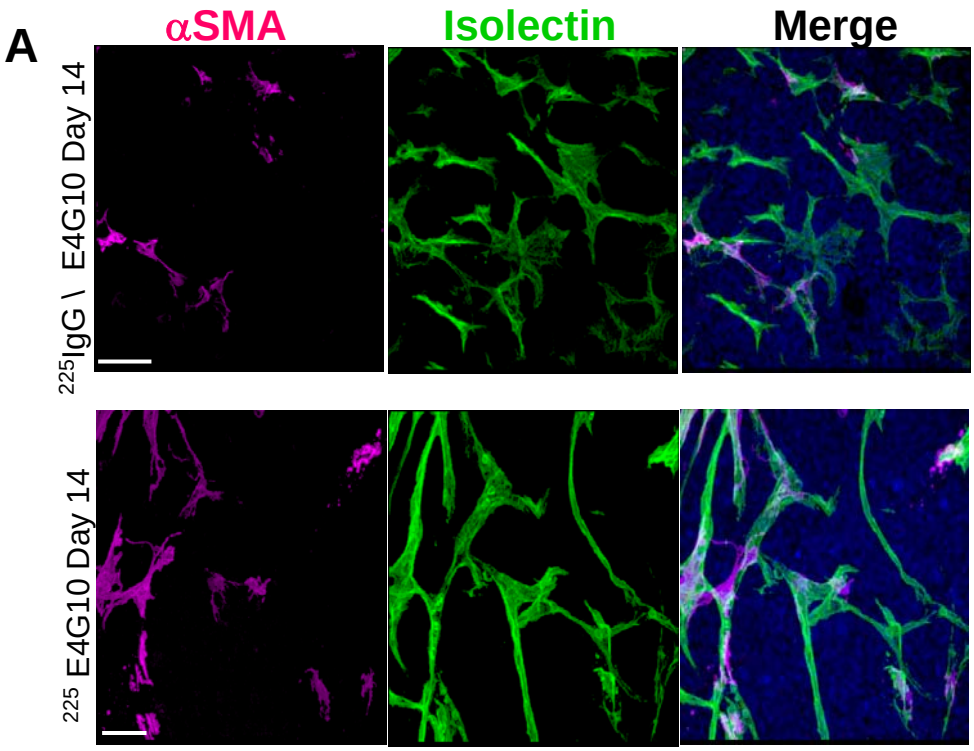

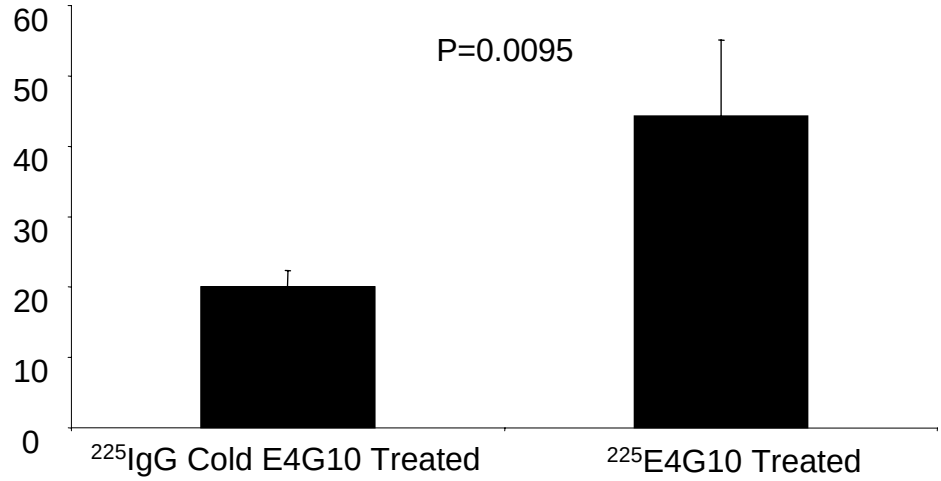

Scale Bar=100micron

Figure 24

Figure 25: ^{225}E4G10 improves pericyte/vessel adhesion

3-dimensional representations of blood vessels from control and treated animals were generated from z-stacks using Zeiss Inside 4D software. Isolectin is represented in red and αSMA is represented in magenta. Arrows highlight pericytes that are loosely adherent.

CD31/α-SMA

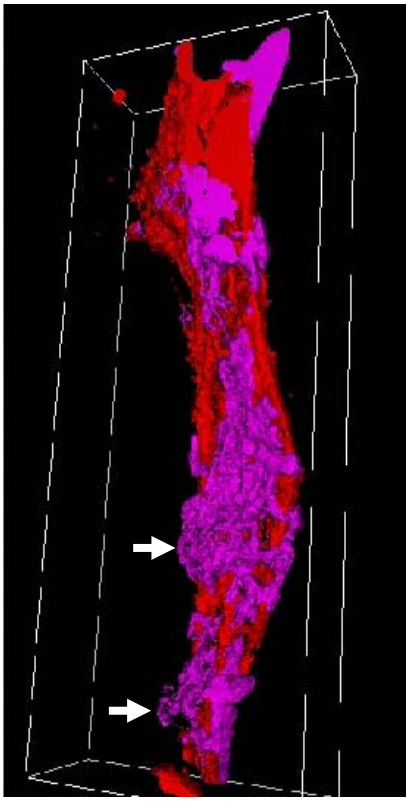

Cold E4G10/^{225}IgG

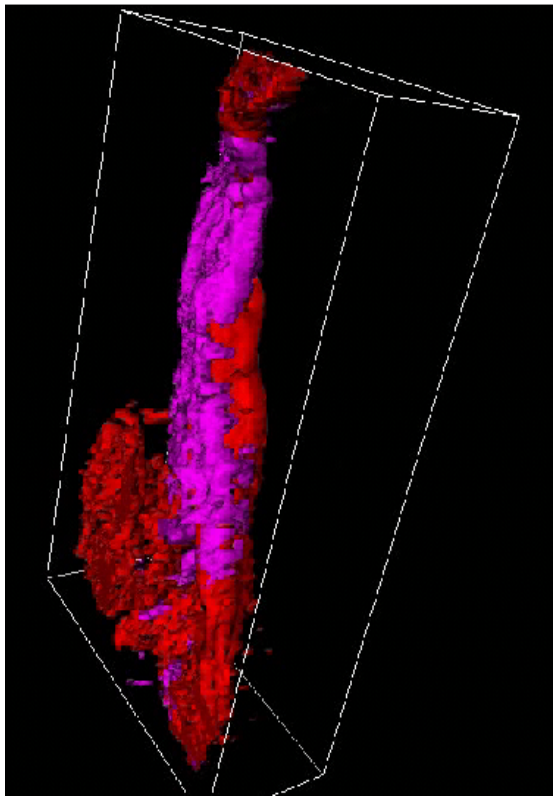

^{225}E4G10

Figure 25

Transcription factor Id1 is expressed in tumor associated ECs and EPCs

Id1 is a helix-loop-helix transcription factor which lacks a DNA binding domain and acts as a negative regulator of other helix-loop-helix proteins. The effects of Id proteins range from cell cycle regulation, to differentiation and lineage determination. Upon dimerizing with another helix-loop-helix protein, Id1 inhibits the binding of that transcription factor to promoter sequences [163, 164]. By this mechanism, Id1 can potentially bind various proteins and effect a wide range of targets as evidenced by the transcriptional profiling comparison between Pten $^{+/-}$ Id1$^{+/+}$ and Pten $^{+/-}$ Id1$^{-/-}$ animals [165]. The role of Id proteins in vascular development was established by the study of Id1 Id3 double knockout animals, which were embryonic lethal. Double knock-out animals had vascular malformations during embryogenesis, such as the inability to sprout or branch into developing tissues. However, by restoring only one copy of either Id1 or Id3, viability was restored. In addition to restoration of viability, vascular development in embryos with three out of four alleles appeared unperturbed. These animals also acquired an impressive tumor resistant and metastatic resistant phenotype associated with poor vascularization of the tumors [166].

A role for Id transcription factor in BM-mediated tumor angiogenesis was established by showing that transplantation of wild type BM rescued tumor growth in the angiogenic defective Id mutant (Id1^{+-}/Id3^{--}) mice [7]. In summary,

Id mutant animals were resistant to tumor growth, associated with a decrease in vessel density. This inability to grow implanted tumors was rescued by the transplantation of WT BM. When comparing WT to Id mutant animals, it was observed that Id mutant BM failed to mobilize EPCs into the blood in response to tumor challenge [7]. Finally, Id was confirmed in tumor endothelium (Figure 26A), but not healthy resting endothelium [167]. It was therefore reasoned that Id1 played a critical role in the mobilization of EPCs.

It was determined that Id1 is expressed in EPCs in response to tumor challenge. WT animals were implanted with LLC tumors and their bone marrow was harvested after 4 days. Lin^- cells were then cytospun and stained for VE-cadherin and Id1. A strong nuclear stain for Id1 was observed in VE-$cadherin^+$ EPCs, but not in other Lin- cells (Figure 26B). In addition to expression within the BM, the expression of Id1 was also confirmed in the EPCs at the periphery of early tumors (Figure 26C). While it was observed that tumor cells occasionally expressed Id1, no other BM-derived cell type could be found expressing Id1 in the tumor.

Figure 26: Id1 is expressed in tumor ECs and EPCs

A: Representative immunofluorescent image of an early vascularized LLC tumor (day 6) demonstrating that Id1 (magenta) is expressed in the nuclei of endothelial cells (marked by CD31, red). **B:** Cytospun immunofluorescent stain of Lin- cells from tumor challenged animals for VE-cadherin (red) and Id1 (magenta). **C:** Representative image of an early avascular LLC tumor periphery (day 4) with VE-cadherin (red) and Id1 (magenta). Bone marrow derived cells are shown in green, DAPI was used to visualize the nuclei, scale bars 10μm.

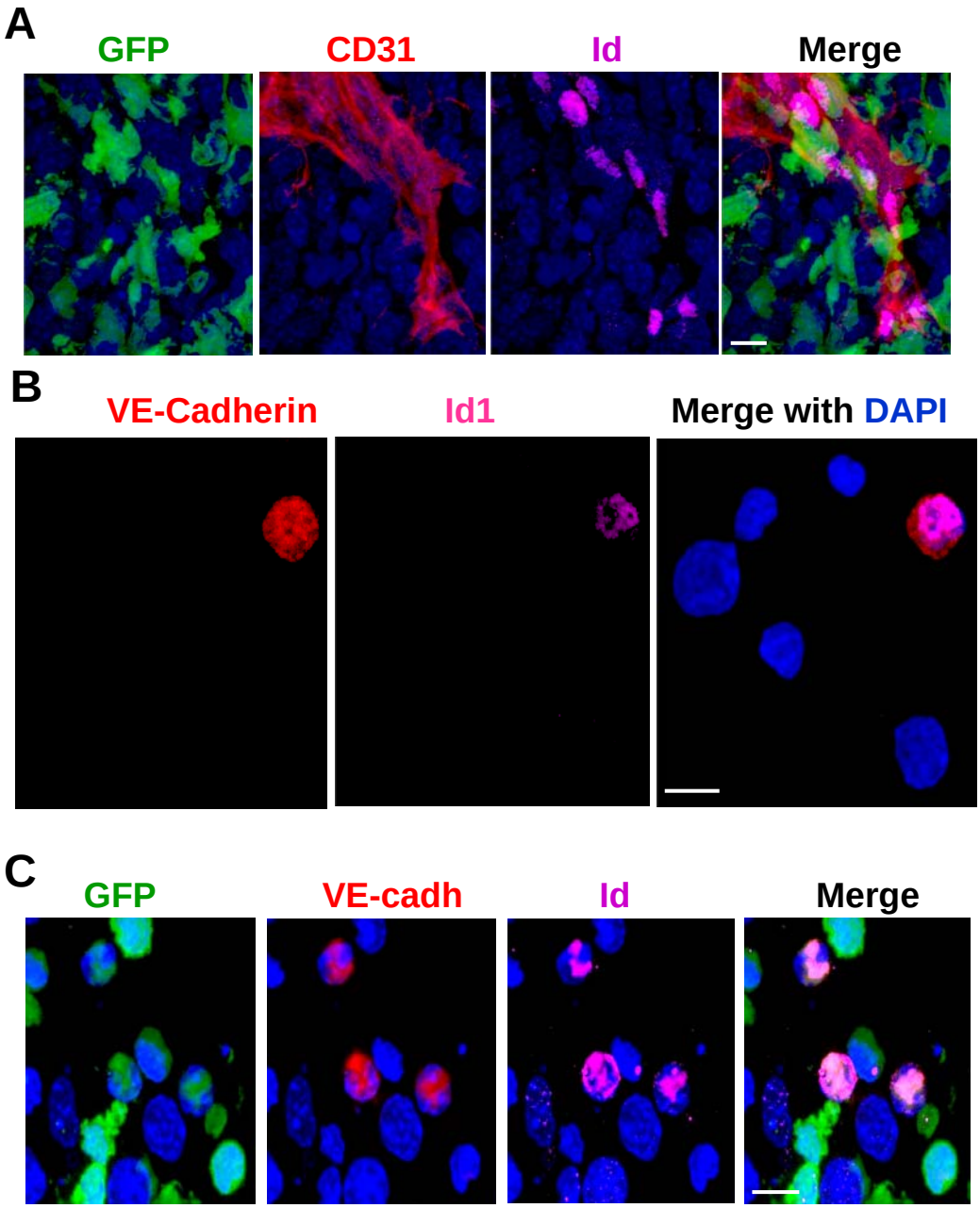

Scale Bars= 10μm

Figure 26

Inhibition of Id1 by lentivirally delivered shRNA

The demonstration that Id1 is preferentially expressed by ECs and EPCs upon tumor challenge presented an opportunity for targeted suppression. However, there is the possibility that the mutant animal somehow compensated for the lack of Id during development. This notion is bolstered by the plasticity of embryonic progenitors marked by endothelial specific adult markers, such as VE-cadherin [168]. Therefore, Id1 suppression via a lentivirally delivered shRNA to fully developed WT adult BM progenitors would mimic knockout conditions without any compensatory mechanisms. A panel of short hairpin RNAs (shRNAs) targeting the Id1 and Id3 genes were designed and screened for effectiveness in suppressing Id1 and Id3 gene expression using a method developed previously [169]. Briefly, fusion proteins consisting of the target gene and a fluorescent reporter were co-transfected with shRNAs. The fluorescence of a cell was directly proportionate to the efficacy of the shRNA. Potent shRNAs targeting Id1 and Id3 mRNA were identified, that effectively reduced endogenous Id1 (>95% reduction), and Id3 (>70% reduction) levels as determined by both real time-polymerase chain reaction (RT-PCR) and Western blotting (Figure 27A-C). The levels of Id1 suppression was, however, slightly compromised when a vector expressing both Id1 and Id3 shRNAs driven by separate U6 promoters was used

Figure 27 shRNA inhibition of Id1 *in vitro*

A: RT-PCR showing reduction in Id1 mRNA levels by an Id1 specific shRNA (Emily Heikamp). **B:** Id3 mRNA levels by a Id3 specific shRNA as compared to a control non specific (NS) shRNA (Emily Heikamp). **C:** Western blot showing reduction in Id1 protein levels by an Id1 specific shRNA in the context of either a single (Id1) or double hairpin (Id1+Id3) construct (Elizabeth Romero). **D:** Vector descriptions of lentiviral constructs expressing shRNAs. U6 promoter driving expression of shRNAs; EFs promoter driving transcription of GFP; cPPT. central polypurine tract; WPRE. Woodchuck hepatitis virus post-trasncription regulatory element; LTR, self inactivating long terminal repeat.

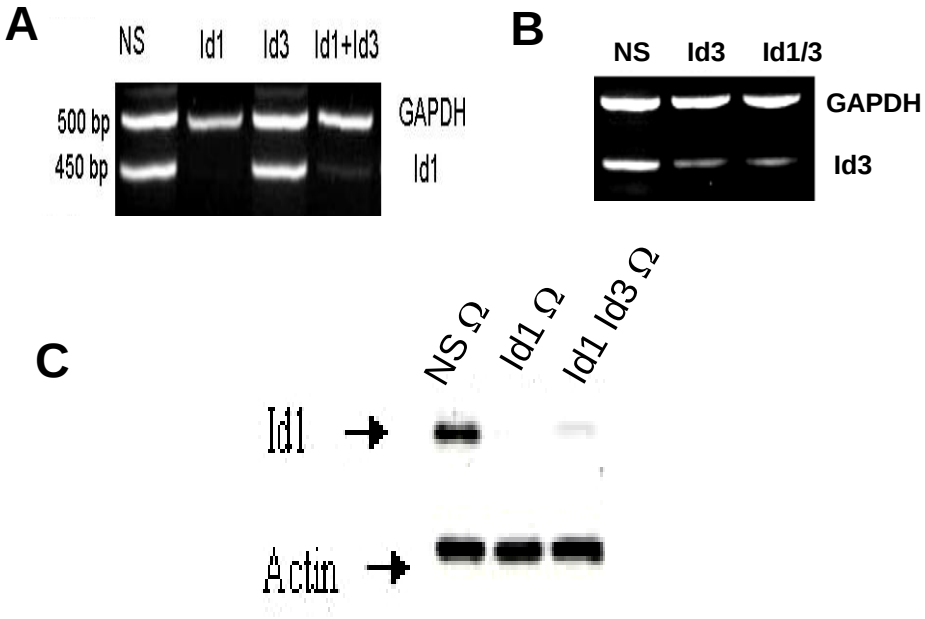
A
NS
Id1
Id3
Id1+Id3
500 bp
450 bp
GAPDH
Id1
B
NS
Id3
Id1/3
GAPDH
Id3
C
NS Ω
Id1 Ω
Id1 Id3 Ω
Id1
Actin
D
LTR
cPPT
U6
Id1
EF1α
GFP
WPRE
LTR
LTR
cPPT
U6
Id1
Id3
U6
EF1α
GFP
WPRE
LTR

Figure 27

(Figure 27B-D). It is possible that the close proximity of the two U6 promoters and their converging direction compromised the transcription of the hairpins.

Retroviral vectors are an attractive tool for gene delivery, specifically the delivery of shRNA. This technology has several advantages. First, these vectors are capable of stably integrating into the genome, greatly reducing the possibility of losing the genetic material with cellular divisions. Retroviral vectors have also been engineered to deliver only the genetic package, and none of the retroviral elements necessary for replication. Particularly, lentivirus has one unique advantage over other retroviral vectors, as it has the capacity to infect non-dividing cells [170, 171]. These properties make lentivirus an excellent choice to use as a delivery method for shRNA into the BM progenitors.

Successful BMTs could be accomplished in two ways. First, total BM could be harvested from donor animals and injected directly into irradiated recipient animals. Alternatively, total BM could be depleted of all mature cells via magnetic separation. This lineage depleted population (Lin^-) could then be transplanted into recipient animals (Figure 28A). Lin- cells were routinely isolated at a purity >95% (Figure28B). A comparison of $5x10^5$ Lin^- cells to $5x10^6$ total BM showed no discernable difference in survival, reconstitution, or response to tumor challenge (Figure 28C and data not shown). Due to the large amount of

virus required to infect unfractionated BM, Lin^- based BMTs were the ideal choice for shRNA BMT experiments.

Figure 28: BMTs with TBM or Lin$^-$ cells yield identical reconstitutions

A: Schematic representation of a bone marrow transplantation experiment utilizing bone marrow depleted of all differentiated cells (Lin$^-$) prior to implantation into recipients. **B:** Flow cytometric analysis was used to determine the purity of the lineage depleted cells. A cocktail of biotin conjugated primary antibodies specific to differentiation markers (identical to the cocktail used for the depletion) was incubated with either total bone marrow (top) or lineage depleted cells. Anti-biotin antibodies conjugated to the APC fluorophore was used as a reporter. **C:** A comparison of BMT animals which received either total BM, or Lin$^-$ cells from GFP$^+$ donors. Error bars represent standard deviation.

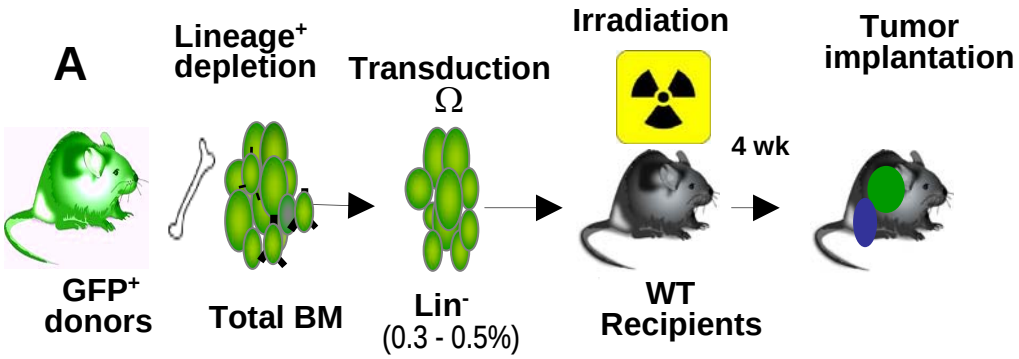
A
Lineage+ depletion
Transduction
Ω
Irradiation
Tumor implantation
4 wk
GFP+ donors
Total BM
Lin-
(0.3 - 0.5%)
WT Recipients

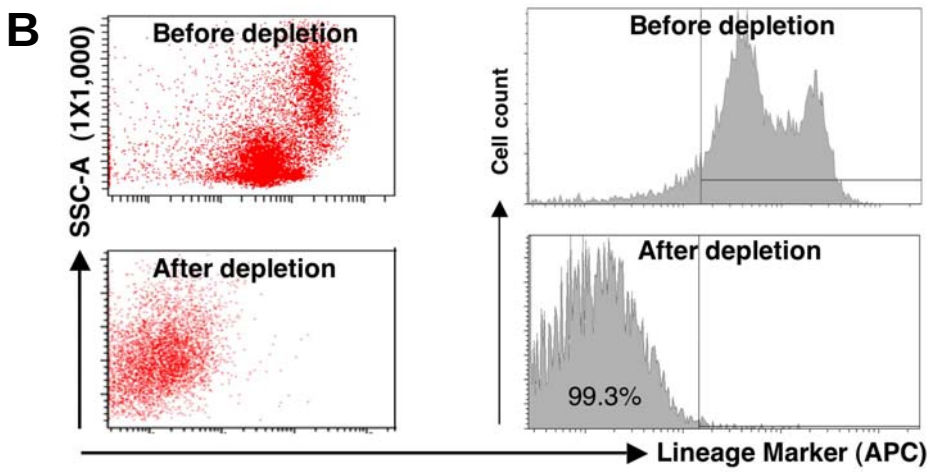
B
Before depletion
After depletion
SSC-A (1X1,000)
Cell count
99.3%
Lineage Marker (APC)

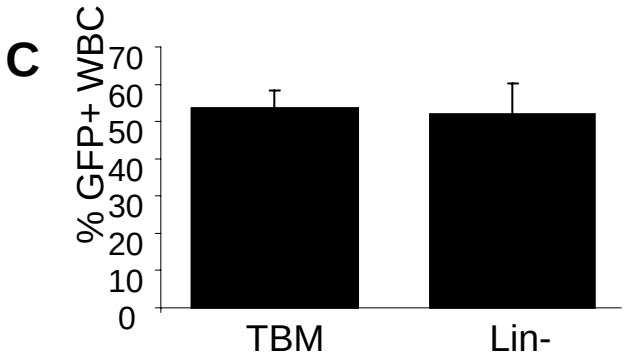
C
% GFP+ WBC
70
60
50
40
30
20
10
0
TBM
Lin-

Figure 28

Lentiviral delivery of shRNAs efficiently infects Lin$^-$ BM cells

WT animals were sacrificed and their bone marrow was depleted of mature cells via magnetic columns in sterile conditions. Lin$^-$ cells were combined with concentrated lentivirus in a 3:1 ratio. It was determined that viral media in excess of 25% of the total transduction media resulted in dramatic cell death (data not shown). Media (either DMEM or SCGM) was free of FBS, but did contain cytokines SCF, IL3, and IL6 to maintain the cells in a healthy state without inducing differentiation. The transduction reaction was then centrifuged on the wells of the plate. This process of spinoculation was found to enhance infection [172]. Transduced cells were maintained in a 37^0C incubator overnight. Transduced cells were rinsed of any excess lentivirus and injected into lethally irradiated hosts.

Small amounts of cells were kept in culture to assess infection by GFP expression. After 4 days in culture post infection, GFP expression was detected in all conditions. Flow cytometric analysis confirms a high level of infection that was remarkably consistent between the Id1, Id1/Id3, and Non-specific (NS) lentiviral constructs (Figure 29). Approximately 80% of all cells were GFP$^+$. I consider this to be an underestimation, due to the overall dim GFP expression and RT-PCR confirmation of greater than 95% reduction in Id1 mRNA levels after

tumor challenge between the Id1, Id1/Id3, and non-specific shRNAs (data not shown).

Figure 29: Efficient transduction of Lin- cells with shRNA lentiviral constructs

Lineage depleted cells were harvested and transduced at 100 MOI with lentiviral vectors endcoding shRNAs directed against non-specific targets (NS), Id1, or Id1 and Id3 together. After 4 days in serum free medium supplemented with SCF, IL3, and IL6, the expression of GFP was analyzed by flow cytometry.

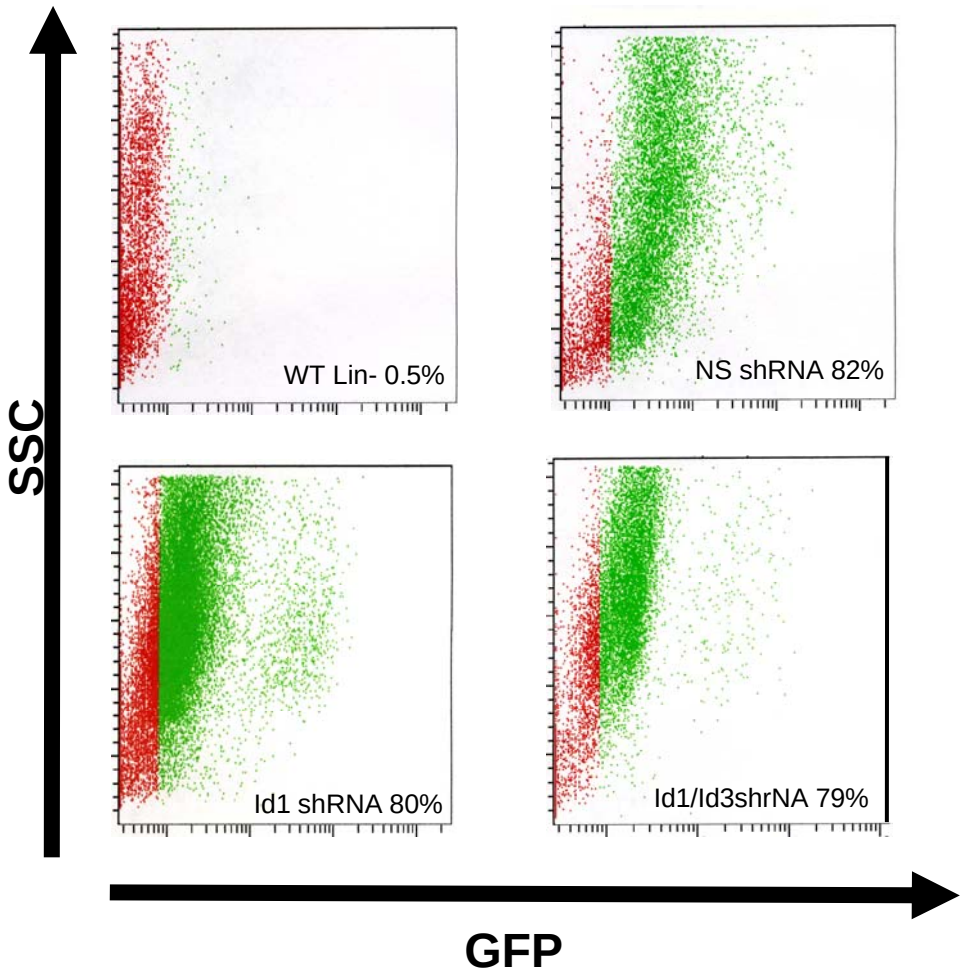

Figure 29

Id shRNAs slow tumor growth with reduced angiogenesis

Animals were allowed to reconstitute with the transduced BM for 4 weeks, following which they were challenged with either B6RV2 or LLC xenografts. B6RV2 tumor growth was marked by a prolonged latency period in the Id1 shRNA BMT animals prior to any significant growth (Figure 30A). After this latency period, the tumors began to grow at a similar rate to the WT and NS shRNA BMTs. LLC tumors showed a slowed tumor growth rate during the entire duration of the 14 day experiment (Figure 30B). Noticably, the Id1 shRNA BMTs maintained a more restricted tumor growth than the Id1/Id3 shRNA BMTs. This growth rate is reflective of the relative Id1 regulation demonstrated by western blot (Fig 27B, C).

Gross visualization of the intradermal tumors taken every two days showed the NS shRNA BMT animal's tumor is engorged in blood (Figure 30). In contrast, the Id1 shRNA BMT animal's tumor is significantly paler. Even when comparing tumors of comparable size (day 6 NS shRNA BMT versus day 14 Id1 shRNA BMT), the Id1 shRNA BMT tumor is still paler.

Immunofluorescent analysis of later tumors reveals a vascular phenotype associated with the reduction of Id1 in the BM. Id1 shRNA tumors displayed a varying vessel density throughout the tumors ranging from the more common large regions devoid of any vasculature to several rare patches of extremely

dense, convoluted, and tortuous vessels (Figure 31). Overall, the vessel density in these tumors was reduced by ~50%. The reduced vessel density is in agreement with the visual analysis (Figure 31).

Figure 30: Tumor growth rates are impaired with shRNAs targeting Id1 and Id3

A: Tumor growth of B6RV2 lymphoma xenografts in non-transplanted wild type mice, non-specific (NS) or a Id1-specific shRNA BMT mice (n= 3 per group). **B:** Tumor growth of LLCs in a non-specific (NS), Id1-specific or Id1 and Id3 shRNA BMT mice (n= 5 each). **C:** LLC tumor morphology (day 2-14) in a non-specific shRNA BMT mice (upper panel), and an Id1-shRNA BMT mice (lower panel). Error bars represent standard deviation.

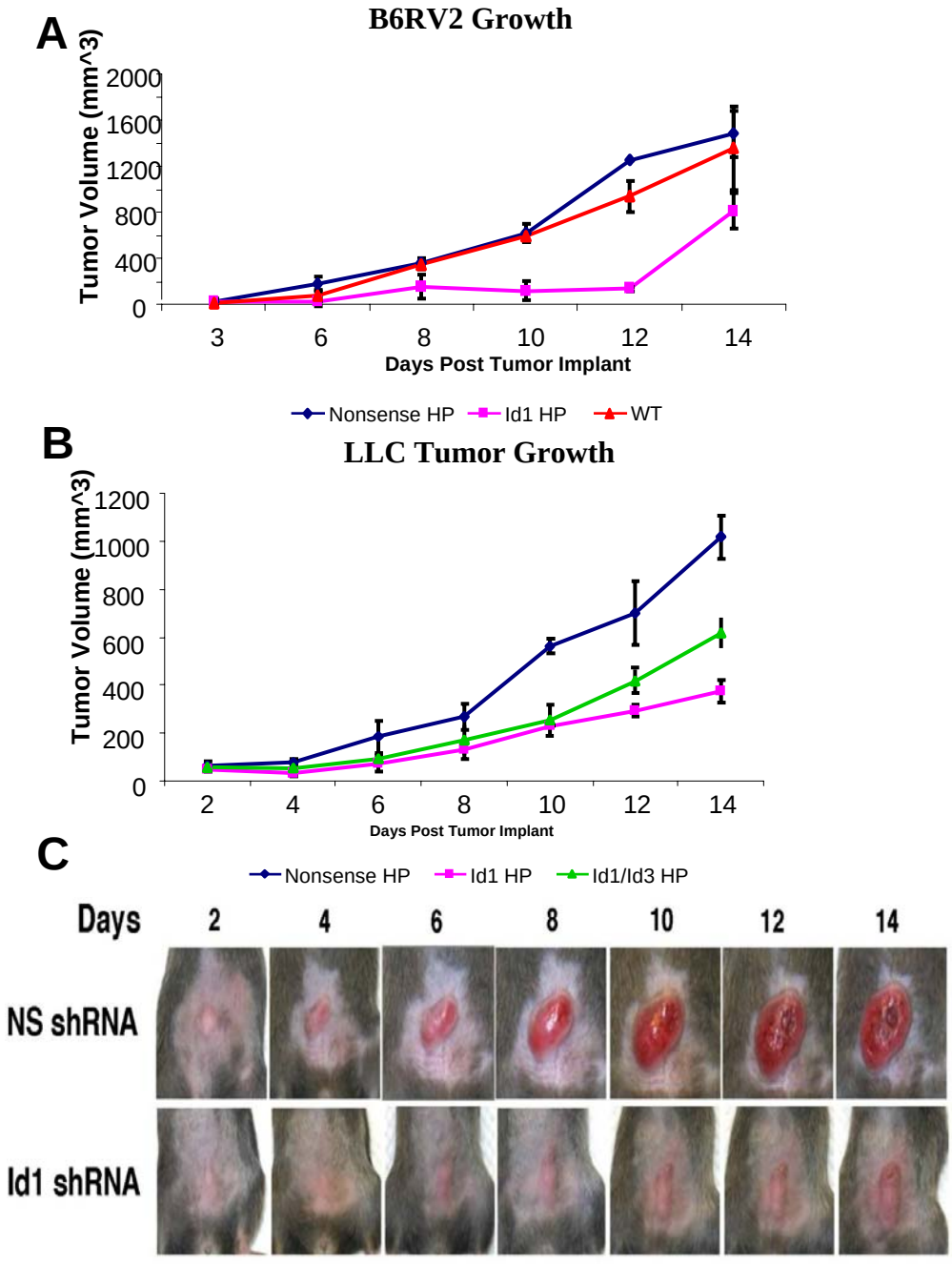
A
B6RV2 Growth
Tumor Volume (mm^3)
2000
1600
1200
800
400
0
3
6
8
10
12
14
Days Post Tumor Implant
Nonsense HP
Id1 HP
WT
B
LLC Tumor Growth
Tumor Volume (mm^3)
1200
1000
800
600
400
200
0
2
4
6
8
10
12
14
Days Post Tumor Implant
C
Nonsense HP
Id1 HP
Id1/Id3 HP
Days
2
4
6
8
10
12
14
NS shRNA
Id1 shRNA

Figure 30

Figure 31: Id1 shRNA BMT reduces vascular density

Representative images of LLC tumors (day 14) from animals transplanted with NS shRNA transduced Lin- cells (top) or Id1 shRNA transduced Lin- cells. Vasculature was visualized by CD31 (red). BM derived cells were visualized by GFP expression (green). Scale bars 100μm.

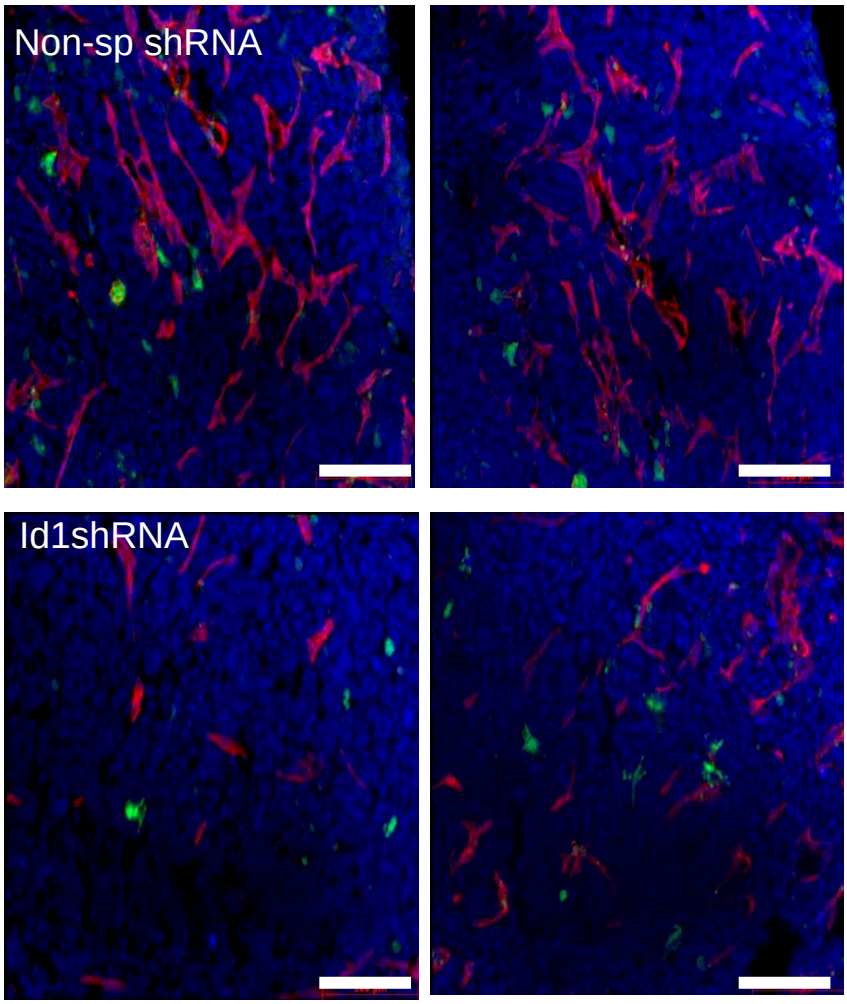

Figure 31

Chapter 3 Discussion

The functional significance of EPCs in angiogenesis-mediated tumor growth was demonstrated by the effective and selective ablation using anti-VE-cadherin antibody, E4G10. Chad May and colleagues were one of the first to report on the E4G10 in 2005 [155]. This report was focused on the generation of two unique VE-cadherin antibodies (E4G10 and BV13) and comparison of the binding conditions. In this report, May *et al* postulated that VE-cadherin is monomeric in the leaky tumor vasculature and a possible target for E4G10. However, no data was provided to demonstrate this hypothesis was correct.

These results differ from that of Liao *et al* which concluded that E4G10 was capable of binding tumor vasculature directly [156]. To demonstrate reduced tumor growth as a response to E4G10, the authors administered large amounts of antibody (1-3mg per animal per injection). They also showed that injections of fluorescent E4G10 antibody stained regions of the tumor which overlapped vascular staining. They concluded the fluorescence detected after the two hours allowed for the antibody to circulate was proof E4G10 bound to the vasculature. These studies are associated with several possible caveats. The first is the large amount of antibody injected. Second, the E4G10 failed to bind the vasculature in a pattern consistent with the localization of VE-cadherin at the intracellular junctions. There are clear regions of the tumor that are avascular, but have

E4G10 staining (see Liao et al figure 5B) which is consistent with antibody leaking into the tumor stroma around the blood vessels. Control experiments with isotype control antibodies at equal concentrations were not presented, as this would have resolved the issue. Conversely, our results are consistent with a report demonstrating E4G10 is only effective in early tumors, and not later tumors [96]. This result is conducive with the binding of E4G10 to the EPCs recruited to early tumors and not to vasculature, which would be leaky regardless of stage.

Recently, several reports have addressed the fate of monomeric VE-cadherin on the surface of mature endothelial cells. VE-cadherin degradation is guided by its phosphorylation in a Src dependent manner. Phosphorylation is enhanced in angiogenic settings, specifically under VEGF stimulation. VE-cadherin is made more susceptible to Src phosphorylation due to its disassociation with the cytoskeleton upon becoming monomeric, a common feature of cadherins. The internalization of VE-cadherin after becoming monomeric, and prior to degradation, has kinetics on a time scale of only several minutes [173-178]. Collectively with the data presented in Figures 18 and 19, these reports establish that there is no opportunity for E4G10 to bind monomeric VE-cadherin on mature endothelial cells. It is therefore more likely that the previous reports describing E4G10 slowing tumor growth were the result of the deleterious effects upon EPCs due to VE-cadherin blockade.

In addition to the work presented here [21], the finding that EPC ablation results in the normalization of tumor vasculature was analyzed in greater depth in collaboration with Dr. David Scheinberg's group at Memorial Sloan-Kettering Cancer Center. Singh Jaggi *et al* used a LNCaP prostate tumor model to study ^{225}E4G10, focusing on the effects on mature vasculature and survival of the animals [162]. Animals were given combinations of treatments including control antibody, ^{225}E4G10, and ^{225}E4G10 combined with the chemotherapeutic Paclitaxel. In agreement with the notion that normalization enhances chemotherapeutic delivery, the combined drug regime doubled the survival rate compared to chemotherapy alone. The normalization of the vasculature was confirmed by increased pericyte coverage, normal basement membranes, and a lack of extravassated red blood cells in the tumor which is indicative of leaky vasculature. There were also no detectable deleterious effects in healthy organs after the ^{225}E4G10 administration. The ability to specifically target EPCs is a great advancement in anti-angiogenic therapy as this leads to the potential of having minimal off-target effects that have hindered broad spectrum anti-angiogenic therapies.

The data presented here has begun to shed light on the effects EPCs have in various tumor models. First, it establishes that EPCs have crucial roles in various tumor types. This common mechanism of tumor growth could result in a

large range of cancers that can be targeted with EPC ablative therapies. It also highlights the differences in tumor biology with regard to EPCs. Note the differences in the growth rates of B6RV2 tumors and LLC tumors when grown in animals with Id1 shRNA BMTs. B6RV2s have a prolonged lag phase followed by rapid growth. LLCs have a steady, but significantly slower growth rates. This may highlight the inherent differences between tumors in their reliance on EPCs, or possibly suggests different methods for coping with the lack of EPCs. Surely, these results provide enthusiasm to study the differing tumor responses to EPC ablation to most effectively design a multifaceted approach that could prolong disease-free survival.

The Id1 shRNA BMT experiments also emphasized the potential rewards for further studying Id1 in EPCs. The Id1 suppression achieved here was distinct from previous studies [7, 165, 166] due to the use of lentivirally delivered Id1 targeting shRNAs as opposed to genetic knockout models. This distinction bypasses any potential compensation for the lack of Id1 during development. This result clearly confirms that the Id1 deficient phenotype is due to its suppression in the BM compartment. Additionally, these results demonstrated the ability to replicate observations made using transgenic animals via the stable introduction of shRNA. As targets are identified that are critical for EPC

function, such as the transcriptional targets of Id1 regulation, this platform will allow for similar studies, without the need for costly genetic models.

CHAPTER 4: Identification and analysis of the EPC lineage

Various studies have aimed to define EPCs based on marker expression of cell populations from peripheral blood [5, 105, 106, 113, 179-183]. However, few have looked within the bone marrow to find more primitive EPCs within the lineage. This study has further defined the phenotype of EPCs and their biological role in tumor angiogenesis. I therefore decided to investigate the lineage of EPCs to: 1)determine the cellular and molecular mechanisms by which EPCs contribute to tumor angiogenesis 2) to determine the identity of a population of progenitors specifically capable of reconstituting the EPC lineage in a bone marrow transplant experiment.

While the analysis of resting EPCs can be used to study various populations, a tumor challenge would activate resting EPCs causing their expansion, mobilization, and differentiation. It has now been shown that EPCs within the BM progenitor compartment, marked by VE-cadherin, are capable of differentiating into mature endothelial cells (Figure 9). The VE-cadherin^{+} EPC population comprises approximately 2-7% of the Lin^{-}. When this population of cells was analyzed in resting animals and their tumor challenged cohorts, there was a striking clearance of EPCs (VE-cadherin^{+} CD11b^{-} Lin^{-}) from the BM. By day 6, these animals had mobilized approximately 80% of their EPCs to the peripheral blood compared to resting levels (Figure 32). Following the clearance

of EPCs, there is a modest rebound in cell numbers after day 6. This clearance of EPCs is in concordance with their arrival at the tumor periphery and the peak of BM contribution to tumor endothelium (Figure 13). This result cannot be attributed to the gross expansion of any other population due to the lack of any detectible increase in the number of progenitors or mature BM cells (data not shown).

Figure 32 VE-cadherin^{+} EPCs from Lin- mobilize in response to tumor challenge

20 animals were burdened with LLC xenograft tumors. At days, 4, 6, 10, and 14 flow cytometry was used to compare the Lin- population of cells and compare it to resting Lin- cells (day 0). EPCs, defined as VE-cadherin+ CD11b-, were quantitated at each time point. Values were normalized based on purity levels, as described. n=5 per group 50,000 events counted per n. Error bars represent standard deviation.

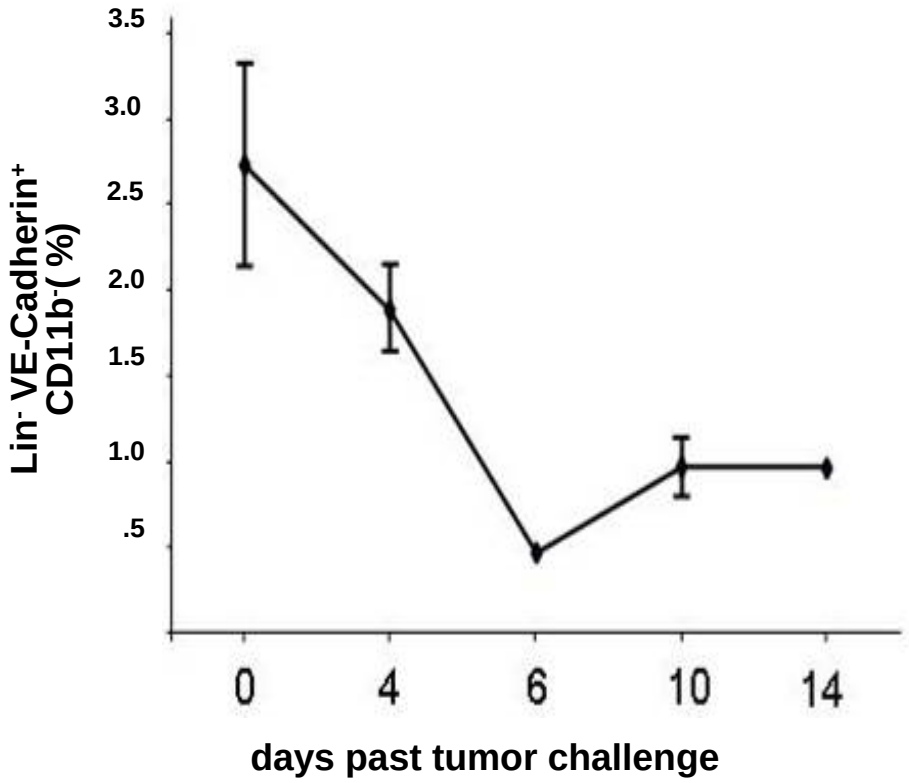
3.5
3.0
2.5
2.0
1.5
1.0
.5
Lin- VE-Cadherin+ CD11b-(%)
0
4
6
10
14
days past tumor challenge

Figure 32

Identification of EPC sub-populations in tumor challenged mice

Encouraged by the observation that VE-cadherin^{+} cells mobilized in response to a tumor challenge, a more in depth analysis with additional markers of endothelial and progenitor cells was performed. This analysis was performed in the context of endothelial markers VE-cadherin and VEGFR2, in addition to progenitor markers c-Kit and Sca1.

c-Kit expression has been associated with the progenitor status of cells within the BM [97, 184, 185]. It is a receptor for Steel Factor (a.k.a. stem cell factor) and can promote progenitor cell viability [186]. c-Kit and VEGFR2 are within the same phylogenetic platelet derived growth factor (PDGF) receptor family and both are located on chromosome 4q12 [187]. It has been demonstrated that the disruption of c-Kit signaling by microRNA-221/222 can inhibit capillary formation of HUVEC cells [188].

Sca1 is also a BM progenitor marker that is often used in conjunction with c-Kit to define the LKS (Lin^{-} c-Kit^{+} $Sca1^{+}$) population, which is highly enriched for cells with long term reconstitution potential. Therefore, it was possible that the analysis of the LKS population in the context of endothelial markers may yield EPCs with reconstitutive potential. Sca1 has also been implicated in endothelial biology. It has been found to be over-expressed on endothelial cells in

the liver in response to tumor challenge [189]. Additionally, Sca1 has previously been used as a marker of EPCs [190].

Analysis of the resting Lin- population revealed the presence of three major populations defined by VE-cadherin, VEGFR2, c-Kit, Sca1, and CD11b as a negative control. Animals were challenged with LLC tumors to determine how these populations respond to tumor challenge in the context of expansion, mobilization, and marker expression. At day 4, 6, and 11 days post tumor challenge, Lin^- BM cells from tumor challenged animals were analyzed with the identical cocktail of antibodies. The numbers of the various populations and their reactivity with each antibody were scrutinized.

The first observation made was that the clearance of VE-$cadherin^+$ cells from the progenitor population was largely due to the clearance of the largest population of cells, defined as VE-$cadherin^+$ c-Kit^+, which were also $VEGFR2^-$ and $Sca1^-$ (Figure 33A). The dominance of this population increases as the EPC population as a whole decreases with the age of the animals (data not shown). At the earliest stage, day 4, there appears to be no clear response, in terms of cell numbers, by the other populations analyzed. However, by day 6 the recovery phase in the EPC population is apparent with the size of all EPC sub-populations reaching numbers exceeding the original resting levels.

Figure 33: VE-cadherin sub-populations respond differently to tumor challenge

A: Bi-exponential scatter plot of Lin- cells showing the expression of VE-cadherin and VEGFR2. Red ovals define the VE-Cadherin populations with and without surface VEGFR2. The blue oval denotes a population of VEGFR2+ VE-cadherin- cells. Error bars represent standard deviation.

B:Lin- cells were isolated from resting and tumor challenged animals and were quantitated based on their expression of VE-cadherin, c-Kit, Sca1, and CD11b. VE-cadherin+ cells were subdivided into 3 distinct sub-populations based on the expression of c-Kit and Sca1. n=5 per group 50,000 events counted per n. Error bars represent standard deviation.

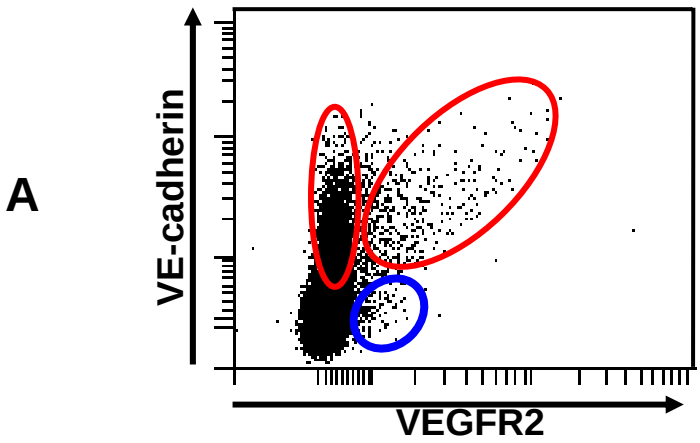
A
VE-cadherin
VEGFR2

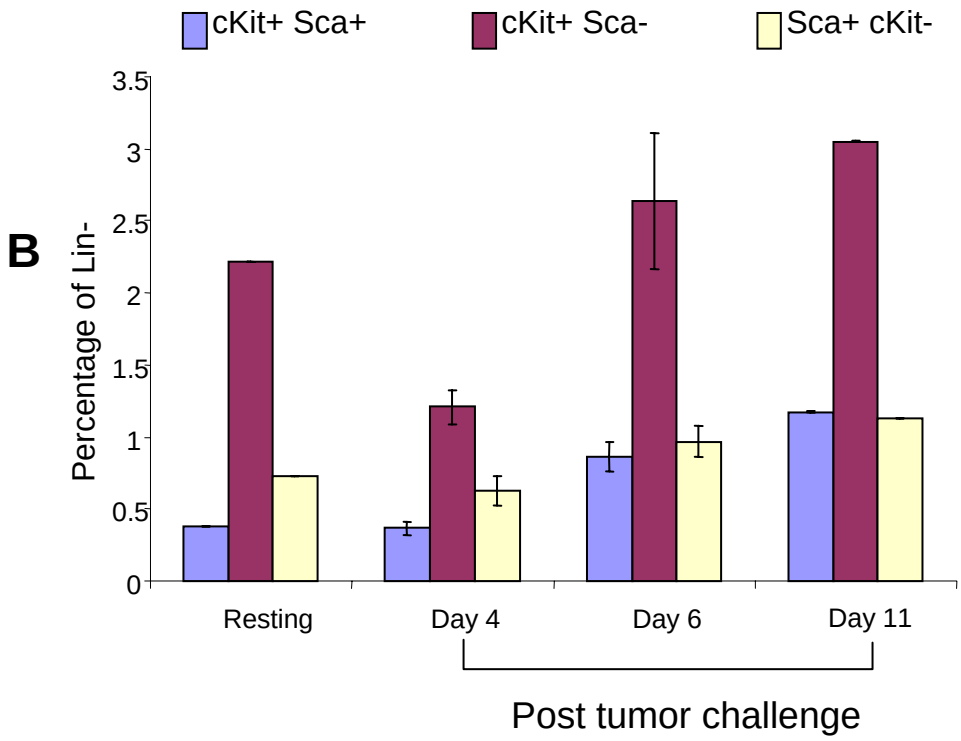
B
cKit+ Sca+
cKit+ Sca-
Sca+ cKit-
Percentage of Lin-
3.5
3
2.5
2
1.5
1
0.5
0
Resting
Day 4
Day 6
Day 11
Post tumor challenge

Figure 33

Marker expression analysis of EPCs under tumor challenge

In addition to the EPC studies focusing on the more abundant VE-cadherin^{+} cells, there is also a rare population of cells defined as VEGFR2^{+} Sca1^{+} VE-cadherin^{-} c-Kit^{-} (Figure 33B). These cells are presumably more primitive than the VE-cadherin marked populations based on the percentage of the population expressing Prominin-1 (CD133), a marker of stem cells [129, 191] in addition to EPCs [5] (Figure 34A). Upon tumor challenge, these cells begin to proliferate rapidly, more than 2 fold by day 4 and 4 fold by day 11 (Figure 34B). This rate of expansion is unparalleled by any other observed population within the BM progenitor pool. This expansion also occurs prior to any expansion observed in cell populations marked by VE-cadherin (Figure 34A). In agreement with the proposed lineage, "mature" cell types are more abundant than primitive cells. Notice, the smaller VEGFR2^{+} population's definition is reversed with respect to the markers of the EPCs found to mobilize from the BM in response to tumor challenge (Figure 34C).

In order to link the presumably more primitive VEGFR2^{+} Sca1^{+} VE-cadherin^{-} c-Kit^{-} cells to the cells found to mobilize in response to tumors VE-cadherin^{+} c-Kit^{+} VEGFR2^{-} Sca1^{-}, the mean fluorescent intensity (MFI) of each marker was analyzed. The MFI is a measurement of the level of receptor

Figure 34: VEGFR2^{+} VE-cadherin^{-} events increase in response to tumor challenge

A: Flow cytometry was used to quantitate the number of cells per 50,000 Lin- cells defined as VEGFR2^{+} Sca1^{+} VE-cadherin^{-} c-Kit^{-} CD11b^{-}, VEGFR2^{+} Sca1^{+} VE-cadherin^{+} c-Kit$^{+/-}$ CD11b^{-}, or VEGFR2^{-} Sca1^{-} VE-cadherin^{+} c-Kit^{+} CD11b^{-} in resting animals. **B:** Quantitation of VEGFR2^{+} VE-cadherin^{-} CD11b^{-} cells in the Lin- fraction of resting and tumor challenged animals. **C:** Histogram of the amount of Prominin1 receptor expressed on the VE-cadherin^{+} VEGFR2^{-} and VE-cadherin^{-} VEGFR2^{+} populations. Error bars represent standard devaitions.

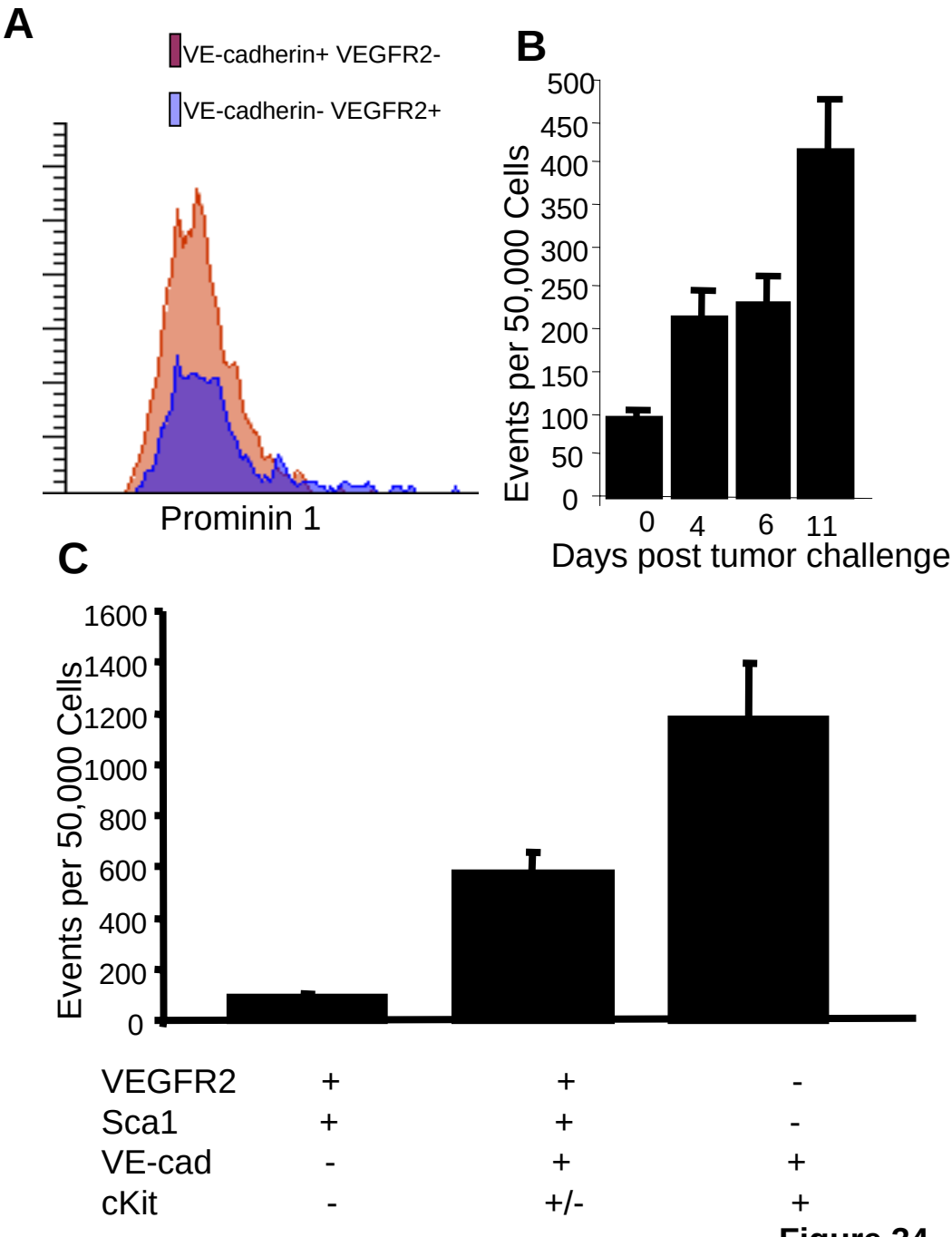
A
VE-cadherin+ VEGFR2-
VE-cadherin- VEGFR2+
Prominin 1
B
Events per 50,000 Cells
500
450
400
350
300
250
200
150
100
50
0
0
4
6
11
Days post tumor challenge
C
Events per 50,000 Cells
1600
1400
1200
1000
800
600
400
200
0
VEGFR2 + + -
Sca1 + + -
VE-cad - + +
cKit - +/- +

Figure 34

presentation on the cell surface. Indeed, the analysis of the markers on the VEGFR2$^+$ VE-cadherin$^-$ cells over the course of tumor challenge showed a dramatic change in the level of receptors expressed. In a resting animal, c-Kit expression on these cells was only detectable on less than 10% of the cells. However, c-Kit expression increased consistently during tumor challenge. By day 11, the c-Kit MFI increased three fold resulting in 85% of VEGFR2$^+$ VE-cadherin$^-$ cells becoming c-Kit$^+$ (Figure 35A).

The most dramatic change observed of any single antigen was Sca1 (Figure 35B). The VEGFR2$^+$ Sca1$^+$ VE-cadherin$^-$ c-Kit$^-$ population of cells were strongly positive for Sca1 in resting animals, however this level of expression dropped two fold by day 4 and four fold by day 11. As robust as the Sca1 loss was, these cells did not become Sca1$^-$ in any significant numbers at any time.

Finally, VEGFR2$^+$ Sca1$^+$ VE-cadherin$^-$ c-Kit$^-$ cells appeared to increase their basal level of VE-cadherin (Figure 35C). This data is not without a significant caveat. As a cell begins to express enough VE-cadherin, it will no longer be considered VE-cadherin$^-$ and would not be included within this population, therefore underestimating the amount of VE-cadherin increase. Together, the changes in the receptor profile of all VEGFR2 and VE-cadherin expressing cells suggest these populations are linked within a single lineage with VEGFR2$^+$ Sca1$^+$ VE-cadherin$^-$ c-Kit$^-$ cells as the most primitive detected, VE-

cadherin^{+} c-Kit^{+} VEGFR2^{-} Sca1^{-} cells capable of mobilizing in response to tumors and VE-cadherin^{+} c-Kit$^{+/-}$ VEGFR2^{+} Sca1^{+} cells as a possible intermediate population.

Figure 35: Tumor challenge affects marker presentation on VEGFR2$^+$ VE-cadherin$^-$ cells

Flow cytometry was used to quantitate the mean fluorescent intensities (MFI) of **A:** c-Kit **B:** Sca1 and **C:** VE-cadherin on VEGFR2$^+$ VE-cadherin$^-$ cells. Error bars represent standard deviation. *Note: As cells increase their expression of VE-cadherin until the point they are considered VE-cadherin$^+$, they will no longer be quantified in this group.*

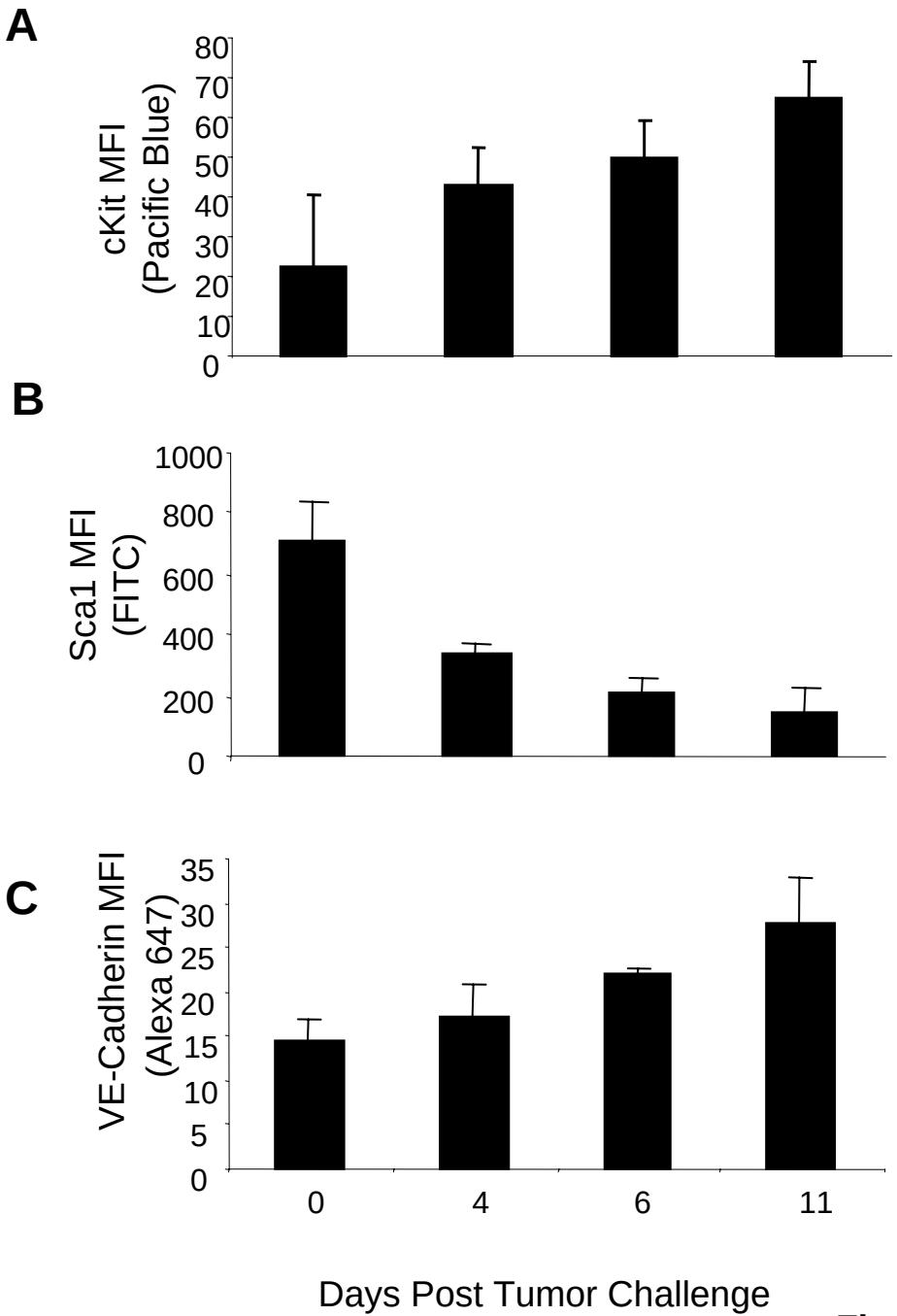
A
cKit MFI (Pacific Blue)
80
70
60
50
40
30
20
10
0
B
Sca1 MFI (FITC)
1000
800
600
400
200
0
C
VE-Cadherin MFI (Alexa 647)
35
30
25
20
15
10
5
0
0
4
6
11
Days Post Tumor Challenge

Figure 35

VEGFR2 is maintained in an intracellular pool of recycling endosomes

The proposed lineage of EPCs within the BM Lin^- contains a critical contradiction to the literature, as EPCs are well known to be defined by VEGFR2 [5]. However, the detection method used only measures the level of VEGFR2 presented on the cell surface. Any VEGFR2 receptor held internally would evade detection. It has recently been observed that VEGFR2 can be maintained internally and possibly indefinitely in short loop recycling endosomes [192]. Gampel and colleagues investigated the intracellular trafficking of VEGFR2 in recycling endosomes. The concept of VEGFR2 recycling endosomes is not surprising. Endosomes marked by the GTPase Rab4 are considered recycling endosomes. As opposed to other endosomes that would direct their payload for degradation, $Rab4^+$ endosomes are capable of returning their contents to the cell surface after only several minutes [193, 194]. The surprising finding made by Gampel, is that within the population of $Rab4^+$ endosomes lie endosomes that are stationary and remain so until the cell is properly stimulated.

The studies of VEGFR2 within $Rab4^+$ endosomes in mature endothelial cells indicated a similar mechanism may be in play within VE-$cadherin^+$ c-Kit^+ $VEGFR2^-$ $Sca1^-$ EPCs. To test this hypothesis, Lin^- cells were harvested, cytospun, fixed, and permeabilized. The use of microscopy for detection allowed for the detection of both membrane bound and internalized VEGFR2. Indeed,

VE-cadherin$^+$ EPCs presented VEGFR2 in two unique manners. The first pattern was VEGFR2 with an overlapping pattern on VE-cadherin on the membrane (Figure 36A). This likely represents the VE-cadherin$^+$ VEGFR2$^+$ cells within the LKS detected by flow cytometry. The second population of VE-cadherin$^+$ cells contained no discernable membrane localized VEGFR2. These cells did, however present VEGFR2 staining colocalizing with subset of the Rab4$^+$ endosomes. These endosomes were cytoplasmically located and represented only a small fraction of the total Rab4$^+$ endosomes (Figure 36B), as expected. Attempts were made to stimulate the EPCs to direct the Rab4$^+$ endosomes containing VEGR2 to the membrane by stimulation with various cytokines at a range of concentrations, however no single cytokine or combination was capable of accomplishing this (data not shown).

Figure 36 VEGFR2 is found on membrane and in cytoplasm

A: Immuno fluorescent staining of cytospun Lin- cells depicting the VEGFR2 (magenta) expression on the membrane of VE-cadherin+ (green) EPCs. **B:** An alternative presentation of VEGFR2 on cytospun Lin- cells colocalizing with cytoplasmic Rab4+ endosomes (red). Scale bar, 2μm.

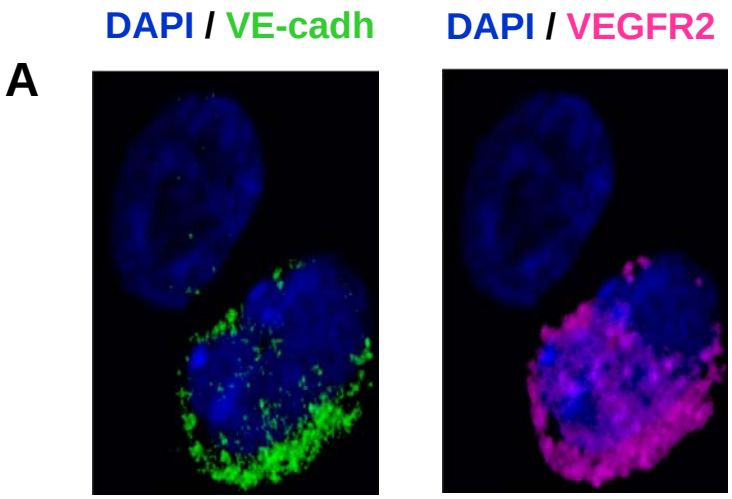
A
DAPI / VE-cadh
DAPI / VEGFR2

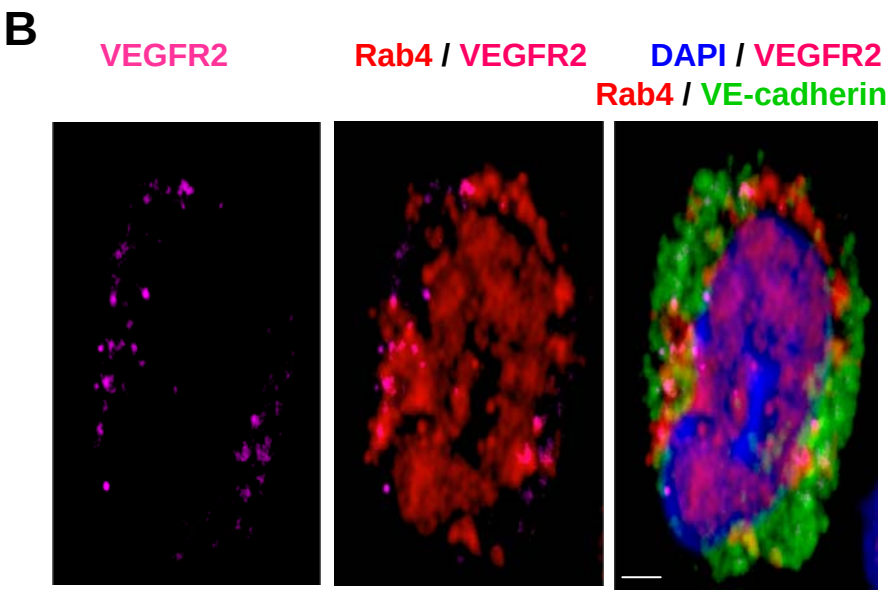
B
VEGFR2
Rab4 / VEGFR2
DAPI / VEGFR2
Rab4 / VE-cadherin

Figure 36

VEGFR2 and VE-cadherin marked cells are incapable of reconstitution

The isolation of a cell type that has the capacity to specifically reconstitute the endothelial lineage in a donor animal could have far reaching implications for cancer patients, heart disease patients, diabetics, and others. I therefore tested if cells in the Lin^- cells marked by either VEGFR2 or VE-cadherin had the capacity to reconstitute the endothelial lineage of recipient animals. Animals constitutively expressing GFP (β-actin GFP) were used as EPC donors. After lineage depletion, progenitors were stained for VEGFR2 and VE-cadherin and sorted into two populations, VE-cadherin$^+$ (which contains ~80% of all VEGFR2$^+$ cells) and VEGFR2$^+$ VE-cadherin$^-$ populations. 5000 VE-cadherin$^+$ cells or 2500 VEGFR2$^+$ cells were implanted into lethally irradiated hosts. Since these cells are not expected to contribute to either hematopoiesis or erythropoiesis, a radioprotective dose of WT GFP$^-$ TBM ($2x10^6$ cells) was also injected to prevent anemia or compromise the immunocompetence of the recipients. Any EPCs from the WT animal were outnumbered by at least 50 fold compared to the sorted GFP$^+$ EPCs, and were therefore not considered to be competing with the sorted GFP$^+$ cells. As a negative control injection, Lin- depleted of all cells marked by VEGFR2 and VE-cadherin were also sorted and injected ($2.5x10^5$).

Animals were allowed to reconstitute for 4 weeks and then challenged with LLC tumors. Early tumors, which are now known to harbor the highest

concentrations of BM-derived EPCs and ECs, were analyzed. As a positive control, GFP^+ TBM transplants were also compared at this time point. The positive control confirms that BM-ECs should be present in the tumor (Figure 37 upper left panel, green box), however neither the VE-cadherin nor VEGFR2 marked populations were capable of contributing to the endothelial lineage. Surprisingly, the negative control, which was thought to be depleted of any cell in the endothelial lineage, fully reconstituted the endothelial lineage (Figure 37, lower right panel). Note that there does appear to be a population of GFP^+ cells in the $VEGFR2^+$ transplant, however it is most likely that this is the result of a small amount of impurities in the sort is bolstered by the lack of reconstitution of $VEGFR2^+$ or VE-$Cadherin^+$ cells in the BM progenitor population (data not shown).

Figure 37: VE-cadherin and VEGFR2 do not define a reconstitutive population

Flow cytometric analysis of LLC tumors (day 8) implanted on BMT animals which received either total bone marrow (TBM, upper left), VE-cadherin^{+} Lin^{-} cells (upper right), VEGFR2^{+} VE-cadherin^{-} cells (lower left), or VEGFR2^{-} VE-cadherin^{-} Lin^{-} cells (lower right) flow sorted from GFP^{+} donors. Green box marks bone marrow-derived endothelial cells. 100,000 events counted per specimen.

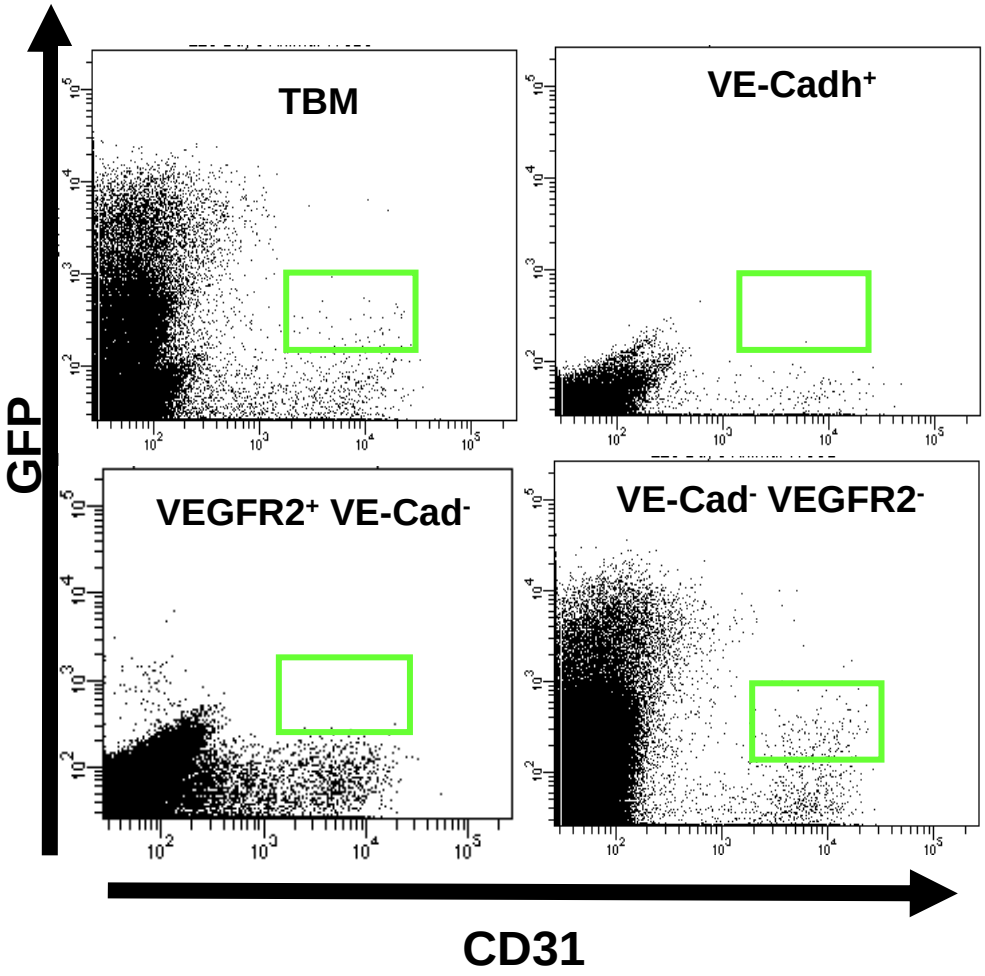

Figure 37

Chapter 4 Discussion

Unfortunately, this proposed lineage of VEGFR2 and VE-cadherin marked EPCs can not be confirmed, and must be considered speculative. The only way to confirm this proposed lineage is to identify a population of cells capable of exclusive reconstitution of EPCs. Despite the repeated efforts, I was unable to identify this population. At this point, the matter of a pure EPC reconstituting cell existing is still an assumption. It is possible that the population of cells responsible for the reconstitution of the endothelial lineage in the bone marrow is also responsible for the reconstitution of one or more additional lineages. However, this does not discredit the proposed lineage. The EPCs described here are defined by two markers that are specific to endothelial cells in the adult animals [5, 126]. EPCs sorted from the BM progenitor population have been confirmed to be bona fide endothelial cells (Figure 9). The exit of EPCs from the BM coincide with their arrival at the periphery of tumors (Figures 33,34). The expression of the various progenitor markers, the change in marker expression upon tumor challenge, and their relative abundance are all consistent with a continuous lineage of EPCs (Figures 34-36, [97, 129, 184, 185, 190, 191]).

As the first findings of even a presumptive lineage of EPCs within the BM, this set of data offers many exciting avenues of further development. One option that offers great promise is the eventual ability to culture and expand pure

EPCs for use in therapeutics. This would require a detailed understanding of the lineage to harvest, expand, and maintain their differentiation status with fidelity. The use of BM progenitor injections have already been shown to be advantageous [39, 40] in repair and the use of pure populations may serve to enhance this.

On the other hand, the ability to specifically inhibit the EPC lineage may have a profound anti-angiogenic phenotype when used in the context of other therapies, such as a vascular disruptive agent which have been shown to induce a influx of mobilized EPCs [195]. For example, a deeper understanding of the retention of a cytoplasmic pool VEGFR2 within $Rab4^{+}$ may result in an opportunity to inhibit EPCs. There are several possibilities to explain how VEGFR2 retention in recycling endosomes that may be utilized in inhibiting EPC fucntion. As several stages in the EPC lineage express VEGFR2, this may be a mechanism to control their responses to VEGF, as I have demonstrated that different populations respond uniquely to tumor challenge (Figure 33). EPCs may exist within even more discreet states within the lineage, and this VEGFR2 retention may prevent premature mobilization of the EPC. Alternatively, VEGF may be one of the final cytokines to signal differentiation into a mature EC. Therefore sequestering VEGFR2 within the cytoplasm may prevent the premature differentiation of EPCs within the BM, maintaining a population of EPCs poised to respond to a specific set of stimuli. Regardless of the reason, the prevention of

VEGFR2 presentation on the membrane acutely on EPCs may serve to temporarily inhibit their function during a specific phase of a cancer therapy without compromising the need for EPCs in their wound healing ability afterwards. However, the inability to identify the mechanism of VEGFR2 stimulation currently makes this a practice in theory, as it may ultimately be discovered a technically infeasible task *in vivo*. Discerning the mechanism of VEGFR2 membrane presentation will be a challenge, as many factors, including structural cues from the progenitor niche, may affect the fate of the $Rab4^{+}$ endosomes.

Chapter 5 Transcriptional profiling to determine the molecular mechanisms of EPC function

The mobilization of EPCs into the peripheral circulation and subsequent differentiation into luminally incorporated BM-ECs constitute a critical step in the initiation of tumor neoangiogenesis. However, the underlying molecular mechanisms that regulate EPC fate determination and their function at the tumor site remain unknown. I have used pure EPC, host-EC, and BM-EC populations in dissecting these pathways by identifying mRNAs that are differentially regulated in response to tumor challenge. In addition to defining key mechanisms underlying the function of these cells, this analysis has the potential to provide novel markers and additional targets for inhibiting angiogenesis.

RNA isolation of flow sorted material

Several options were available for the isolation of cells for transcriptional profiling, including laser capture microscopy and magnetic sorting. However, I took advantage of the endothelial cell definitions devised by flow cytometry (see chapters 2 and 3). Fortunately, the definitions of endothelial cells at various stages were well established by flow cytometry, which was directly transferable to fluorescence-activated cell sorting (FACS).

Because the limited number of cells available in early tumors was a major bottleneck in performing reliable microarray analysis, it was necessary to

optimize RNA isolation and linear amplification. Multiple methods of RNA extraction were evaluated for their ability to isolate RNA from flow sorted samples. Specifically, two commercially available kits have been designed for the isolation of RNA from small amounts of starting material, one from Arcturus and the other from Stratagene. These kits were compared for their ability to recover RNA from live or mildly fixed cells. Fixed cells had the potential to prevent RNA degradation during the sorting procedure.

Lungs were chosen as a control organ due to the presence of a large amount of endothelial cells which were clearly defined by flow cytometry (data not shown). Lungs were dissociated, and either fixed in 1% formalin or left live. The quality of the RNA extractions was then determined on Agilent's Bioanalyzer using the Pico 6000 RNA assay. As seen in Figure 38, the Arcturus protocol was superior to Stratagene's in terms of RNA integrity. Note the lack of 28S ribosomal peaks in the Stratagene isolated material. Both methods of RNA isolation failed to yield reliable material from fixed samples. I therefore used collagenase to dissociate cells, and serum-free media for direct sorting (this enhanced cell viability, data not shown). After collection, cells were pelleted and RNA was extracted using a modified Arcturus protocol (see materials and methods, protocol modification optimized by Anirban Paul, Huang Laboratory, CSHL).

Figure 38: Optimizing RNA extraction from sorted cells

Equivalent amounts of cells were havested identically in each of two commercially available RNA isolation kits after a 3 hour incubation with or without fixation by 1% formalin. Arrows denote 18S and 28S ribosomal peaks, where detectable. RNA was analyzed via Agilent RNA 6000 Pico-chip.

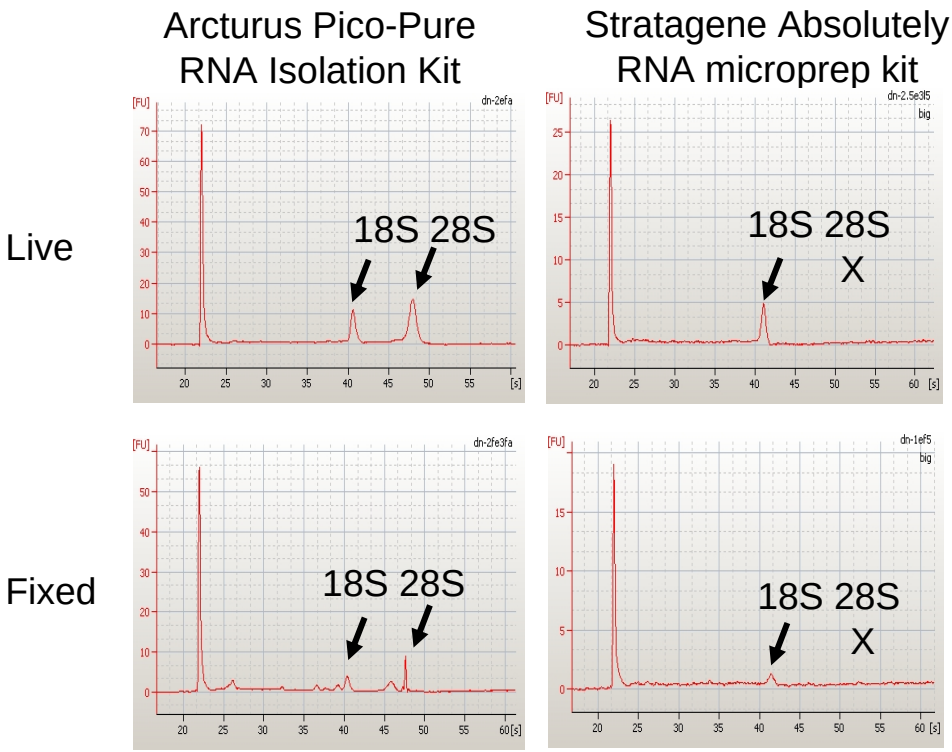
Arcturus Pico-Pure
RNA Isolation Kit
Stratagene Absolutely
RNA microprep kit
Live
Fixed
18S 28S
18S 28S
X
18S 28S
18S 28S
X

Figure 38

RNA and aRNA quality from flow sorted material

Conventional gel based or spectrophotometric assays do not provide a reliable quantitation of small amounts of the initial harvest RNA. I therefore used the Agilent BioAnalyzer platform; which is capable of quantitating RNA with samples smaller than 1ng. Furthermore, the Bioanalyzer software is able to discern RNA quality by examining multiple parameters in the output trace files and calculating an RNA integrity number (RIN) [196]. RINs range from 1 (poor) to 10 (perfect). RINs were routinely achieved between 7 and 10 (Figure 39A). Occasionally, small cell populations (X<500 cells), yielded too little RNA to be accurately measured by the BioAnalyzer (Figure 39B). Notably, these small populations still provided sufficient quantity of aRNA after two rounds of amplification for array hybridization (Figure 39C).

I also performed analysis of the aRNA size range following two rounds of amplification, since such a protocol has been reported to generate products of smaller size [197]. Sizes ranged from 500bp to 700bp, which was fairly consistent from comparatively large (500,000 cells) and small populations (x<500 cells) as assayed using Agilent's BioAnalyzer RNA 6000 Nano Chip in a smear analysis assay (data not shown). The amplified material was then hybridized to the Affymetrix chip (Mouse genome 430A 2.0). The lowest amount of cellular material to yield a satisfactory array was ~250 cells. Following hybridization, the

Affymetrix hybridization control metrics were used to pass image data (see materials and methods). Chips that had unsatisfactory quality metrics were not included in the data analysis. Robust multichip analysis (RMA) was used to normalize file data for further analysis [198].

Figure 39: RNA quality of flow sorted and amplified material

A: Agilent RNA 6000 Pico chip analysis of RNA sorted from a day 5 tumor defined as $CD31^{+}$ GFP^{+} $Isolectin^{+}$ $CD11b^{-}$. **B:** Analysis of a population of EPCs obtained from a day 5 tumor in a BMT animal, defined as GFP^{+} $VE\text{-}cadherin^{+}$ $CD31^{low}$ $CD11b^{-}$. **C:** aRNA traces after two rounds of amplification of the material from **B**.

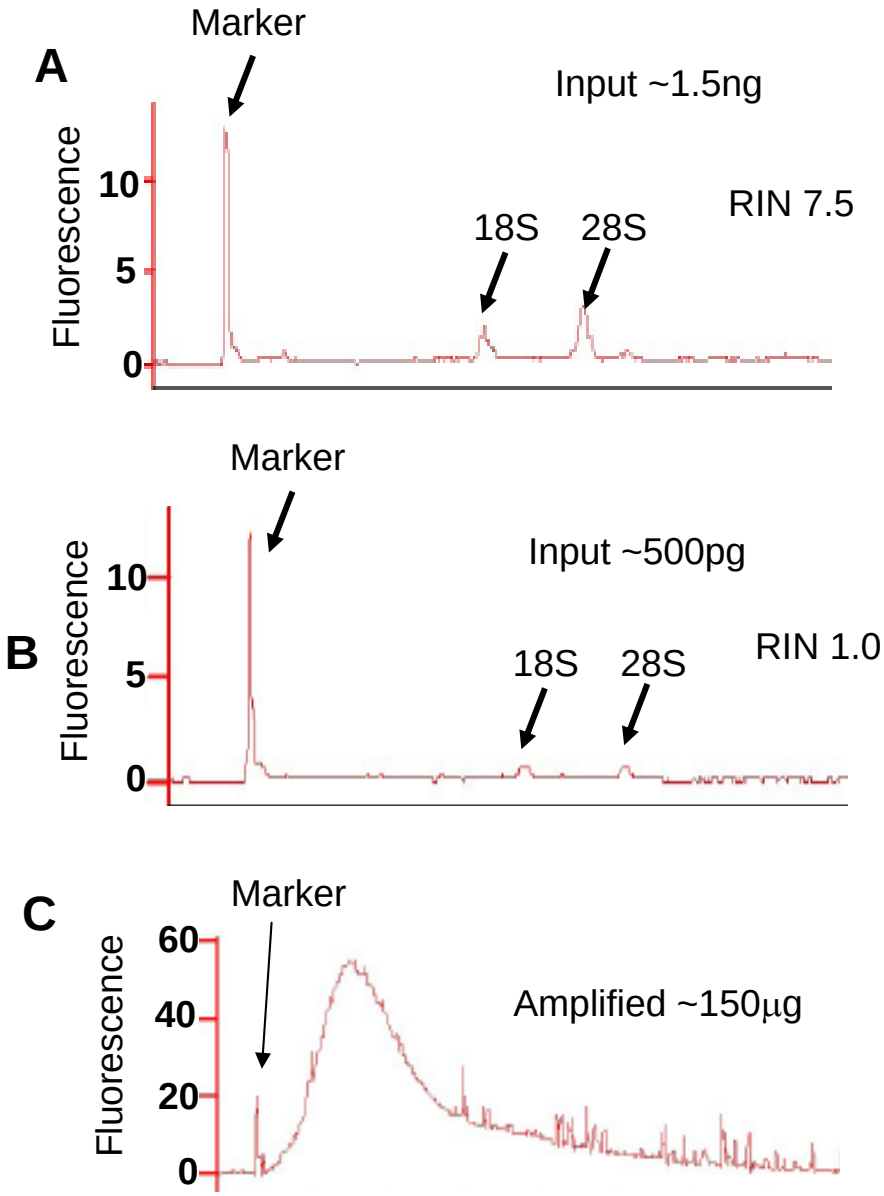
A
Marker
Input ~1.5ng
Fluorescence
10
5
0
18S
28S
RIN 7.5
B
Marker
Input ~500pg
Fluorescence
10
5
0
18S
28S
RIN 1.0
C
Marker
Fluorescence
60
40
20
0
Amplified ~150µg

Figure 39

Comparison of EPCs, BM-ECs, and host-ECs from tumors

GFP^+ BMT animals were challenged with LLC tumors, and tumors were harvested from days 4-8 after implantation. As described before, EPCs were (GFP^+ VE-cadherin$^+$ $CD31^{low}$ $CD11b^-$), BM-ECs ($CD31^+$ Isolectin$^+$ GFP^+ $CD11b^-$), and Host ECs ($CD31^+$ Isolectin$^+$ GFP^- $CD11b^-$) were isolated by FACS. Following RNA isolation, amplification, and hybridization in triplicate, the chips were normalized, and a hierarchical cluster was created (prepared in Bioconductor, R package). The hierarchy depicted a relationship between the three populations and their replicates (Figure 40).

As expected, each population clustered with biological replicate experiments. Of the three populations, the BM-ECs clustered particularly tightly. While EPCs and host-ECs still clustered with each other, their looser correlation could possibly be due to heterogeneity within the host-EC population and asynchronous EPCs. Notably, BM-ECs and EPCs clustered separately suggesting differences in gene expression patters among these groups. BM-ECs were more similar to host-ECs than EPCs. This observation is also confirmed by normalized log ratio data in a scatter plot of averaged groups between BM-ECs v host-ECs and EPCs v BM-ECs (Figure 41A,B).

Figure 40: Cluster Dendogram of EPCs, BM-ECs, and host-ECs from tumors

A representative cluster dendogram based on the similarity and disimilarities between EPCs, BM-ECs, host-ECs. Correlations were derived from the normalized log scale ratios.

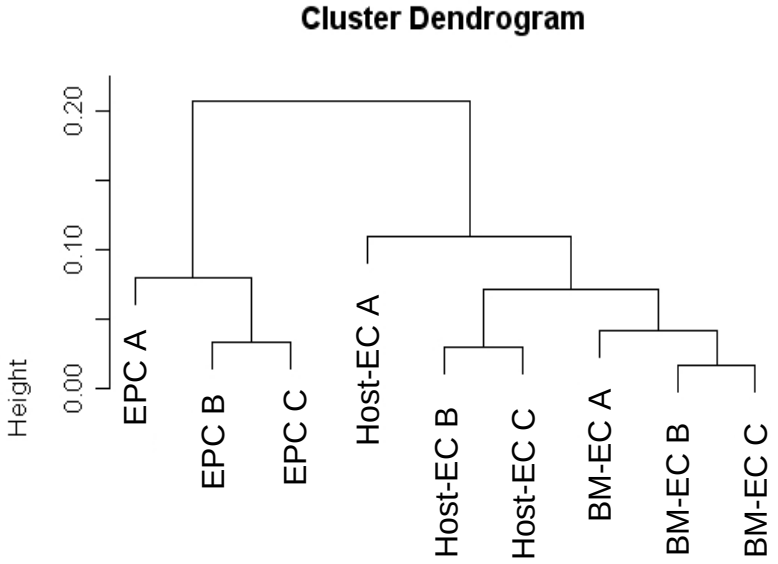
Cluster Dendrogram
Height
0.00
0.10
0.20
EPC A
EPC B
EPC C
Host-EC A
Host-EC B
Host-EC C
BM-EC A
BM-EC B
BM-EC C

Figure 40

Figure 41: Scatter plot of Host-EC v BM-EC and BM-EC v EPC

A: Normalized log ratio data is presented as a scatter plot visualization from Host-ECs (n=3) and from BM-ECs (n=3). **B:** Scatter plot visualization of averaged signals averaged from BM-ECs (n=3) and from EPCs (n=3). Scatter plot drawn with Array Assist software.

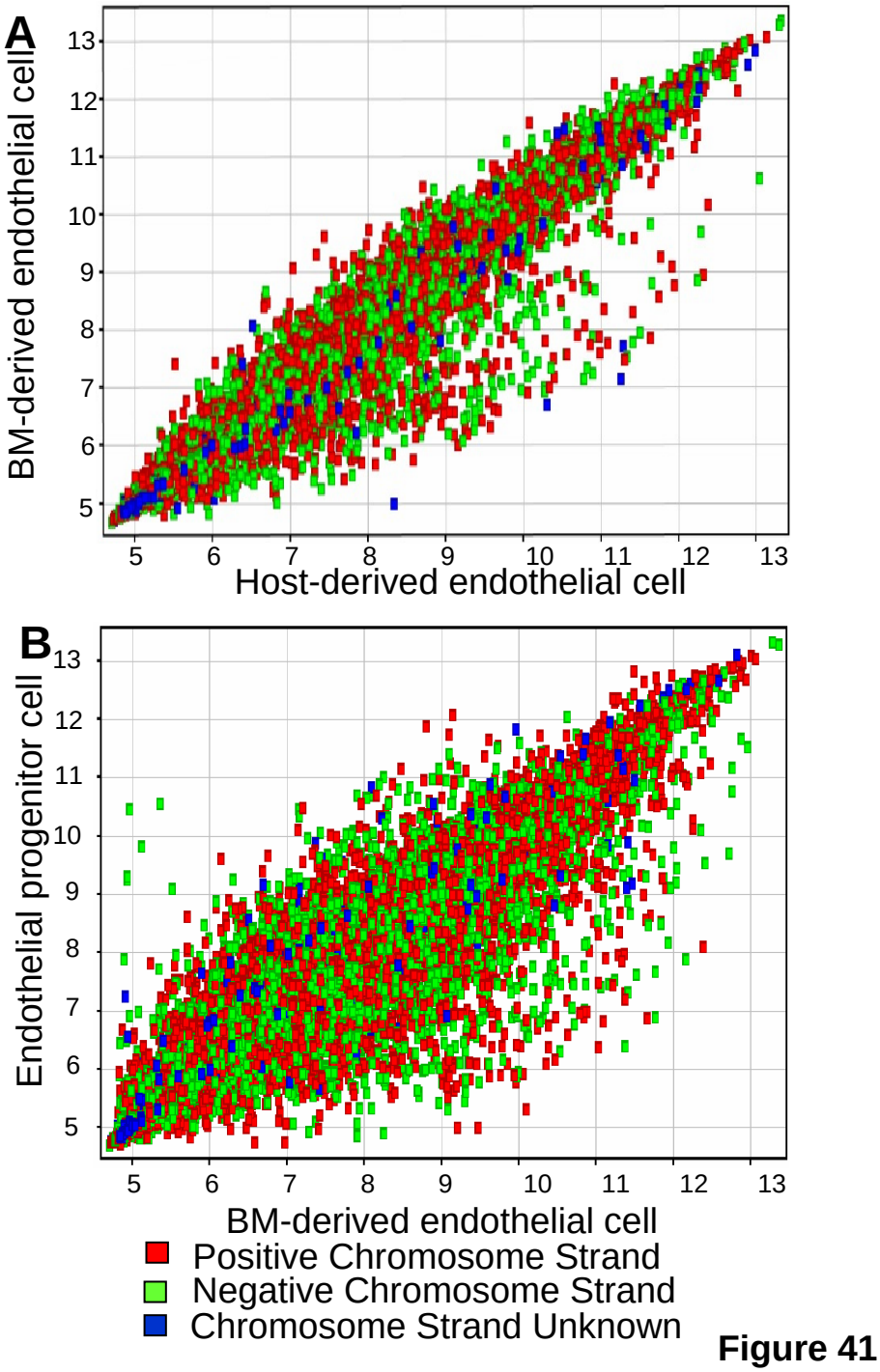
A
BM-derived endothelial cell
Host-derived endothelial cell
B
Endothelial progenitor cell
BM-derived endothelial cell
Positive Chromosome Strand
Negative Chromosome Strand
Chromosome Strand Unknown

Figure 41

BM-ECs and EPCs have distinct angiogenic and ECM profiles

The chip used, GeneChip Mouse Genome 430A 2.0, represents approximately 14,000 mouse genes. Between the three populations analyzed, 19 targets were differentially regulated with an adjusted P value under 0.0002, 352 targets with an adjusted P value under 0.002, and 2258 targets under 0.02. Statistical significance was calculated by one-way Anova, the P-value was adjusted to account for false discovery rates (FDR, Benjamini and Hochberg). A list of genes involved in angiogenesis was generated for comparison to study the differences between populations. Only statistically significant genes were included, in addition to several genes that showed very large differences. This comparison is represented as a heat-map depicting either higher or lower signal intensity (Figure 42).

Angiogenic, Progenitor, and Hematopoietic Markers: As shown in Figure 42, EPCs expressed higher levels of Thy1, a known progenitor marker [199]. Pecam1 (CD31) expression was also upregulated as EPCs differentiate into BM-ECs, consistent with the levels of CD31 protein observed before (Figure 3). EPCs express higher levels of CD45 (Ptprc) in agreement with previous studies [21, 200]. There was also a correlation between the EPC/BM-EC/host-EC populations and control populations of hematopoietic origin, tumor-derived GFP^+ $CD11b^+$ $CD31^-$ cells. This population displayed lower intensities for transcripts of

Figure 42: Heat map comparing BM-ECs to EPCs

Major angiogenic genes and comparitively disregulated genes between BM-ECs and EPCs was generated. Genes are either up (green) or down (red) regulated.

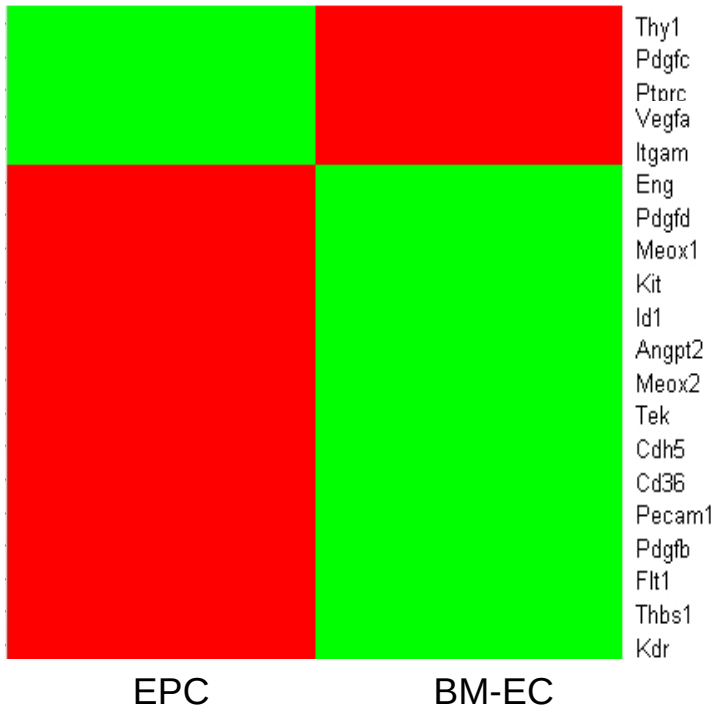
Thy1
Pdgfc
Ptprc
Vegfa
Itgam
Eng
Pdgfd
Meox1
Kit
Id1
Angpt2
Meox2
Tek
Cdh5
Cd36
Pecam1
Pdgfb
Flt1
Thbs1
Kdr
EPC
BM-EC
Up-regulated
Down-regulated

Figure 42

endothelial genes, such as VEGFR2, VE-Cadherin, and CD31 while expressing higher levels of hematopoietic transcripts, such as CD11b (data not shown)

Surprisingly, many other genes associated with endothelial biology suggest a remarkable divergence between EPCs and BM-EC. For example, BM-ECs expressed higher levels thrombospondin (Thbs1), which is a potent anti-angiogenic compound. BM-ECs also express higher levels of CD36, one of the receptors for thrombospondin [201]. BM-ECs also express higher levels of Tie2 (Tek) and its corresponding ligand, angiopoietin 2 (angpt2) [202].

Extracellar Matrix: Extracellular matrix (ECM) components showed varying levels of expression between EPCs and BM-ECs. Several collagens and procollagens showed higher expression in EPCs, while others were expressed higher in BM-ECs. However, there was little difference between the expression level of these ECM components between BM-ECs and host-ECs (Table 2). ECM components are well known to have varying effects on angiogenesis [17, 203-208]. Interestingly, one of the pro-collagens is the precursor for endostatin (Col18a1). Endostatin is a potent anti-angiogenic compound which is released upon the degradation of the ECM [209].

Chemokines and Receptors: Chemokines and their receptors are critical for both immune and non-immune cells for communication and co-localization [210, 211]. A comparison of chemokines and chemokine receptors shows a

Table 2: Selected extracellular matrix associated genes with statistically significant changes in expression compared to BM-ECs.

Gene Symbol	Gene Name	Genbank	Host-EC vs BM-EC	BM-EC vs EPC	P.value
Col15a1	collagen, type XV, alpha 1	AF011450	1.55	7.94	0.00326406
Col18a1	procollagen, type XVIII, alpha 1	NM_009929	1.30	7.77	0.00690662
Col4a1	procollagen, type IV, alpha 1	BF158638	1.55	9.83	0.0016399
Col4a2	procollagen, type IV, alpha 2	BC013560	1.41	7.19	0.00083716
Col5a2	procollagen, type V, alpha 2	AV229424	1.05	-5.26	0.04657566
Col5a3	procollagen, type V, alpha 3	NM_016919	1.03	-3.91	0.00609152
Col6a1	procollagen, type VI, alpha 1	NM_009933	1.28	-4.75	0.00789236
Col6a2	procollagen, type VI, alpha 2	BI455189	1.17	-5.17	0.00734533
Col16a1	procollagen, type XVI, alpha 1	BB766878	1.02	-2.02	0.02191113

Table 3: Selected chemokine and receptor genes with statistically significant changes in expression between Host ECs, BM-ECs, and EPCs.

Gene Symbol	Gene Name	Genbank	Host-EC vs BM EC	BM-EC vs EPC	P.value
Ccl25	chemokine (C-C motif) ligand 25	NM_009138	1.01	2.36	0.00978
Ccl7	chemokine (C-C motif) ligand 7	AF128193	-2.57	-1.07	0.003038
Ccr1	chemokine (C-C motif) receptor type 1	AV231648	-9.69	1.51	0.010592
Ccr2	chemokine (C-C motif) receptor type 2	BB148128	-6.682	4.31	0.006907
Cxcl10	Chemokin (C-X-C motif) ligand 10	NM_021274	1.61	-8.14	0.026587
Cxcl11	Chemokin (C-X-C motif) ligand 11	NM_019494	1.78	-5.67	0.041232
Cxcl12	Chemokin (C-X-C motif) ligand 12	NM_013655	-1.09	-19.330	0.00426
Cxcl16	Chemokin (C-X-C motif) ligand 16	BC019961	-5.09	2.15	0.017317
Cxcl4	Chemokin (C-X-C motif) ligand 4	NM_019932	-9.71	2.81	0.034901
Cxcl7	Chemokin (C-X-C motif) ligand 7	NM_023785	-5.05	-3.38	0.040885
Cxcr4	chemokin (C-X-C motif) receptor 4	D87747	1.64	-2.61	0.01619

unique profile for the EPCs, BM-ECs, and host-ECs. This result suggests that each cell type may have a distinct sensitivity to chemokines within their microenvironment. Collectively, these transcriptional profiling experiments demonstrate that distinct gene expression signatures were obtained from EPCs, BM-ECs, and host-ECs which may be indicative of their respective functions.

Transcriptional profiling target validation

Select candidates obtained from the transcriptional profiling experiments were subjected to validation *in vivo*. Two endothelial genes with known angiogenic roles were selected from the list of genes with significantly different expression. VE-cadherin (cdh5) and Tie2 (Tek) were both found to be up regulated in BM-ECs compared to host-ECs (Figure 42). BMT animals were challenged with LLC tumors and subjected to flow cytometric analysis. The ECs were then gated for their expression of Tie2 which revealed it is expressed on a larger proportion of BM-ECs than on host-ECs (Figure 43A). Interestingly, BM-ECs also express higher levels of Angiopoietin-2 (angpt2) compared to host-ECs. Angiopoietin 2, a ligand for Tie2, can either behave agonistically or antagonistically in a context dependent manner with other cytokines, such as VEGF. One of these functions is to promote vascular stability through Tie2 [212-215]. With respect to VE-cadherin, MFI measurements showed a 2 fold increase of receptor density on the cell surface of BM-ECs (Figure 43B). One of the effects of angiogenic stimuli is the down-regulation of VE-cadherin [173, 174, 176, 177], suggesting the possibility that host-ECs are sensitized to angiogenic factors or simply in a higher state of angiogenic activation compared to BM-ECs.

To determine if the vascular phenotype of tumors correlates with EPC/BM-EC contribution (early tumors) and their subsequent dilution (late

tumors), a kinetic analysis of tumors was performed following Isolectin injection to estimate vessel functionality. Endothelial cells, $CD31^+$ $CD11b^-$, were measured for both their ability to bind Isolectin (% of $Isolectin^+$ ECs, Figure 43Ctop) and the strength of this binding (Isolectin MFI on ECs, Figure 43Cbottom). Both the functionality of the ECs and their ability to bind Isolectin, a measure of their exposure to blood flow, decreased as a function of tumor growth. Coincidentally, the peak of EC function in blood vessels corresponds with the EPC/BM-EC peak at day 6 (Figure 43C, red box).

Figure 43: Endothelial markers and functional kinetics of tumor vasculature

A: Quantiation of the percentage of cells expressing Tie2 receptor on BM-ECs, $CD31^+$ GFP^+ $Isolectin^+$ $CD11b^-$, and Host-ECs, $CD31^+$ GFP^- $Isolectin^+$ $CD11b^-$. **B:** Quantitation of the mean fluorescent intensity (MFI) of VE-cadherin (Qdot 705 conjugate) on BM-ECs and Host-ECs. **C:** BMTs (n=5 per time point) were given a 50mg injection of Isolectin GSIB4 (Pacific Blue conjugate) and analyzed by flow cytometry at days 4, 6, 10, and 14. Quantiatation of Isolectin presence (top) and intensity (bottom) on ECs is shown with peak EPC/BM-EC contribution noted by the red box. Error bars represent standard deviation.

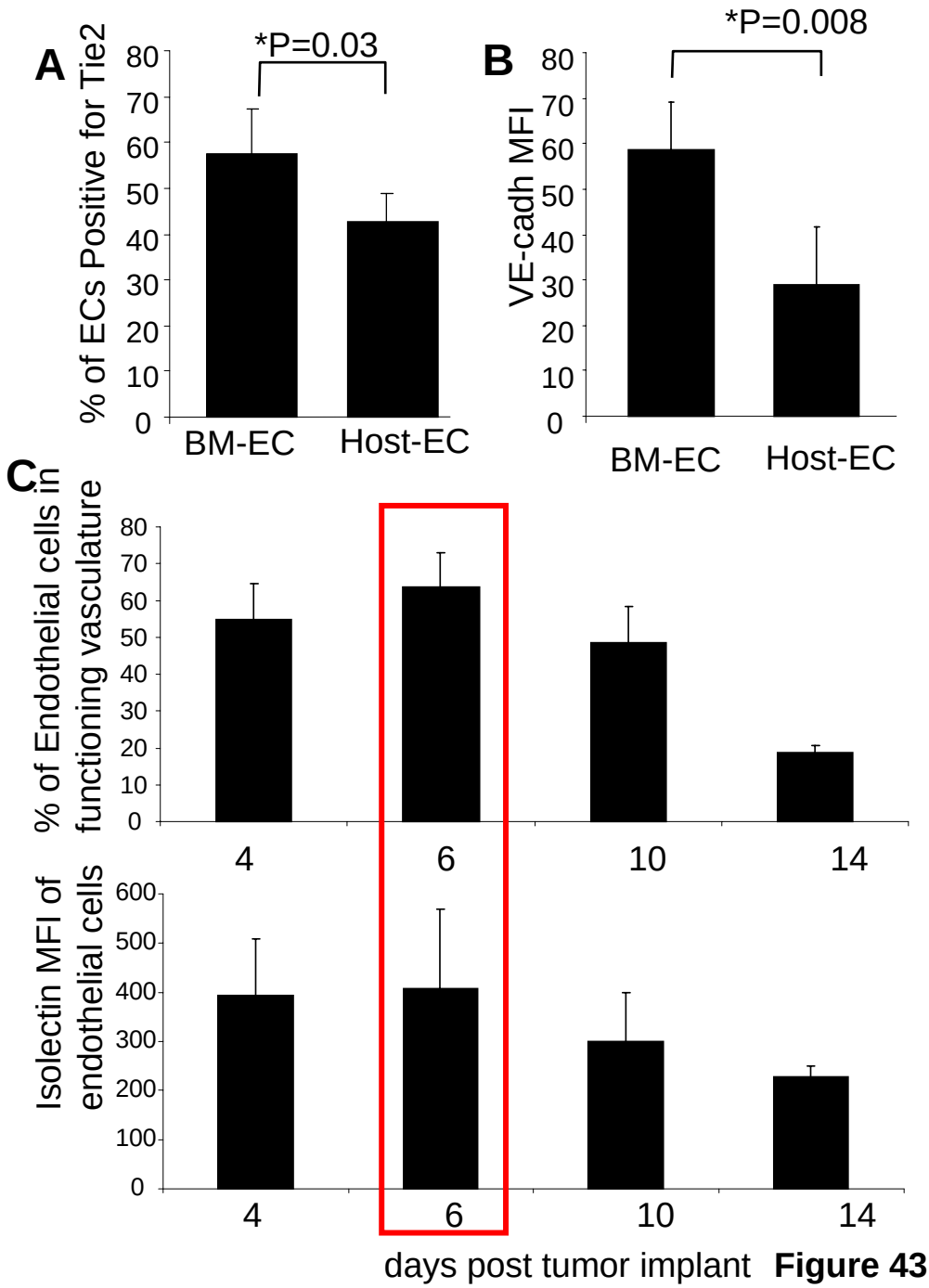
A
*P=0.03
% of ECs Positive for Tie2
80
70
60
50
40
30
20
10
0
BM-EC
Host-EC
B
*P=0.008
VE-cadh MFI
80
70
60
50
40
30
20
10
0
BM-EC
Host-EC
C
% of Endothelial cells in functioning vasculature
80
70
60
50
40
30
20
10
0
4
6
10
14
Isolectin MFI of endothelial cells
600
500
400
300
200
100
0
4
6
10
14
days post tumor implant

Figure 43

Chapter 5 Discussion

Transcriptional profiling has great potential to provide mechanistic insights into tumor angiogenesis. Indeed, genome-wide transcriptional profiling has unveiled critical aspects of tumor vasculature, as compared to normal endothelium (reviewed in [216]). Candidates, such as the tumor endothelial marker (TEM) family of markers [217-220], roundabout 4 (ROBO4) [220, 221], and endothelin 1 [220, 221] have been identified from multiple profiling experiments.

The work described in this study has shown that tumor progression is associated with distinct populations of ECs derived from the bone marrow and the host. These populations can be reliably harvested and profiled for their mRNA expression changes. The transcription profiles of EPCs, BM-ECs, and host-ECs provide some tantalizing cues as to molecular mechanisms that govern the formation of neovasculature in growing tumors. EPCs appeared to express various ECM related proteins that may be one of the initial responses in preparing the microenvironment to be conducive for recruitment of host vessels from the periphery of the tumor. This may be mediated in concert with the expression of various chemokines and their receptors, which provide direction to the surrounding host-ECs. The profiles of the host-ECs compared to the BM-ECs suggest the possibility that host-ECs may be stimulated into a more angiogenic

state, while the BM-ECs may act as a stabilizing force. Note that BM-ECs upregulate PDGF (β and δ isoforms) and downregulate VEGFa following differentiation (Figure 42), which is likely to promote pericyte coverage and vessel stabilization. Also, BM-ECs have upregulated negative regulators of angiogenesis, including angiopoietin 2, thrombospondin 1, and their corresponding receptors. Also observed, was upregulation of Meox2 compared to host-ECs (data not shown). Meox2 (growth arrest-specific homeobox) is capable of inhibiting the activation of endothelial cells [222]. A potential model based on these findings is that vessel incorporated BM-ECs exert a stabilizing force on the developing vasculature, as depicted in Figure 44. Possibly, BM-ECs stabilize the vasculature by secreting various factors (PDGFb, PDGFd, angiopoietin 2, thrombospondin1), and by attracting pericytes to further support the vasculature. This model may also partially explain how BM-ECs are diluted as a function of tumor growth, as described in Figures 13 and 14. Possibly, as tumor vasculature loses the stabilizing effects of BM-ECs, it gains the characteristic chaotic and dysfunctional nature of tumor endothelium, as seen in Figure 43C.

A number of chemokines and chemokine receptors were also observed to show differential regulation. In addition to migration and recruitment, these receptors may also regulate the attraction/repulsion of certain hematopoietic cell types (Figure 45). The various cell types which colocalize with the endothelium

Figure 44: Model of stabilizing BM-ECs

Model depicing a blood vessel composed of both host-derived endothelial cells (red cells) and BM-derived endothelial cells (green cells), with secreted factors (blue arrows) and pericytes (pink cells) focused around the regions of BM-ECs. Continued neovasculature is sprouting from regions not associated with BM-ECs.

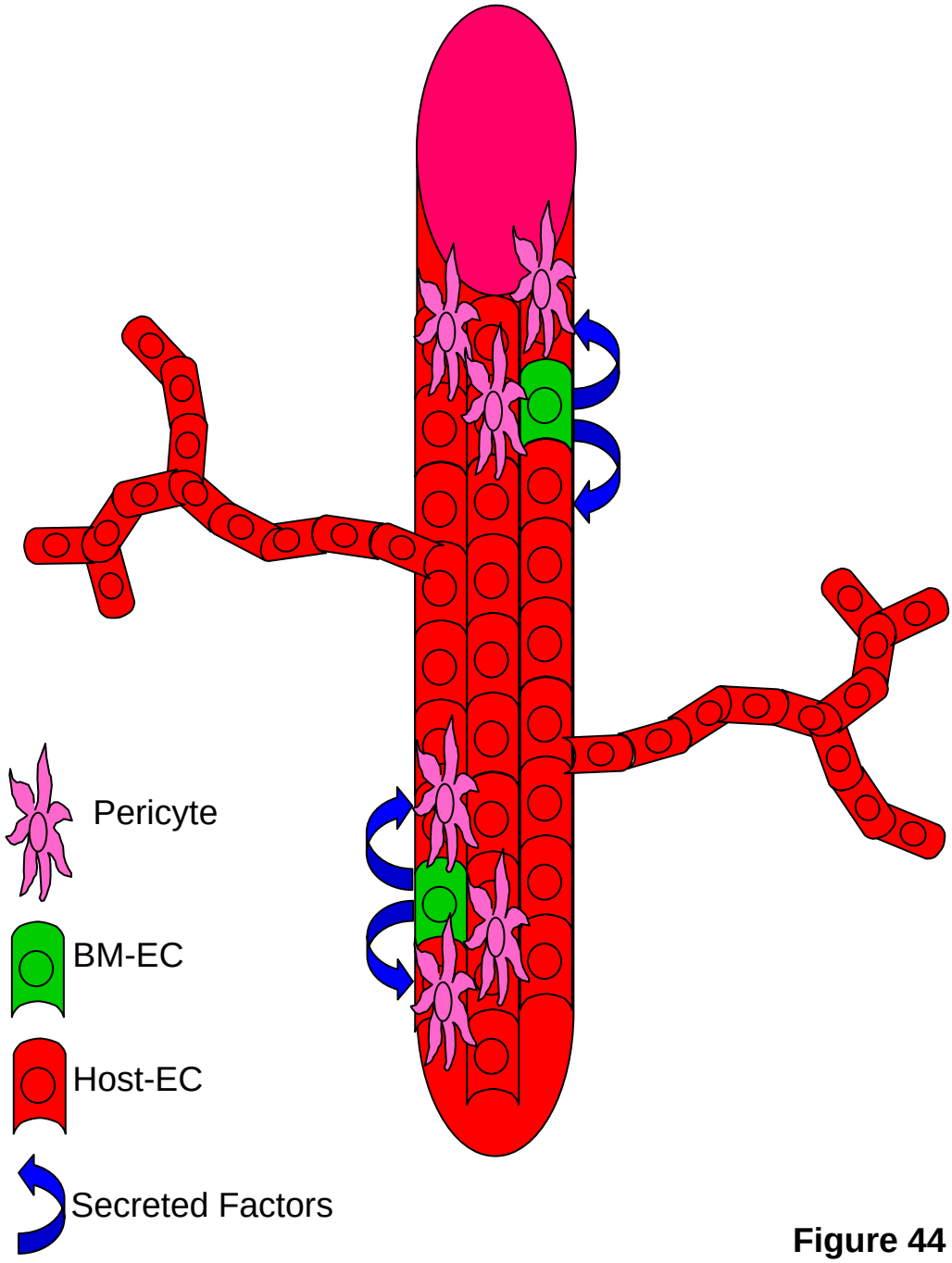

Figure 44

Figure 45: Model of chemokines and their role in angiogenesis

A model showing the possible result of different chemokines and receptors expressed on both host-derived endothelial cells (red cells) and BM-derived endothelial cells (green cells) and the neighboring cells.

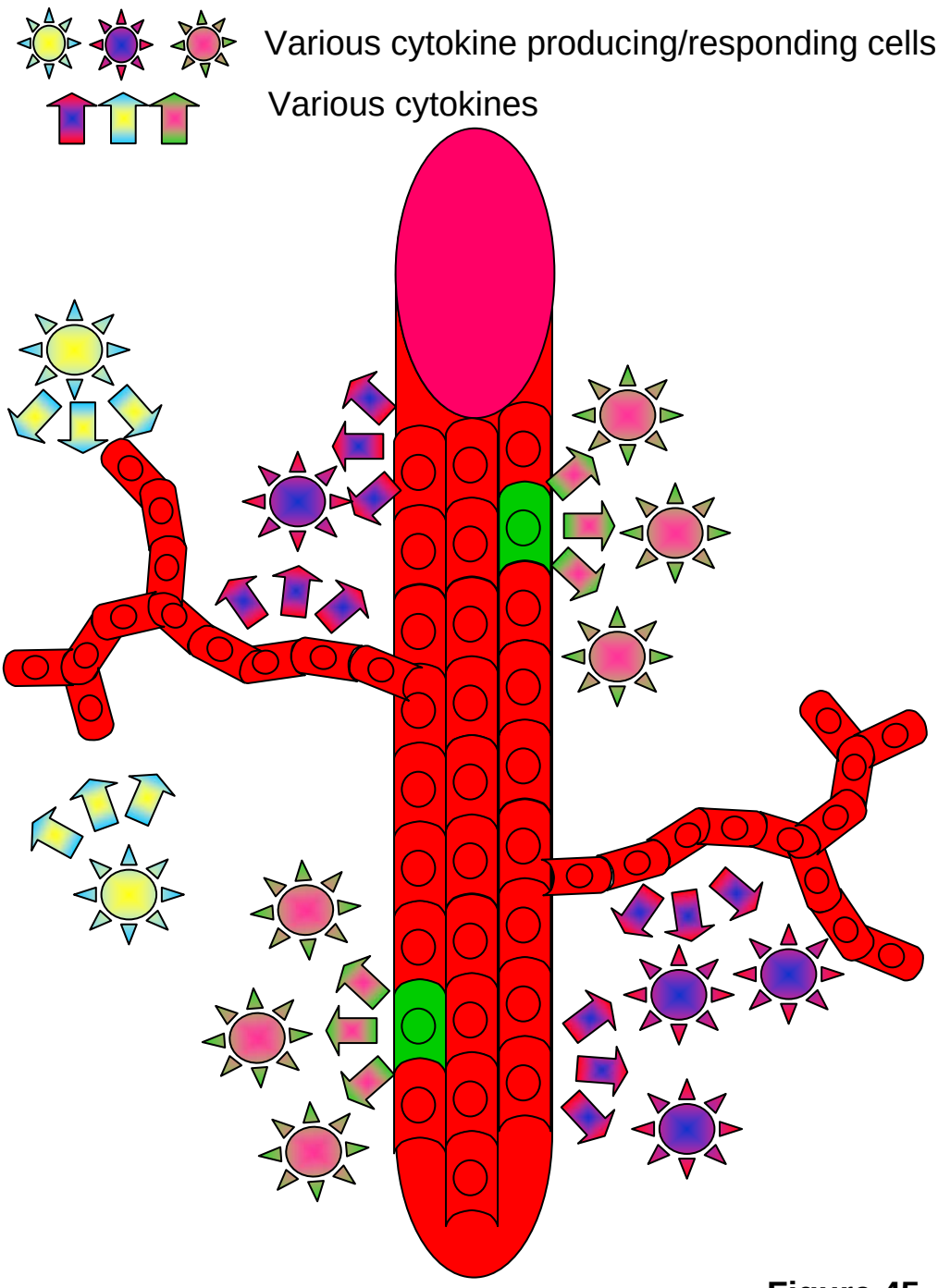
Various cytokine producing/responding cells
Various cytokines

Figure 45

(i.e. pericytes, leukocytes, etc) may further provide paracrine roles in supporting vessel growth perivascularly. Targeted cells may be the proangiogenic hematopoietic cells, such as BM-derived Tie2-expressing monocytes [23], macrophages [34], recruited BM-derived circulating cells [37], pericyte progenitors [30], infiltrating neutrophils [36], and vascular leukocytes [152] which have been described in the literature.

The validation of these candidate genes, and the expression patterns used to generate multiple hypothesis, will be subject to future investigation. Regardless of the exact interactions between EPCs, BM-ECs, and host-ECs, the discrete profiles between these populations suggest that each cell type plays a distinct role in the progression of tumor angiogenesis. Each cell type may also have value as anticancer therapeutic targets, as demonstrated with the E4G10-mediate EPC ablation, which resulted in severe angiogenesis inhibition and impaired growth.

Chapter 6 Conclusions and Perspectives

Non-tumor directed cancer therapeutics

Antiangiogenic cancer therapies hold great promises for the treatment of various cancers [223]. Indeed, the first FDA approved anti-angiogenic cancer drug, which targeted VEGF, Bevacizumab (Avastin) [67] has provided an overall survival benefit in colorectal, breast, and lung cancer patients when combined with conventional chemotherapy. Although Avastin had early success, patients receiving a single class of angiogenesis inhibitors eventually relapse and succumb to the disease. It is possible that the tumor is capable of compensating for the lack of response by one angiogenic pathway by emphasizing another [95]. Despite the limitations of the first drug of its class, such results are potentially only the beginning of a class of drugs targeting specific components of angiogenesis. Multiple hematopoietic populations have been also demonstrated to contribute to tumor angiogenesis [23, 30, 34, 36, 37, 152] and these cell populations may also come to represent therapeutic targets. As new studies, such as this work and others [217], continue to further the understanding of the contributions of these various cells to tumor progression, more viable therapeutic treatments will undoubtedly be discovered. The clear understanding of the lineage and function of cells contributing to tumor angiogenesis allowed for the logical design of targeted therapeutics. Using combination of BM transplantation, mouse genetic

models and functional genomic approaches I have characterized the EPC phenotype in detail, and demonstrated the precise spatial and temporal contribution of EPCs to the neovascularization of growing transplanted and spontaneous tumors *in vivo*. The validity of targeting EPCs may not have been realized without understanding both the kinetics of their contribution to tumor vasculature and the status of VE-cadherin on the cell surface. This work has demonstrated how a detailed analysis of a particular cell type, the EPC, can direct the proper and effective use of a novel therapeutic. This experimental framework can be applied to varying tumor types and microenvironment components to yield similar results.

Exploiting the normalization of tumor vasculature [159] for improved chemotherapeutic delivery will be joined by various other metrics of tumor development. These metrics may be based on polyvariate flow cytometry and transcriptional profiling as described here. It is not only important to understand the critical flaws within the cancer genome that cause the disease, but also the interactions of tumor cells with neighboring cells creating the permissive microenvironment for the tumor to grow. Comparisons to large-scale profiling of ECs from various healthy tissues and at discrete stages of disease progression will identify angiogenic components that are potentially tumor specific, such results are already being achieved [216].

Quantitation of the abundance of particular cells comprising the microenvironment within the tumor bed may be sufficient to direct clinicians to the most beneficial treatments. Large scale quantitation of cellular components from human tumors could then be indexed with treatment regime. After several years, a correlation could be found between the most successful combinations of treatment and microenvironment profile. Additionally, the work done here demonstrates that it is possible to generate a profile of various populations from a single sample. These profiles can be combined with genome wide profiles of the cancer cells to map the pathways that the tumor is utilizing to stimulate both endothelial and other stromal components. This offers the possibility for a truly high detailed profile of the microenvironment to more accurately define the status of the microenvironment. When utilized in a clinical setting, these studies offer the possibility of predicting the therapeutic agent that has maximal benefit to the patient.

Materials and Methods

Cell lines and growth conditions

The murine lymphoma cell line B6RV2 [7], Lewis lung carcinoma cell line LLCs/D122 (provided by Lea Eisenbach, Wiesmann Institute of Science, Rehovot, Israel), and melanoma cell line B16F0 (ATCC) were used for generating tumors in C57BL/6 mice. 293T cells were used as packagers and titer determinants for lentiviral constructs. LLCs, 293Ts, and B16F0 were maintained in DMEM supplemented with 10% fetal bovine serum. B6RV2 cells were maintained in RPMI with 15% FBS. Murine endothelial cells, mHEVc were cultured as described [144, 224].

Designing and cloning of shRNAs ShRNAs targeting Id1 and Id3 genes were designed using the software (http://www.cshl.org/public/SCIENCE/hannon.html). shRNA sequences (two complementary ~83nt DNA oligos) were annealed and cloned directly into U6 promoter-containing vector using a ligation-independent cloning method[169]. shRNAs modeled after human microRNA30 (miR30) comprised of the hairpin stem of 22nt dsRNA and a 19nt loop from human miR30. The target sequences used for generating Id1shRNA were 5' AACGGCGAGATCAGTGCCTTGG 3', and for Id3 shRNA was 5'ATGGATGAGCTTCGATCTTAA 3'. The entire U6 promoter- shRNA

cassette was transferred into lentiviral vectors by gateway clonase recombination reaction (Invitrogen, CA). shRNA targeting firefly luciferase served as a non-specific control. Effective shRNAs were identified using a screening method [169]. In order to minimize off-target effects, a BLAST homology search (based on sense and antisense sequences) was systematically performed to ensure that a single mRNA sequence was targeted.

Lentiviral constructs, virus generation and transductions

The parent self-inactivating lentiviral vector was provided by D. Torono [University of Geneva, Switzerland], into which a ccdB gateway recombination cassette was inserted at the SalI restriction site. For cloning two shRNAs in the same vector one of the two XhoI site was mutated by using a pair of primers with an intential mismatch covering the XhoI site. DPNI treatment was then used to digest all the parental plasmid after a PCR. *E. Coli* were then transformed with the PCR product and colonies were screened for a lack of XhoI restriction activity at the desired site. A second ccdB cassette was inserted at the XhoI site. Lentiviruses expressing expressing shRNAs under the U6 promoter were produced by calcium phosphate transfection of lentiviral DNA constructs into the 293T retroviral packaging cells. 293T cells were plated in 15cm dishes at a density of $3.0x10^6 – 3.5x10^6$ cells to achieve approximately 30% confluence at the

time of transfection. Precipitation was allowed to form overnight and replaced the following morning. At this time, all plates were assessed for precipitate formation by phase contrast microscopy and for successful trasnfection by GFP expression. Plates with less than 30% transfection efficiency were discarded. Transfected plates were allowed to incubate with 20mls of DMEM 10%FBS for 48 hours. Viral particles pseudotyped with vesicular stomatities viral envelope (VSVG) were collected by harvesting supernatants from the packagers, and filtered through a 0.45 μM membrane (Millipore). Concentrated lentiviral stocks were produced by centrifugation of supernatants (25,000 rpm for 2 hrs) over a 20% sucrose gradient. Virus was collected by washing the pellet with 3% BSA in serum free medium and allowed an overnight incubation at 4^{o}. Virus from all tubes was then combined, aliquoted, and snap-frozen in liquid nitrogen. Titers were determined as described [225]. Briefly, 293Ts were infected at a density of $8x10^{6}$ cells per well. Wells were infected with 5μl, 0.5μl, or 0.05 μl of concentrated lentivirus in duplicate. Flow cytometry was used for the detection of GFP expression. Only wells with between 1% and 10% of GFP^{+} cells were considered accurate enough for the determination of infectious units per ml (IFU). Lentiviral transductions of lin^{-} BM cells were generally performed in serum-free StemSpan™ SFEM media (Stem Cell Technologies), in the absence of (B6RV2) or in the presence of cytokines (LLCs).

BM isolation, Lin$^-$ cell purification and transplantation.

GFP transgenics, C57BL/6-Tg (ACTbEGFP)10sb/J or FVB.Cg-Tg(GFPU)5Nagy/J (The Jackson Laboratory, Bar Harbor, Maine), were used as the donor strain. In these strains, GFP is driven by a hybrid chicken β-actin promoter and cytomegalovirus intermediate early enhancer. BM cells were harvested by flushing femurs and tibias of adult animals. 1 X 10^7 total BM cells were transplanted into lethally irradiated (1100 rads) recipients. Lin$^-$ cells were enriched using the Lineage Cell Depletion Kit (CD5, CD45R (B220), CD11b, anti-Ly-6G (Gr-1), 7-4, and Ter119 antibodies) and a magnetic separation device, MACS (Milteyni Biotech, Auburn, CA). The purity of the Lin$^-$ fraction was determined using a fluorescent antibody specific for lineage specific markers by flow cytometry. Typical purities are greater than 95%. All animal protocols were reviewed and approved by the CSHL Animal Care and Use Committee.

Flow cytometry, tumor growth, immunohistochemistry and microscopy

C57BL/6 mice were inoculated intradermally with (5 X 10^6 - 2 X 10^7 LLC/D122 or B6RV2 cells, or with 5 X 10^5 B16F0 cells and tumor size was monitored (width X 0.5 length^2). Animals were first anesthetized with 20% urethane. Once limp, cardiac perfusion through the right ventricle replaced the blood with

phosphate buffer (PB) at a rate of 3mls/min. Tumors were excised from sacrificed animals, minced, and then digested at 37°C for 45-60 min with an enzyme cocktail (Collagenase A, elastase, and DNase I, Roche Applied Science) and filtered through a 30-μm strainer. Cells were rinsed several times to remove all residual enzymes. Single cell suspensions were pre-blocked with Fc block (CD16/CD32, BD Biosciences PharMingen) and then incubated with the following primary antibodies from Pharmingen: rat IgG2aκ and IgG2aκ isotype control, CD31/PECAM-1 (clone MEC 13.3); VE-cadherin/CD144 (clone 11D4.1); CD11b (clone M1/70.), VEGFR2/Flk1 (clone avas12alpha1). Labeled cell populations were measured by LSRII flow cytometer (Beckton Dickenson), compensation for multivariate experiments was performed with FACS Diva software (Becton Dickinson Immunocytometry Systems, Franklin Lakes, New Jersey, USA). Flow cytometry analysis was performed using a variety of controls such as, isotype antibodies, FMO samples [226], and unstained samples for determining appropriate gates, voltages, and compensations required in multivariate flow cytometry. Tumor bearing mice were anesthetized and then perfused with PB followed by 4% paraformaldehyde. Typically, the same animals were used for both flow cytometry and microscopy. A tumor was implanted on the left and right flanks of the animal. After perfusion with PB, the right tumor was removed for enzymatic digestion. Perfusion continued with

paraformaldehyde and the left tumor was harvested for microscopic analysis. In some cases animals were injected with Alexa Fluor 647 conjugated isolectin GS-IB4 or Choleratoxin β subunit (50μg for 10min, Molecular Probes) prior to phosphate buffer perfusion. Tumors were incubated overnight in paraformaldehyde, followed by 20% sucrose, and cryoembedded in Tissue-tek O.C.T. embedding compound (Electron Microscopy Sciences).

Immunohistochemistry was performed using the primary antibodies, Prominin1 (Clone 13A4) (eBiosciences), Endoglin (clone MJ7/18), CD45RB (Clone 16A), pan CD45 (Clone 30-F11), CD41 (Clone MWREQ30) (BD Pharmingen), and E4G10 (ImClone) in addition to antibodies described for flow cytometry on ~30μM thick sections. GFP positive cells were detected by their own signal.

Fluorescent images of endothelium that contained donor-derived endothelial cells were obtained using a computerized Zeiss fluorescent microscope (Axiovert 200M), fitted with an apotome and a HRM camera. Images were analyzed by using Axiovision 4.5 software. The average depth of the optical sections was 30μm, with a resolution of 0.275-0.35 μm.

Peripheral Blood Analysis

Animals were first lightly warmed under a bulb and placed in a small animal restrainer. The ventral tail artery was then cut with a razor at a 45^{o} angle. 5-10 drops of blood was then collected into 1ml of anticoagulant (5mM EDTA, 0.05% NaN_3). Mononuclear cells were then separated from the red blood cells (RBC) by either RBC lysis (PharmLyse, BD Bioscience) or Histopaque (Sigma-Aldrich). Cells were then analyzed by flow cytometry as described.

Cytospin

For the analysis of small cell populations in suspension, approximately $5x10^4$ cells were resuspended in 200µl of PBS. Cells were then place in a cytofunel and spun at 600 rpm for 4 minutes. A hydrophobic barrier was placed around the cells and 4% paraformaldehyde was used to fix the cells for 5 minutes. Subsequent immunofluorescent analysis followed as described.

RNA Isolation and Amplification

Cells were either collagenased treated from lung and tumor isolation, or isolated from magnetic separation of BM. A quickened collagenase treatment was employed with excessive mincing, 6mg of collagenase, and 25 minutes at 37^{o}. Cells were resuspended in DMEM with 0.5% BSA for staining and flow sorting. Cells were also collected from the sorter into DMEM with 0.5% BSA kept at 4^{o}.

Collected cells were then pelleted and resuspended in 50µl of extraction buffer for the Arcturus Picopure RNA isolation kit. RNA quantity and quality were ascertained by the Agilent Bioanalyzer platform using the Pico-chip. Two-round RNA amplifications were performed using Ambion's Message Amp II kit with the second round (round 1 6hr, round 2 14hr) in vitro translation using Biotin-11 DUTPs.

Microarray and Data Analysis

RNA quality was assesed on an Agilent 2100 Bioanalyzer, RNA 6000 Pico Series II Chips (Agilent, Palo Alto, CA, USA). Samples with assesed by a RIN score, 7.5 or greater were passed. When enough material was not available for accurate RIN score, the presence of 18S and 28S ribosomal bands were passed. Total RNA was amplified by a modified Eberwine Technique, using a Message Amp II kit (Ambion, Austin, TX) for 2 rounds of amplification [227]. Quantity was assesed by Nanodrop ND-1000 (Nanodrop Technologies, Wilmington, DE). aRNA smear analysis for 3' bias was perfromed on select samples using Agilent 2100 Bioanalyzer RNA 6000 Pico Series II Chips (Agilent, Palo Alto, CA, USA) . Samples were then prepared for hybridization, hybridized, washed, and scanned according to the manufacturer's instructions on MOE 430A 2.0 GeneChips (Affymetrix, Santa Clara, CA). Affymetrix QC metrics were used to

pass the image data. The Bioconductor R based software was used for the data analysis. RMA algorithm implemented in the Affymetrix package of the Bioconductor was applied to perform low-level analysis (Background correction, normalization and summarization) of the probes [228]. Higher level statistical analysis were done using the "limma" package of the Bioconductor [229]. Supplemental Figures were generated using Array Assist (Stratagene, La Jolla, CA)

EPC differentiation assay

Total BM cells from GFP transgenic animals were first enriched for Lin^- cells as described before. Lin- cells were incubated with VE-cadherin (Alexa Fluor 647) and CD11b (Alexa Fluor 750) antibodies. Using multivariate flow sorting a pure GFP^+ EPC population (VE-$cadherin^+$ $CD11b^-$) was collected by FACS Aria (BD Biosciences). Approximately 5000 EPCs were co-cultured with 5 X 10^4 murine endothelial cells, mHEVc (gift from Cook-Mills) on matrigel (BD Biosciences) supplemented with Medium 200 and LSGS (Cascade Biologics). Similarly, EPCs (1 X 10^3) and hematopoietic cells (approximately 5 X 10^4) were flow sorted from early tumors (day 4) derived from GFP^+ BMT animals and co-cultured with 5 X 10^4 murine endothelial cells. Low CD31 expression on EPCs was confirmed with a PE conjugated CD31 antibody. Cells were cultured in

phenol-red free DMEM with 2% FBS and 10ng/ml VEGF. Immunostaining was directly performed on matrigels with VCAM (clone 429, MVCAM.A, BD Pharmingen), and CD31/PECAM-1 (clone MEC 13.3) antibody after fixation with 4% paraformaldehyde.

Spontaneous tumor model

Male PyMT mice (obtained from mouse models of human cancer consortium, NCI) on a FVB/N background were randomly bred with FVB/N females (Jackson Labs) lacking the PyMT transgene to obtain female mice heterozygous for the PyMT transgene. These female carriers developed mammary tumors by 5-6 which were staged according to Lin et al. [148]. Bone marrow donors in the FVB/N background were FVB.Cg-Tg(GFPU)5Nagy/J which also drove GFP by a CMV enhanced β-actin promoter. However, this line is maintained as a homozygous strain. BMTs were either performed on 1 week old animals intraperitonealy or at 4 week old animals via tail vein. All procedures involving mice were conducted in accordance with protocols reviewed and approved by the CSHL Animal Care and Use Committee.

Conjugation of antibodies to fluorophores

Only antibodies free of protein buffers, such as BSA, FBS, and gelatin, were capable of being conjugated to either succinimydil esters or quantum dots. For ester conjugations, bulk dye was purchased from Molecular Probes, resuspended in DMSO, desiccated in 10μg aliquots, and stored frozen. Exact antibody concentrations were determined using a Nanodrop. Antibodies were brought to a concentration of 1mg/ml in 100μl of PBS and buffered with 10μl of 1M sodium bicarbonate (pH 7.4). The pellet of dye was then resuspended by the antibody and incubated for anywhere from 15 to 90 minutes, depending on the fluorophore and antibody. Conjugated antibody was then purified from unincorporated dyes by passage over Biospin P30 Gel (Biorad). The degree of labeling (DOL) was calculated from readings taken from the nanodrop by the following formula: A_{max}/(Extinction Coefficient*((A_{280}-(A_{max}*Correction Factor))/IgG Extinction Coefficient)). DOLs between 3 and 6 were typical.

Preparation and administration of radioimmunoconjugate

^{225}Ac (Oak Ridge National Laboratory, Oak Ridge, TN) was conjugated to E4G10 (a gift from ImClone, New York) using a two-step labeling method, as described [158, 230] and performed by collaborators Jaggi and Scheinberg. Radio-purity and immunoreactivity of the radioimmunoconjugate (RIC) was determined, as described [230]. Mice were anesthetized and injected

intravenously with the RIC in100µl at days 3, 5, 8, and 12 (50 nCi, 0.6 ug antibody per administration)

Statistical Analysis

Analysis of different treatment groups were performed using the Mann-Whitney T test.

Bibliography:

1. Folkman, J., *Angiogenesis in cancer, vascular, rheumatoid and other disease.* Nat Med, 1995. **1**(1): p. 27-31.
2. Risau, W., *Mechanisms of angiogenesis.* Nature, 1997. **386**(6626): p. 671-4.
3. Carmeliet, P. and R.K. Jain, *Angiogenesis in cancer and other diseases.* Nature, 2000. **407**(6801): p. 249-57.
4. Kopp, H.G., C.A. Ramos, and S. Rafii, *Contribution of endothelial progenitors and proangiogenic hematopoietic cells to vascularization of tumor and ischemic tissue.* Curr Opin Hematol, 2006. **13**(3): p. 175-81.
5. Asahara, T., et al., *Isolation of putative progenitor endothelial cells for angiogenesis.* Science, 1997. **275**(5302): p. 964-7.
6. Shi, Q., et al., *Utilizing granulocyte colony-stimulating factor to enhance vascular graft endothelialization from circulating blood cells.* Ann Vasc Surg, 2002. **16**(3): p. 314-20.
7. Lyden, D., et al., *Impaired recruitment of bone-marrow-derived endothelial and hematopoietic precursor cells blocks tumor angiogenesis and growth.* Nat Med, 2001. **7**(11): p. 1194-201.
8. Chambers, A.F., A.C. Groom, and I.C. MacDonald, *Dissemination and growth of cancer cells in metastatic sites.* Nat Rev Cancer, 2002. **2**(8): p. 563-72.
9. Gupta, G.P. and J. Massague, *Cancer metastasis: building a framework.* Cell, 2006. **127**(4): p. 679-95.
10. Weigelt, B., J.L. Peterse, and L.J. van 't Veer, *Breast cancer metastasis: markers and models.* Nat Rev Cancer, 2005. **5**(8): p. 591-602.
11. Indraccolo, S., et al., *Interruption of tumor dormancy by a transient angiogenic burst within the tumor microenvironment.* Proc Natl Acad Sci U S A, 2006. **103**(11): p. 4216-21.
12. Grey, A.M., et al., *Purification of the migration stimulating factor produced by fetal and breast cancer patient fibroblasts.* Proc Natl Acad Sci U S A, 1989. **86**(7): p. 2438-42.
13. Matsumoto, K., et al., *A study of an in vitro model for invasion of oral squamous cell carcinoma.* J Oral Pathol Med, 1989. **18**(9): p. 498-501.
14. Hu, M., et al., *Distinct epigenetic changes in the stromal cells of breast cancers.* Nat Genet, 2005. **37**(8): p. 899-905.
15. Micke, P. and A. Ostman, *Tumour-stroma interaction: cancer-associated fibroblasts as novel targets in anti-cancer therapy?* Lung Cancer, 2004. **45 Suppl 2**: p. S163-75.

16. Kalluri, R. and M. Zeisberg, *Fibroblasts in cancer.* Nat Rev Cancer, 2006. **6**(5): p. 392-401.
17. Hamano, Y., et al., *Physiological levels of tumstatin, a fragment of collagen IV alpha3 chain, are generated by MMP-9 proteolysis and suppress angiogenesis via alphaV beta3 integrin.* Cancer Cell, 2003. **3**(6): p. 589-601.
18. Maeshima, Y., et al., *Tumstatin, an endothelial cell-specific inhibitor of protein synthesis.* Science, 2002. **295**(5552): p. 140-3.
19. Tanjore, H. and R. Kalluri, *The role of type IV collagen and basement membranes in cancer progression and metastasis.* Am J Pathol, 2006. **168**(3): p. 715-7.
20. Carmeliet, P., *Angiogenesis in life, disease and medicine.* Nature, 2005. **438**(7070): p. 932-6.
21. Nolan, D.J., et al., *Bone marrow-derived endothelial progenitor cells are a major determinant of nascent tumor neovascularization.* Genes Dev, 2007. **21**(12): p. 1546-58.
22. Camien, M.N. and R.C. Warner, *Denaturation of covalently closed circular DNA. Kinetics, comparison of several DNAs, mechanism and ionic effects.* J Biol Chem, 1986. **261**(13): p. 6026-33.
23. De Palma, M., et al., *Tie2 identifies a hematopoietic lineage of proangiogenic monocytes required for tumor vessel formation and a mesenchymal population of pericyte progenitors.* Cancer Cell, 2005. **8**(3): p. 211-26.
24. De Palma, M., et al., *Targeting exogenous genes to tumor angiogenesis by transplantation of genetically modified hematopoietic stem cells.* Nat Med, 2003. **9**(6): p. 789-95.
25. Labeur, C., et al., *Design of a new class of amphipathic helical peptides for the plasma apolipoproteins that promote cellular cholesterol efflux but do not activate LCAT.* Arterioscler Thromb Vasc Biol, 1997. **17**(3): p. 580-8.
26. Lin, E.Y., et al., *Colony-stimulating factor 1 promotes progression of mammary tumors to malignancy.* J Exp Med, 2001. **193**(6): p. 727-40.
27. Benelli, R., et al., *Neutrophils as a key cellular target for angiostatin: implications for regulation of angiogenesis and inflammation.* Faseb J, 2002. **16**(2): p. 267-9.
28. Chavakis, T., et al., *Regulation of neovascularization by human neutrophil peptides (alpha-defensins): a link between inflammation and angiogenesis.* Faseb J, 2004. **18**(11): p. 1306-8.
29. Hacker, C., et al., *Transcriptional profiling identifies Id2 function in dendritic cell development.* Nat Immunol, 2003. **4**(4): p. 380-6.

30. Song, S., et al., *PDGFRbeta+ perivascular progenitor cells in tumours regulate pericyte differentiation and vascular survival.* Nat Cell Biol, 2005. **7**(9): p. 870-9.
31. Singh, R.K. and I.J. Fidler, *Regulation of tumor angiogenesis by organ-specific cytokines.* Curr Top Microbiol Immunol, 1996. **213 (Pt 2)**: p. 1-11.
32. Bando, H. and M. Toi, *Tumor angiogenesis, macrophages, and cytokines.* Adv Exp Med Biol, 2000. **476**: p. 267-84.
33. Coussens, L.M. and Z. Werb, *Inflammation and cancer.* Nature, 2002. **420**(6917): p. 860-7.
34. Pollard, J.W., *Tumour-educated macrophages promote tumour progression and metastasis.* Nat Rev Cancer, 2004. **4**(1): p. 71-8.
35. Kaplan, R.N., et al., *VEGFR1-positive haematopoietic bone marrow progenitors initiate the pre-metastatic niche.* Nature, 2005. **438**(7069): p. 820-7.
36. Nozawa, H., C. Chiu, and D. Hanahan, *Infiltrating neutrophils mediate the initial angiogenic switch in a mouse model of multistage carcinogenesis.* Proc Natl Acad Sci U S A, 2006. **103**(33): p. 12493-8.
37. Grunewald, M., et al., *VEGF-Induced Adult Neovascularization: Recruitment, Retention, and Role of Accessory Cells.* Cell, 2006. **124**(1): p. 175-89.
38. Rajantie, I., et al., *Adult bone marrow-derived cells recruited during angiogenesis comprise precursors for periendothelial vascular mural cells.* Blood, 2004.
39. Orlic, D., et al., *Transplanted adult bone marrow cells repair myocardial infarcts in mice.* Ann N Y Acad Sci, 2001. **938**: p. 221-9; discussion 229-30.
40. Balsam, L.B., et al., *Haematopoietic stem cells adopt mature haematopoietic fates in ischaemic myocardium.* Nature, 2004. **428**(6983): p. 668-73.
41. Gothert, J.R., et al., *Genetically tagging endothelial cells in vivo: bone marrow-derived cells do not contribute to tumor endothelium.* Blood, 2004. **104**(6): p. 1769-77.
42. Spring, H., et al., *Chemokines direct endothelial progenitors into tumor neovessels.* Proc Natl Acad Sci U S A, 2005. **102**(50): p. 18111-6.
43. Zhang, N., et al., *Tracking angiogenesis induced by skin wounding and contact hypersensitivity using a Vegfr2-luciferase transgenic mouse.* Blood, 2004. **103**(2): p. 617-26.
44. Folkman, J., P. Hahnfeldt, and L. Hlatky, *Cancer: looking outside the genome.* Nat Rev Mol Cell Biol, 2000. **1**(1): p. 76-9.

45. Stoler, D.L., et al., *The onset and extent of genomic instability in sporadic colorectal tumor progression.* Proc Natl Acad Sci U S A, 1999. **96**(26): p. 15121-6.
46. Greenberger, S., et al., *Transcription-controlled gene therapy against tumor angiogenesis.* J Clin Invest, 2004. **113**(7): p. 1017-24.
47. Glover, D.J., H.J. Lipps, and D.A. Jans, *Towards safe, non-viral therapeutic gene expression in humans.* Nat Rev Genet, 2005. **6**(4): p. 299-310.
48. Schwartz, J.J. and S. Zhang, *Peptide-mediated cellular delivery.* Curr Opin Mol Ther, 2000. **2**(2): p. 162-7.
49. Jackson, D.A., S. Juranek, and H.J. Lipps, *Designing nonviral vectors for efficient gene transfer and long-term gene expression.* Mol Ther, 2006. **14**(5): p. 613-26.
50. Martin, M.E. and K.G. Rice, *Peptide-guided gene delivery.* Aaps J, 2007. **9**(1): p. E18-29.
51. Wolff, J.A., et al., *Direct gene transfer into mouse muscle in vivo.* Science, 1990. **247**(4949 Pt 1): p. 1465-8.
52. Zhang, G., et al., *Expression of naked plasmid DNA injected into the afferent and efferent vessels of rodent and dog livers.* Hum Gene Ther, 1997. **8**(15): p. 1763-72.
53. Choate, K.A. and P.A. Khavari, *Direct cutaneous gene delivery in a human genetic skin disease.* Hum Gene Ther, 1997. **8**(14): p. 1659-65.
54. Gao, X., K.S. Kim, and D. Liu, *Nonviral gene delivery: what we know and what is next.* Aaps J, 2007. **9**(1): p. E92-104.
55. O'Brien, J. and S.C. Lummis, *An improved method of preparing microcarriers for biolistic transfection.* Brain Res Brain Res Protoc, 2002. **10**(1): p. 12-5.
56. Dean, D.A., et al., *Electroporation as a method for high-level nonviral gene transfer to the lung.* Gene Ther, 2003. **10**(18): p. 1608-15.
57. Kim, H.J., et al., *Ultrasound-mediated transfection of mammalian cells.* Hum Gene Ther, 1996. **7**(11): p. 1339-46.
58. Liu, F., Y. Song, and D. Liu, *Hydrodynamics-based transfection in animals by systemic administration of plasmid DNA.* Gene Ther, 1999. **6**(7): p. 1258-66.
59. Templeton, N.S., et al., *Improved DNA: liposome complexes for increased systemic delivery and gene expression.* Nat Biotechnol, 1997. **15**(7): p. 647-52.
60. Wu, G.Y. and C.H. Wu, *Receptor-mediated gene delivery and expression in vivo.* J Biol Chem, 1988. **263**(29): p. 14621-4.

61. Kommareddy, S. and M. Amiji, *Antiangiogenic gene therapy with systemically administered sFlt-1 plasmid DNA in engineered gelatin-based nanovectors.* Cancer Gene Ther, 2007. **14**(5): p. 488-98.
62. Wei, J., et al., *Embryonic endothelial progenitor cells armed with a suicide gene target hypoxic lung metastases after intravenous delivery.* Cancer Cell, 2004. **5**(5): p. 477-88.
63. Chung-Faye, G.A., et al., *In vivo gene therapy for colon cancer using adenovirus-mediated, transfer of the fusion gene cytosine deaminase and uracil phosphoribosyltransferase.* Gene Ther, 2001. **8**(20): p. 1547-54.
64. Huber, B.E., et al., *Metabolism of 5-fluorocytosine to 5-fluorouracil in human colorectal tumor cells transduced with the cytosine deaminase gene: significant antitumor effects when only a small percentage of tumor cells express cytosine deaminase.* Proc Natl Acad Sci U S A, 1994. **91**(17): p. 8302-6.
65. Matsuzaki, Y., et al., *Unexpectedly efficient homing capacity of purified murine hematopoietic stem cells.* Immunity, 2004. **20**(1): p. 87-93.
66. Verheul, H.M. and H.M. Pinedo, *Possible molecular mechanisms involved in the toxicity of angiogenesis inhibition.* Nat Rev Cancer, 2007. **7**(6): p. 475-85.
67. Presta, L.G., et al., *Humanization of an anti-vascular endothelial growth factor monoclonal antibody for the therapy of solid tumors and other disorders.* Cancer Res, 1997. **57**(20): p. 4593-9.
68. Miller, K.D., *Issues and challenges for antiangiogenic therapies.* Breast Cancer Res Treat, 2002. **75 Suppl 1**: p. S45-50; discussion S57-8.
69. Ferrara, N., et al., *Discovery and development of bevacizumab, an anti-VEGF antibody for treating cancer.* Nat Rev Drug Discov, 2004. **3**(5): p. 391-400.
70. Motzer, R.J., et al., *Sunitinib malate for the treatment of solid tumours: a review of current clinical data.* Expert Opin Investig Drugs, 2006. **15**(5): p. 553-61.
71. Wilhelm, S., et al., *Discovery and development of sorafenib: a multikinase inhibitor for treating cancer.* Nat Rev Drug Discov, 2006. **5**(10): p. 835-44.
72. Baffert, F., et al., *Cellular changes in normal blood capillaries undergoing regression after inhibition of VEGF signaling.* Am J Physiol Heart Circ Physiol, 2006. **290**(2): p. H547-59.
73. Goodlad, R.A., et al., *Inhibiting vascular endothelial growth factor receptor-2 signaling reduces tumor burden in the ApcMin/+ mouse model of early intestinal cancer.* Carcinogenesis, 2006. **27**(10): p. 2133-9.

74. Huang, J., et al., *Regression of established tumors and metastases by potent vascular endothelial growth factor blockade.* Proc Natl Acad Sci U S A, 2003. **100**(13): p. 7785-90.
75. McCarty, M.F., et al., *ZD6474, a vascular endothelial growth factor receptor tyrosine kinase inhibitor with additional activity against epidermal growth factor receptor tyrosine kinase, inhibits orthotopic growth and angiogenesis of gastric cancer.* Mol Cancer Ther, 2004. **3**(9): p. 1041-8.
76. Podar, K., et al., *The small-molecule VEGF receptor inhibitor pazopanib (GW786034B) targets both tumor and endothelial cells in multiple myeloma.* Proc Natl Acad Sci U S A, 2006. **103**(51): p. 19478-83.
77. Polverino, A., et al., *AMG 706, an Oral, Multikinase Inhibitor that Selectively Targets Vascular Endothelial Growth Factor, Platelet-Derived Growth Factor, and Kit Receptors, Potently Inhibits Angiogenesis and Induces Regression in Tumor Xenografts.* Cancer Res, 2006. **66**(17): p. 8715-21.
78. Wood, J.M., et al., *PTK787/ZK 222584, a novel and potent inhibitor of vascular endothelial growth factor receptor tyrosine kinases, impairs vascular endothelial growth factor-induced responses and tumor growth after oral administration.* Cancer Res, 2000. **60**(8): p. 2178-89.
79. Karp, J.E., et al., *Targeting vascular endothelial growth factor for relapsed and refractory adult acute myelogenous leukemias: therapy with sequential 1-beta-d-arabinofuranosylcytosine, mitoxantrone, and bevacizumab.* Clin Cancer Res, 2004. **10**(11): p. 3577-85.
80. Motzer, R.J., et al., *Sunitinib in patients with metastatic renal cell carcinoma.* Jama, 2006. **295**(21): p. 2516-24.
81. Herbst, R.S. and A.B. Sandler, *Non-small cell lung cancer and antiangiogenic therapy: what can be expected of bevacizumab?* Oncologist, 2004. **9 Suppl 1**: p. 19-26.
82. Kabbinavar, F., et al., *Phase II, randomized trial comparing bevacizumab plus fluorouracil (FU)/leucovorin (LV) with FU/LV alone in patients with metastatic colorectal cancer.* J Clin Oncol, 2003. **21**(1): p. 60-5.
83. Robert, C., et al., *Subungual splinter hemorrhages: a clinical window to inhibition of vascular endothelial growth factor receptors?* Ann Intern Med, 2005. **143**(4): p. 313-4.
84. Scappaticci, F.A., et al., *Surgical wound healing complications in metastatic colorectal cancer patients treated with bevacizumab.* J Surg Oncol, 2005. **91**(3): p. 173-80.

85. Heymach, J.V., et al., *Phase II study of the antiangiogenic agent SU5416 in patients with advanced soft tissue sarcomas.* Clin Cancer Res, 2004. **10**(17): p. 5732-40.
86. Hurwitz, H., et al., *Bevacizumab plus irinotecan, fluorouracil, and leucovorin for metastatic colorectal cancer.* N Engl J Med, 2004. **350**(23): p. 2335-42.
87. Kuenen, B.C., et al., *Dose-finding and pharmacokinetic study of cisplatin, gemcitabine, and SU5416 in patients with solid tumors.* J Clin Oncol, 2002. **20**(6): p. 1657-67.
88. Cobleigh, M.A., et al., *A phase I/II dose-escalation trial of bevacizumab in previously treated metastatic breast cancer.* Semin Oncol, 2003. **30**(5 Suppl 16): p. 117-24.
89. Sane, D.C., L. Anton, and K.B. Brosnihan, *Angiogenic growth factors and hypertension.* Angiogenesis, 2004. **7**(3): p. 193-201.
90. Sica, D.A., *Angiogenesis inhibitors and hypertension: an emerging issue.* J Clin Oncol, 2006. **24**(9): p. 1329-31.
91. Lehmann, J., et al., *Adjuvant cisplatin plus methotrexate versus methotrexate, vinblastine, epirubicin, and cisplatin in locally advanced bladder cancer: results of a randomized, multicenter, phase III trial (AUO-AB 05/95).* J Clin Oncol, 2005. **23**(22): p. 4963-74.
92. Yang, J.C., et al., *A randomized trial of bevacizumab, an anti-vascular endothelial growth factor antibody, for metastatic renal cancer.* N Engl J Med, 2003. **349**(5): p. 427-34.
93. Drevs, J., et al., *Soluble markers for the assessment of biological activity with PTK787/ZK 222584 (PTK/ZK), a vascular endothelial growth factor receptor (VEGFR) tyrosine kinase inhibitor in patients with advanced colorectal cancer from two phase I trials.* Ann Oncol, 2005. **16**(4): p. 558-65.
94. Motzer, R.J., et al., *Activity of SU11248, a multitargeted inhibitor of vascular endothelial growth factor receptor and platelet-derived growth factor receptor, in patients with metastatic renal cell carcinoma.* J Clin Oncol, 2006. **24**(1): p. 16-24.
95. Casanovas, O., et al., *Drug resistance by evasion of antiangiogenic targeting of VEGF signaling in late-stage pancreatic islet tumors.* Cancer Cell, 2005. **8**(4): p. 299-309.
96. Lamszus, K., et al., *Inhibition of glioblastoma angiogenesis and invasion by combined treatments directed against vascular endothelial growth factor receptor-2, epidermal growth factor receptor, and vascular endothelial-cadherin.* Clin Cancer Res, 2005. **11**(13): p. 4934-40.

97. Briddell, R.A., et al., *Further phenotypic characterization and isolation of human hematopoietic progenitor cells using a monoclonal antibody to the c-kit receptor.* Blood, 1992. **79**(12): p. 3159-67.
98. Suratt, B.T., et al., *Human pulmonary chimerism after hematopoietic stem cell transplantation.* Am J Respir Crit Care Med, 2003. **168**(3): p. 318-22.
99. Poulsom, R., et al., *Bone marrow contributes to renal parenchymal turnover and regeneration.* J Pathol, 2001. **195**(2): p. 229-35.
100. Larrivee, B., et al., *Minimal contribution of marrow-derived endothelial precursors to tumor vasculature.* J Immunol, 2005. **175**(5): p. 2890-9.
101. Bertolini, F., et al., *The multifaceted circulating endothelial cell in cancer: towards marker and target identification.* Nat Rev Cancer, 2006. **6**(11): p. 835-45.
102. Baumann, C.I., et al., *PECAM-1 is expressed on hematopoietic stem cells throughout ontogeny and identifies a population of erythroid progenitors.* Blood, 2004. **104**(4): p. 1010-6.
103. Schmeisser, A., et al., *Monocytes coexpress endothelial and macrophagocytic lineage markers and form cord-like structures in Matrigel under angiogenic conditions.* Cardiovasc Res, 2001. **49**(3): p. 671-80.
104. Harder, R., et al., *Dissection of murine lymphocyte-endothelial cell interaction mechanisms by SV-40-transformed mouse endothelial cell lines: novel mechanisms mediating basal binding, and alpha 4-integrin-dependent cytokine-induced adhesion.* Exp Cell Res, 1991. **197**(2): p. 259-67.
105. Peichev, M., et al., *Expression of VEGFR-2 and AC133 by circulating human CD34(+) cells identifies a population of functional endothelial precursors.* Blood, 2000. **95**(3): p. 952-8.
106. Gill, M., et al., *Vascular trauma induces rapid but transient mobilization of VEGFR2(+)AC133(+) endothelial precursor cells.* Circ Res, 2001. **88**(2): p. 167-74.
107. Fujiyama, S., et al., *Bone marrow monocyte lineage cells adhere on injured endothelium in a monocyte chemoattractant protein-1-dependent manner and accelerate reendothelialization as endothelial progenitor cells.* Circ Res, 2003. **93**(10): p. 980-9.
108. Gulati, R., et al., *Diverse origin and function of cells with endothelial phenotype obtained from adult human blood.* Circ Res, 2003. **93**(11): p. 1023-5.
109. Chavakis, E., et al., *Role of beta2-integrins for homing and neovascularization capacity of endothelial progenitor cells.* J Exp Med, 2005. **201**(1): p. 63-72.

110. Rehman, J., et al., *Peripheral blood "endothelial progenitor cells" are derived from monocyte/macrophages and secrete angiogenic growth factors.* Circulation, 2003. **107**(8): p. 1164-9.
111. Yang, L., et al., *Expansion of myeloid immune suppressor Gr+CD11b+ cells in tumor-bearing host directly promotes tumor angiogenesis.* Cancer Cell, 2004. **6**(4): p. 409-21.
112. Urbich, C., et al., *Cathepsin L is required for endothelial progenitor cell-induced neovascularization.* Nat Med, 2005. **11**(2): p. 206-13.
113. Hildbrand, P., et al., *The role of angiopoietins in the development of endothelial cells from cord blood CD34+ progenitors.* Blood, 2004. **104**(7): p. 2010-9.
114. Garmy-Susini, B. and J.A. Varner, *Circulating endothelial progenitor cells.* Br J Cancer, 2005. **93**(8): p. 855-8.
115. Shalaby, F., et al., *Failure of blood-island formation and vasculogenesis in Flk-1-deficient mice.* Nature, 1995. **376**(6535): p. 62-6.
116. Shalaby, F., et al., *A requirement for Flk1 in primitive and definitive hematopoiesis and vasculogenesis.* Cell, 1997. **89**(6): p. 981-90.
117. Eichmann, A., et al., *Ligand-dependent development of the endothelial and hemopoietic lineages from embryonic mesodermal cells expressing vascular endothelial growth factor receptor 2.* Proc Natl Acad Sci U S A, 1997. **94**(10): p. 5141-6.
118. Urbich, C., et al., *Relevance of monocytic features for neovascularization capacity of circulating endothelial progenitor cells.* Circulation, 2003. **108**(20): p. 2511-6.
119. Yoder, M.C., et al., *Redefining endothelial progenitor cells via clonal analysis and hematopoietic stem/progenitor cell principals.* Blood, 2007. **109**(5): p. 1801-9.
120. Katayama, N., et al., *Stage-specific expression of c-kit protein by murine hematopoietic progenitors.* Blood, 1993. **82**(8): p. 2353-60.
121. Mayo, J.G., *Biologic characterization of the subcutaneously implanted Lewis lung tumor.* Cancer Chemother Rep 2, 1972. **3**(1): p. 325-30.
122. Hermiston, M.L., Z. Xu, and A. Weiss, *CD45: a critical regulator of signaling thresholds in immune cells.* Annu Rev Immunol, 2003. **21**: p. 107-37.
123. Hathcock, K.S., et al., *CD45 expression by B cells. Expression of different CD45 isoforms by subpopulations of activated B cells.* J Immunol, 1992. **149**(7): p. 2286-94.
124. Thomas, M.L. and E.J. Brown, *Positive and negative regulation of Src-family membrane kinases by CD45.* Immunol Today, 1999. **20**(9): p. 406-11.

125. Irie-Sasaki, J., et al., *CD45 is a JAK phosphatase and negatively regulates cytokine receptor signalling.* Nature, 2001. **409**(6818): p. 349-54.
126. Dejana, E., G. Bazzoni, and M.G. Lampugnani, *Vascular endothelial (VE)-cadherin: only an intercellular glue?* Exp Cell Res, 1999. **252**(1): p. 13-9.
127. Coultas, L., K. Chawengsaksophak, and J. Rossant, *Endothelial cells and VEGF in vascular development.* Nature, 2005. **438**(7070): p. 937-45.
128. Muller, W.A., et al., *PECAM-1 is required for transendothelial migration of leukocytes.* J Exp Med, 1993. **178**(2): p. 449-60.
129. Miraglia, S., et al., *A novel five-transmembrane hematopoietic stem cell antigen: isolation, characterization, and molecular cloning.* Blood, 1997. **90**(12): p. 5013-21.
130. Fargeas, C.A., D. Corbeil, and W.B. Huttner, *AC133 antigen, CD133, prominin-1, prominin-2, etc.: prominin family gene products in need of a rational nomenclature.* Stem Cells, 2003. **21**(4): p. 506-8.
131. Fonsatti, E., et al., *Endoglin: An accessory component of the TGF-beta-binding receptor-complex with diagnostic, prognostic, and bioimmunotherapeutic potential in human malignancies.* J Cell Physiol, 2001. **188**(1): p. 1-7.
132. Gougos, A. and M. Letarte, *Primary structure of endoglin, an RGD-containing glycoprotein of human endothelial cells.* J Biol Chem, 1990. **265**(15): p. 8361-4.
133. Bodey, B., et al., *Over-expression of endoglin (CD105): a marker of breast carcinoma-induced neo-vascularization.* Anticancer Res, 1998. **18**(5A): p. 3621-8.
134. Kumar, S., et al., *Breast carcinoma: vascular density determined using CD105 antibody correlates with tumor prognosis.* Cancer Res, 1999. **59**(4): p. 856-61.
135. Saad, R.S., et al., *Endoglin (CD105) and vascular endothelial growth factor as prognostic markers in colorectal cancer.* Mod Pathol, 2004. **17**(2): p. 197-203.
136. Li, C., et al., *Both high intratumoral microvessel density determined using CD105 antibody and elevated plasma levels of CD105 in colorectal cancer patients correlate with poor prognosis.* Br J Cancer, 2003. **88**(9): p. 1424-31.
137. Wikstrom, P., et al., *Endoglin (CD105) is expressed on immature blood vessels and is a marker for survival in prostate cancer.* Prostate, 2002. **51**(4): p. 268-75.

138. Romani, A.A., et al., *The risk of developing metastatic disease in colorectal cancer is related to CD105-positive vessel count.* J Surg Oncol, 2006. **93**(6): p. 446-55.
139. Elices, M.J., et al., *VCAM-1 on activated endothelium interacts with the leukocyte integrin VLA-4 at a site distinct from the VLA-4/fibronectin binding site.* Cell, 1990. **60**(4): p. 577-84.
140. Haraldsen, G., et al., *Cytokine-regulated expression of E-selectin, intercellular adhesion molecule-1 (ICAM-1), and vascular cell adhesion molecule-1 (VCAM-1) in human microvascular endothelial cells.* J Immunol, 1996. **156**(7): p. 2558-65.
141. Gao, J.X. and A.C. Issekutz, *Mac-1 (CD11b/CD18) is the predominant beta 2 (CD18) integrin mediating human neutrophil migration through synovial and dermal fibroblast barriers.* Immunology, 1996. **88**(3): p. 463-70.
142. Thomas, M.L., *The leukocyte common antigen family.* Annu Rev Immunol, 1989. **7**: p. 339-69.
143. Mitjavila-Garcia, M.T., et al., *Expression of CD41 on hematopoietic progenitors derived from embryonic hematopoietic cells.* Development, 2002. **129**(8): p. 2003-13.
144. Cook-Mills, J.M., J.S. Gallagher, and T.L. Feldbush, *Isolation and characterization of high endothelial cell lines derived from mouse lymph nodes.* In Vitro Cell Dev Biol Anim, 1996. **32**(3): p. 167-77.
145. Fidler, I.J., *Biological behavior of malignant melanoma cells correlated to their survival in vivo.* Cancer Res, 1975. **35**(1): p. 218-24.
146. Guy, C.T., R.D. Cardiff, and W.J. Muller, *Induction of mammary tumors by expression of polyomavirus middle T oncogene: a transgenic mouse model for metastatic disease.* Mol Cell Biol, 1992. **12**(3): p. 954-61.
147. Desai, K.V., et al., *Initiating oncogenic event determines gene-expression patterns of human breast cancer models.* Proc Natl Acad Sci U S A, 2002. **99**(10): p. 6967-72.
148. Lin, E.Y., et al., *Progression to malignancy in the polyoma middle T oncoprotein mouse breast cancer model provides a reliable model for human diseases.* Am J Pathol, 2003. **163**(5): p. 2113-26.
149. Pennell, N.A., S.D. Hurley, and W.J. Streit, *Lectin staining of sheep microglia.* Histochemistry, 1994. **102**(6): p. 483-6.
150. Sahagun, G., et al., *Purification of murine endothelial cell cultures by flow cytometry using fluorescein-labeled griffonia simplicifolia agglutinin.* Am J Pathol, 1989. **134**(6): p. 1227-32.

151. Janes, P.W., S.C. Ley, and A.I. Magee, *Aggregation of lipid rafts accompanies signaling via the T cell antigen receptor.* J Cell Biol, 1999. **147**(2): p. 447-61.
152. Conejo-Garcia, J.R., et al., *Vascular leukocytes contribute to tumor vascularization.* Blood, 2005. **105**(2): p. 679-81.
153. Duda, D.G., et al., *Evidence for incorporation of bone marrow-derived endothelial cells into perfused blood vessels in tumors.* Blood, 2006. **107**(7): p. 2774-6.
154. Minami, E., et al., *Extracardiac progenitor cells repopulate most major cell types in the transplanted human heart.* Circulation, 2005. **112**(19): p. 2951-8.
155. May, C., et al., *Identification of a transiently exposed VE-cadherin epitope that allows for specific targeting of an antibody to the tumor neovasculature.* Blood, 2005. **105**(11): p. 4337-44.
156. Liao, F., et al., *Selective targeting of angiogenic tumor vasculature by vascular endothelial-cadherin antibody inhibits tumor growth without affecting vascular permeability.* Cancer Res, 2002. **62**(9): p. 2567-75.
157. McDevitt, M.R., et al., *Tumor therapy with targeted atomic nanogenerators.* Science, 2001. **294**(5546): p. 1537-40.
158. McDevitt, M.R., et al., *Design and synthesis of 225Ac radioimmunopharmaceuticals.* Appl Radiat Isot, 2002. **57**(6): p. 841-7.
159. Jain, R.K., *Normalization of tumor vasculature: an emerging concept in antiangiogenic therapy.* Science, 2005. **307**(5706): p. 58-62.
160. Mayer, R.J., *Two steps forward in the treatment of colorectal cancer.* N Engl J Med, 2004. **350**(23): p. 2406-8.
161. Tong, R.T., et al., *Vascular normalization by vascular endothelial growth factor receptor 2 blockade induces a pressure gradient across the vasculature and improves drug penetration in tumors.* Cancer Res, 2004. **64**(11): p. 3731-6.
162. Singh Jaggi, J., et al., *Selective alpha-particle mediated depletion of tumor vasculature with vascular normalization.* PLoS ONE, 2007. **2**: p. e267.
163. Norton, J.D., *ID helix-loop-helix proteins in cell growth, differentiation and tumorigenesis.* J Cell Sci, 2000. **113 (Pt 22)**: p. 3897-905.
164. Norton, J.D., et al., *Id helix-loop-helix proteins in cell growth and differentiation.* Trends Cell Biol, 1998. **8**(2): p. 58-65.
165. Ruzinova, M.B., et al., *Effect of angiogenesis inhibition by Id loss and the contribution of bone-marrow-derived endothelial cells in spontaneous murine tumors.* Cancer Cell, 2003. **4**(4): p. 277-89.

166. Lyden, D., et al., *Id1 and Id3 are required for neurogenesis, angiogenesis and vascularization of tumour xenografts.* Nature, 1999. **401**(6754): p. 670-7.
167. de Candia, P., et al., *Angiogenesis impairment in Id-deficient mice cooperates with an Hsp90 inhibitor to completely suppress HER2/neu-dependent breast tumors.* Proc Natl Acad Sci U S A, 2003. **100**(21): p. 12337-42.
168. Kim, I., O.H. Yilmaz, and S.J. Morrison, *CD144 (VE-cadherin) is transiently expressed by fetal liver hematopoietic stem cells.* Blood, 2005. **106**(3): p. 903-5.
169. Kumar, R., D.S. Conklin, and V. Mittal, *High-throughput selection of effective RNAi probes for gene silencing.* Genome Res, 2003. **13**(10): p. 2333-40.
170. Zufferey, R., et al., *Self-inactivating lentivirus vector for safe and efficient in vivo gene delivery.* J Virol, 1998. **72**(12): p. 9873-80.
171. Naldini, L., et al., *In vivo gene delivery and stable transduction of nondividing cells by a lentiviral vector.* Science, 1996. **272**(5259): p. 263-7.
172. O'Doherty, U., W.J. Swiggard, and M.H. Malim, *Human immunodeficiency virus type 1 spinoculation enhances infection through virus binding.* J Virol, 2000. **74**(21): p. 10074-80.
173. Xiao, K., et al., *Mechanisms of VE-cadherin processing and degradation in microvascular endothelial cells.* J Biol Chem, 2003. **278**(21): p. 19199-208.
174. Xiao, K., et al., *p120-Catenin regulates clathrin-dependent endocytosis of VE-cadherin.* Mol Biol Cell, 2005. **16**(11): p. 5141-51.
175. Nawroth, R., et al., *VE-PTP and VE-cadherin ectodomains interact to facilitate regulation of phosphorylation and cell contacts.* Embo J, 2002. **21**(18): p. 4885-95.
176. Gavard, J. and J.S. Gutkind, *VEGF controls endothelial-cell permeability by promoting the beta-arrestin-dependent endocytosis of VE-cadherin.* Nat Cell Biol, 2006. **8**(11): p. 1223-34.
177. Lambeng, N., et al., *Vascular endothelial-cadherin tyrosine phosphorylation in angiogenic and quiescent adult tissues.* Circ Res, 2005. **96**(3): p. 384-91.
178. Izumi, G., et al., *Endocytosis of E-cadherin regulated by Rac and Cdc42 small G proteins through IQGAP1 and actin filaments.* J Cell Biol, 2004. **166**(2): p. 237-48.
179. Burger, P.E., et al., *Fibroblast growth factor receptor-1 is expressed by endothelial progenitor cells.* Blood, 2002. **100**(10): p. 3527-35.

180. Ferrari, N., et al., *Bone marrow-derived, endothelial progenitor-like cells as angiogenesis-selective gene-targeting vectors.* Gene Ther, 2003. **10**(8): p. 647-56.
181. Hristov, M., W. Erl, and P.C. Weber, *Endothelial progenitor cells: isolation and characterization.* Trends Cardiovasc Med, 2003. **13**(5): p. 201-6.
182. Kanayasu-Toyoda, T., et al., *CD31 (PECAM-1)-bright cells derived from AC133-positive cells in human peripheral blood as endothelial-precursor cells.* J Cell Physiol, 2003. **195**(1): p. 119-29.
183. Salven, P., et al., *VEGFR-3 and CD133 identify a population of CD34+ lymphatic/vascular endothelial precursor cells.* Blood, 2003. **101**(1): p. 168-72.
184. Gunji, Y., et al., *Human primitive hematopoietic progenitor cells are more enriched in KITlow cells than in KIThigh cells.* Blood, 1993. **82**(11): p. 3283-9.
185. Okada, S., et al., *Enrichment and characterization of murine hematopoietic stem cells that express c-kit molecule.* Blood, 1991. **78**(7): p. 1706-12.
186. Ikuta, K. and I.L. Weissman, *Evidence that hematopoietic stem cells express mouse c-kit but do not depend on steel factor for their generation.* Proc Natl Acad Sci U S A, 1992. **89**(4): p. 1502-6.
187. Gu, J. and X. Gu, *Natural history and functional divergence of protein tyrosine kinases.* Gene, 2003. **317**(1-2): p. 49-57.
188. Poliseno, L., et al., *MicroRNAs modulate the angiogenic properties of HUVECs.* Blood, 2006. **108**(9): p. 3068-71.
189. Luna, G., J. Paez, and J.E. Cardier, *Expression of the hematopoietic stem cell antigen Sca-1 (LY-6A/E) in liver sinusoidal endothelial cells: possible function of Sca-1 in endothelial cells.* Stem Cells Dev, 2004. **13**(5): p. 528-35.
190. Urao, N., et al., *Erythropoietin-mobilized endothelial progenitors enhance reendothelialization via Akt-endothelial nitric oxide synthase activation and prevent neointimal hyperplasia.* Circ Res, 2006. **98**(11): p. 1405-13.
191. Yin, A.H., et al., *AC133, a novel marker for human hematopoietic stem and progenitor cells.* Blood, 1997. **90**(12): p. 5002-12.
192. Gampel, A., et al., *VEGF regulates the mobilization of VEGFR2/KDR from an intracellular endothelial storage compartment.* Blood, 2006. **108**(8): p. 2624-31.
193. Schmid, S.L. and I. Mellman, *Isolation of functionally distinct endosome subpopulations by free-flow electrophoresis.* Prog Clin Biol Res, 1988. **270**: p. 35-49.

194. Mayorga, L.S., et al., *Inhibition of endosome fusion by phospholipase A2 (PLA2) inhibitors points to a role for PLA2 in endocytosis.* Proc Natl Acad Sci U S A, 1993. **90**(21): p. 10255-9.
195. Shaked, Y., et al., *Therapy-induced acute recruitment of circulating endothelial progenitor cells to tumors.* Science, 2006. **313**(5794): p. 1785-7.
196. Schroeder, A., et al., *The RIN: an RNA integrity number for assigning integrity values to RNA measurements.* BMC Mol Biol, 2006. **7**: p. 3.
197. Wilson, C.L., et al., *Amplification protocols introduce systematic but reproducible errors into gene expression studies.* Biotechniques, 2004. **36**(3): p. 498-506.
198. Harr, B. and C. Schlotterer, *Comparison of algorithms for the analysis of Affymetrix microarray data as evaluated by co-expression of genes in known operons.* Nucleic Acids Res, 2006. **34**(2): p. e8.
199. Araki, H., et al., *Chromatin-modifying agents permit human hematopoietic stem cells to undergo multiple cell divisions while retaining their repopulating potential.* Blood, 2007. **109**(8): p. 3570-8.
200. Duda, D.G., et al., *A protocol for phenotypic detection and enumeration of circulating endothelial cells and circulating progenitor cells in human blood.* Nat Protoc, 2007. **2**(4): p. 805-10.
201. Haviv, F., et al., *Thrombospondin-1 mimetic peptide inhibitors of angiogenesis and tumor growth: design, synthesis, and optimization of pharmacokinetics and biological activities.* J Med Chem, 2005. **48**(8): p. 2838-46.
202. Asahara, T., et al., *Tie2 receptor ligands, angiopoietin-1 and angiopoietin-2, modulate VEGF-induced postnatal neovascularization.* Circ Res, 1998. **83**(3): p. 233-40.
203. Nyberg, P., L. Xie, and R. Kalluri, *Endogenous inhibitors of angiogenesis.* Cancer Res, 2005. **65**(10): p. 3967-79.
204. Corpechot, C., et al., *Hypoxia-induced VEGF and collagen I expressions are associated with angiogenesis and fibrogenesis in experimental cirrhosis.* Hepatology, 2002. **35**(5): p. 1010-21.
205. Hangai, M., et al., *Matrix metalloproteinase-9-dependent exposure of a cryptic migratory control site in collagen is required before retinal angiogenesis.* Am J Pathol, 2002. **161**(4): p. 1429-37.
206. Marneros, A.G. and B.R. Olsen, *The role of collagen-derived proteolytic fragments in angiogenesis.* Matrix Biol, 2001. **20**(5-6): p. 337-45.
207. Peacock, D.J., M.L. Banquerigo, and E. Brahn, *Angiogenesis inhibition suppresses collagen arthritis.* J Exp Med, 1992. **175**(4): p. 1135-8.

208. Seandel, M., et al., *Growth factor-induced angiogenesis in vivo requires specific cleavage of fibrillar type I collagen.* Blood, 2001. **97**(8): p. 2323-32.
209. Folkman, J., *Antiangiogenesis in cancer therapy--endostatin and its mechanisms of action.* Exp Cell Res, 2006. **312**(5): p. 594-607.
210. Fernandez, E.J. and E. Lolis, *Structure, function, and inhibition of chemokines.* Annu Rev Pharmacol Toxicol, 2002. **42**: p. 469-99.
211. Murdoch, C. and A. Finn, *Chemokine receptors and their role in vascular biology.* J Vasc Res, 2000. **37**(1): p. 1-7.
212. Daly, C., et al., *Angiopoietin-2 functions as an autocrine protective factor in stressed endothelial cells.* Proc Natl Acad Sci U S A, 2006. **103**(42): p. 15491-6.
213. Gu, J., et al., *Hypoxia-induced up-regulation of angiopoietin-2 in colorectal cancer.* Oncol Rep, 2006. **15**(4): p. 779-83.
214. Harfouche, R. and S.N. Hussain, *Signaling and regulation of endothelial cell survival by angiopoietin-2.* Am J Physiol Heart Circ Physiol, 2006. **291**(4): p. H1635-45.
215. Tsutsui, S., et al., *Angiopoietin 2 expression in invasive ductal carcinoma of the breast: its relationship to the VEGF expression and microvessel density.* Breast Cancer Res Treat, 2006. **98**(3): p. 261-6.
216. Mittal, V. and D.J. Nolan, *Genomics and proteomics approaches in understanding tumor angiogenesis.* Expert Rev Mol Diagn, 2007. **7**(2): p. 133-47.
217. St Croix, B., et al., *Genes expressed in human tumor endothelium.* Science, 2000. **289**(5482): p. 1197-202.
218. Beaty, R.M., et al., *PLXDC1 (TEM7) is identified in a genome-wide expression screen of glioblastoma endothelium.* J Neurooncol, 2007. **81**(3): p. 241-8.
219. Madden, S.L., et al., *Vascular gene expression in nonneoplastic and malignant brain.* Am J Pathol, 2004. **165**(2): p. 601-8.
220. Nanda, A. and B. St Croix, *Tumor endothelial markers: new targets for cancer therapy.* Curr Opin Oncol, 2004. **16**(1): p. 44-9.
221. Seth, P., et al., *Magic roundabout, a tumor endothelial marker: expression and signaling.* Biochem Biophys Res Commun, 2005. **332**(2): p. 533-41.
222. Gorski, D.H. and A.J. Leal, *Inhibition of endothelial cell activation by the homeobox gene Gax.* J Surg Res, 2003. **111**(1): p. 91-9.
223. Kerbel, R. and J. Folkman, *Clinical translation of angiogenesis inhibitors.* Nat Rev Cancer, 2002. **2**(10): p. 727-39.

224. Tudor, K.S., T.L. Deem, and J.M. Cook-Mills, *Novel alpha 4-integrin ligands on an endothelial cell line.* Biochem Cell Biol, 2000. **78**(2): p. 99-113.
225. Salmon, P., et al., *High-level transgene expression in human hematopoietic progenitors and differentiated blood lineages after transduction with improved lentiviral vectors.* Blood, 2000. **96**(10): p. 3392-8.
226. Perfetto, S.P., P.K. Chattopadhyay, and M. Roederer, *Seventeen-colour flow cytometry: unravelling the immune system.* Nat Rev Immunol, 2004. **4**(8): p. 648-55.
227. Van Gelder, R.N., et al., *Amplified RNA synthesized from limited quantities of heterogeneous cDNA.* Proc Natl Acad Sci U S A, 1990. **87**(5): p. 1663-7.
228. Irizarry, R.A., et al., *Summaries of Affymetrix GeneChip probe level data.* Nucleic Acids Res, 2003. **31**(4): p. e15.
229. Smyth, G.K., *Linear models and empirical bayes methods for assessing differential expression in microarray experiments.* Stat Appl Genet Mol Biol, 2004. **3**: p. Article3.
230. Borchardt, P.E., et al., *Targeted actinium-225 in vivo generators for therapy of ovarian cancer.* Cancer Res, 2003. **63**(16): p. 5084-90.